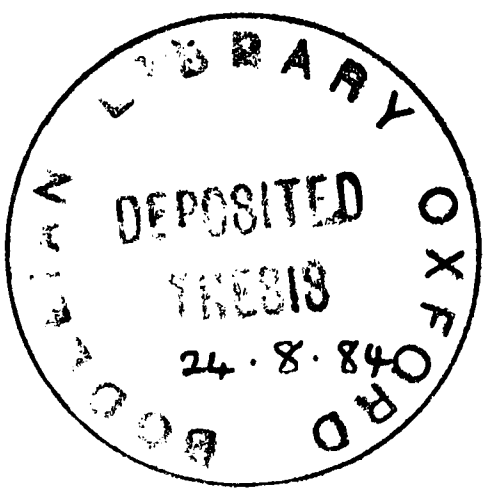

STUDIES IN APPLIED BIOELECTROCHEMISTRY

by

Graham Davis

Dissertation submitted for the degree of

Doctor of Philosophy in the honours school of

Physical Sciences (Chemistry)

University of Oxford

The Queen's College, Oxford

Hilary Term 1984

To my Mother

Contents

Abstract of the thesis entitled "Studies in Applied Bioelectrochemistry" submitted by Graham Davis, The Queen's College, University of Oxford for the degree of Doctor of Philosophy, Hilary Term 1984.

This thesis descibes the development of bioelectrochemical systems for application as biomedical analytical devices and fuel cells based on biological catalysts.

A range of ferrocene derivatives in the oxidised, ferricinium ion, form act as electron acceptors for the enzyme glucose oxidase. Kinetic information for these reactions was obtained by using the electrochemical technique of D. C. cyclic voltammetry. An amperometric enzyme electrode for the detection of glucose was devised based upon 1,1'-dimethylferrocene. The enzyme electrode was constructed using graphite foil as the base sensor on to which the ferrocene was doped and glucose oxidase covalently immobilised. In gravimetrically prepared buffered solutions of glucose the electrode gave a current proportional to the bulk glucose concentration in the range 1-30mM, which encompasses the range over which a diabetic's body glucose may vary. The electrode response is independent of pH, has a temperature coefficient of ca. 4%/°C and is insensitive to many potentially interfering substances found in biological samples. The electrode was used to assay both plasma and whole-blood samples from diabetics.

The enzyme electrode was also used to monitor changes in glucose concentration. An electrochemical assay was devised involving a coupled sequence of enzymes which consume glucose at a rate determined by the activity of the enzyme creatine kinase. This assay for creatine kinase may be useful in the diagnosis of acute myocardial infarction.

The ferricinium ion was studied as a general electron acceptor for oxido-reductases and a range of electrochemically coupled enzymatic oxidation reaction devised. These systems form the basis for the development of amperometric enzyme electrodes for detecting pyruvate, lactate, alcohols, sarcosine, xanthine, aldehydes, isocitrate, NADH, NADPH and carbon monoxide.

An alternative use for an amperometric enzyme electrode is as an anodic half-cell of a fuel cell. A biofuel cell based upon the oxidation of methanol by the quinoprotein alcohol dehydrogenase was developed.

Acknowledgements

First and foremost to my supervisor Dr Allen Hill for help, advice and considerable encouragement.

To all the members of the "HAOH group" especially Dr Tony Cass, Nick Walton and Nigel Oliver.

To Dr Monika Green for collaborating with experiments on creatine kinase.

To Prof John Higgins and members of his group at the Cranfield Institute of Technology.

To Bill Aston for obtaining the data presented in figures 7.12 and 7.13.

To Dr John Pickup at Guy's Hospital, London for providing blood samples from human diabetics.

To Dr John Colby at Sunderland Polytechnic for providing samples of carbon monoxide oxido-reductase.

To the SERC and Genetics International, Inc. for financial support.

Finally, to Miss Txed for her forgiving nature whilst producing this thesis.

CHAPTER 1

INTRODUCTION

CHAPTER 2

ELECTROCHEMICAL THEORY AND BACKGROUND

CHAPTER 5

CREATINE KINASE ASSAY USING THE GLUCOSE ENZYME ELECTRODE

CHAPTER 6

ELECTROCHEMICALLY COUPLED ENZYMATIC OXIDATION REACTIONS

CHAPTER 7

METHANOL BASED BIOELECTROCHEMICAL FUEL CELL

General abbreviations

O	oxidised form
R	reduced form
i_p	peak current
i_p^a	anodic peak current
i_p^c	cathodic peak current
i_f	Faradaic current
n	number of electrons
F	Faraday's constant
A	area of electrode
D_o	diffusion coefficient of oxidised species
E	potential
E^o	redox potential
$E_{1/2}$	half-wave potential
R	gas constant
T	degrees Kelvin
ν	rate of voltage sweep
C_o	concentration of O
a	$nF\nu/RT$
k_f	pseudo-first order rate constant
k	second order rate constant
i_k	kinetically controlled current
i_d	diffusion controlled current

SCE	saturated calomel electrode
NHE	normal hydrogen electrode
ΔG	free energy
W_u	available work
ΔH	enthalpy
ΔS	entropy
E	enzyme
S	substrate
P	product
ES	enzyme-substrate complex
k_1	rate of ES formation
k_2	rate of product formation
ϕ_s	membrane permeability
[S]	bulk substrate concentration
$[S]_o$	substrate concentration within enzyme layer
K_M	Michaelis-Menten constant
V^*	volume of enzyme layer
FPLC	fast protein liquid chromatography
IU	international enzyme unit
RMM	relative molecular mass
NCN	carbodiimide
cp	cyclopentadienyl
EC	Enzyme Commision number

CHAPTER 1

INTRODUCTION

1.1.1 Analytical applications of enzymes

The value of enzymes in quantitative assays has been apparent for many years. A variety of properties make these biocatalysts particularly appealing in analyses. Perhaps the most important is the specificity of enzymes, which allows their use for the determination of substrate concentration without prior separation from a complex mixture. Until recently, the instability, scarcity and expense of enzymes discouraged their wider use in analytical chemistry. During the 1970's, considerable effort was focused on improving commercial scale enzyme purification procedures. Latterly, this has resulted in over 10% of the 2000 known enzymes becoming available in a purified form and at relatively low cost. As a consequence, analysts in areas as diverse as water quality control, pollution monitoring, clinical chemistry and fermentation control regularly use a range of enzyme based assays (1-3).

1.1.2 Immobilised enzymes

Whilst enzymes have conventionally been used in solution, significant analytical advantages may be achieved by immobilisation on to an insoluble support; these include, increased enzyme

stability and the repetitive use of a single batch of enzyme. A wide range of support materials and immobilisation methods are now available and this may increase the use of enzymes as routine laboratory tools.

1.1.3 Transducer-immobilised enzymes

A number of analytical devices have been developed by immobilising an enzyme on to the surface of a transducer which is capable of detecting a physical or chemical change caused by the action of the enzyme. Transducers that have been used in this way include thermometric (4), spectrophotometric (5), luminescent (6) and electrochemical (7) devices. The most widely known example of a transducer bound enzyme probe is the so-called enzyme electrode. These devices combine the specificity and affinity of a biological catalyst for its substrate with the analytical power of electrochemistry. In an enzyme electrode, the function of the enzyme is to generate (or consume) an electro-active species in a stoichiometric relationship to its substrate. The former is then detected electrochemically.

1.1.4 Enzyme Immobilization at an electrode

Both physical and chemical methods can be used to immobilise an enzyme at an electrode (8). In general, physical methods where the enzyme is adsorbed on to the electrode, entrapped behind a membrane

covering the electrode, or occluded within a gel matrix, are less stable than those based on chemical methods. Chemical methods include those where the enzyme is coupled either *via* a cross-linking agent to itself or another protein, or, directly to funtional groups on the electrode surface. Functional groups of enzymes that are open to chemical modification include α- and ϵ-amino groups, α-,β- and δ-carboxyl groups, sulphydryl groups and phenolic groups, and the imidazole portion of hystidine residues. These methods have been extensively reviewed by Chibata and others (8-13). Cyanuric chloride and carbodiimide respectively, can be used to covalently couple enzymes to hydroxyl and carboxyl functional groups on the surface of graphite, eqs 1.1 and 1.2.

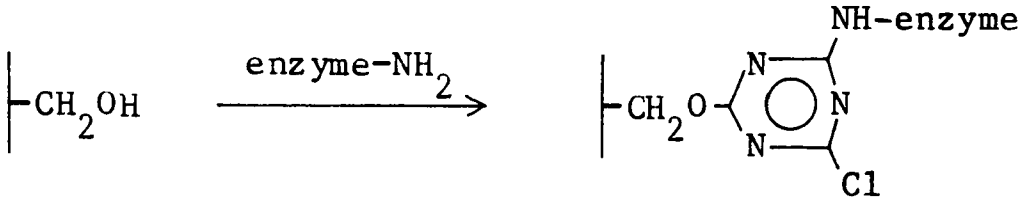

[1.1]

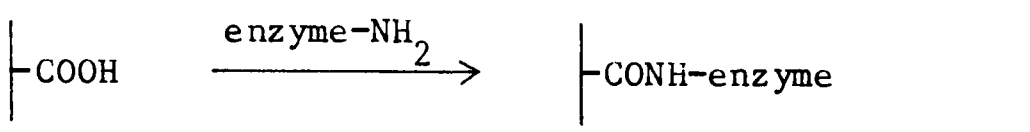

[1.2]

Whilst cyanuric chloride reacts exclusively with lysine residues, carbodiimides are less selective and will couple *via* lysine, tyrosine, cysteine, aspartic acid and glutamic acid residues (13).

1.1.5 Effect of immobilisation on enzyme kinetics

Kinetic differences have been observed (13) between the solution phase and immobilised forms of many enzymes. These differences have been ascribed to three main processes: mass

transfer becoming rate limiting; steric and orientational factors; and micro-environmental effects. Since mass transfer is a first order effect with respect to substrate, the effect can be to increase the apparent first order kinetic region. (For an enzyme electrode, slow mass transfer can increase the linear range, thereby increasing the region which is useful analytically). Considering steric factors, the enzyme may be immobilised in such an orientation that the active site is patially blocked. Whilst this phenomenon has not been studied in detail, it may contribute to changes in enzyme kinetics. Micro-environmental effects are related to partitioning of kinetic effectors such as hydrogen ion, substrate, product, activator or inhibitor between the bulk solution and the immobilised enzyme layer.

1.1.6 Effect of immobilisation on enzyme stability

The stability of the enzyme in an immobilised form is an important factor since in many cases the rate of decrease in enzyme activity is reduced after immobilisation (13). Three types of stability can be measured: thermal stability, storage stability and operational stability. Thermal stability is defined as the ability of the enzyme to function at elevated temperatures without denaturation. Storage stability relates to loss of activity under a defined storage protocol. Operational stability is associated with the rate of decrease in the amount of enzyme activity, for an enzyme electrode this can be equated with the rate of change in the

calibration coefficient.

1.1.7 Construction and operation of an enzyme electrode

An enzyme electrode is constructed by immobilising a layer of enzyme close to the surface of an electrode. A measurement can be made by operating the device in either the potentiometric or amperometric mode. In addition to the enzyme electrode, a reference electrode is necessary with a circuit for measuring either the current flow, or the potential difference between the electrodes. When operating amperometrically, a source of potential is required to drive the current.

By placing the enzyme electrode into an electrolyte of suitable pH that contains the substrate of the enzyme, enzymatic conversion of substrate to product can occur within the immobilised layer. Since the reaction only occurs in the enzyme layer, a concentration gradient of both substrate and product is generated by the reaction. After some time interval, ca. 30-600 s, a steady-state condition will be obtained in which the rate of supply and the rate of consumption of the substrate are equal. Over a limited concentration range, a steady-state current (or potential) related to the bulk concentration of the substrate will be realised. This forms the analytical basis of an enzyme electrode. The relationship of the steady-state electrochemical response is linear in an amperometric device and logarithmic in a potentiometric device. As an alternative

to making a steady-state measurement, the bulk substrate concentration can be determined from an initial rate measurement (7).

1.1.8 Analytical applications of enzyme electrodes

In principle, the scope for applications of enzyme electrodes is limited only by the number of enzymes that are available, provided that a suitable transducer can be devised.

Potentiometric detection has usually been applied to enzyme electrodes in which an ionic species is produced (or consumed) by the reaction, e.g. H^+, NH_4^+, CN^- and I^-. These species can be detected with ion-selective electrodes. Various configurations are summarised in table 1.1 (14-19). Enzyme electrodes based on amperometric detection are most often applied to devices incorporating an oxido-reductase where the enzyme generates (or consumes) an electro-active molecule. When using an oxidase or dehydrogenase, it is often necessary to add a co-reagent, usually oxygen or $NAD(P)^+$. Table 1.2, summarises a number of amperometric enzyme electrodes that have been developed (20-28).

There are a number of reasons, table 1.3, for the interest in enzyme electrodes as analytical devices. As stated previously, the most important reason is that they offer a convenient and straightforward method for determining the concentration of a

Table 1.1 Potentiometric enzyme electrodes

Substrate	Enzyme	Species	Electrode	Ref
urea	urease	H^+	pH/glass	14
penicillin	penicillinase	"	"	15
glucose	β-glucosidase	"	"	14
L-amino acids	L-amino acid oxidase	NH_4^+	mono-cation	16
creatine	creatinase	"	"	17
uric acid	uric acid oxidase	CO_2	CO_2-selective	18
glucose	glucose oxidase	I^-	Iodide-selective	19

Table 1.2 Amperometric enzyme electrodes

Substrate	Enzyme	Species	Electrode	Ref
glucose	glucose oxidase	O_2	platinum	20
alcohols	alcohol oxidase	"	"	21
amino acids	amino acid oxidase	"	"	22
uric acid	uric acid oxidase	"	"	23
diamines	diamine oxidase	"	"	24
glucose	glucose oxidase	H_2O_2	"	25
alcohols	alcohol oxidase	"	"	26
ethanol	alcohol dehydrogenase	NADH	carbon	27
lactate	lactate dehydrogenase	$Fe(CN)_6^{3-}$	platinum	28

Table 1.3 Advantages of enzyme elecrtodes

Sample pre-treatment minimal

Non-destuctive towards sample

Small sample volume ca. 20-1000µl

Electrode calibrated versus standard samples

Wide range and sensitivity

Rapid response ca. 30-600 s

particular species in a complex mixture. In addition, pretreatment of the sample is minimal and unlike spectrophotometric assays turbidity is not a problem. As with pH electrodes, devices are relatively easy to operate and calibrate. The use of an enzyme electrode does not normally lead to the destruction of the sample, so additional components may be assayed subsequently. The range of concentrations over which enzyme electrodes are reported to give a response is wide, ca. 10^{-5}-10^{-1}M (7). The lower limit of detection is determined by three factors: the magnitude of other electroactive species (background), the sensitivity of the technique and the reproducibility of these parameters.

Devices respond quickly, since the steady-state response is usually attained within 30-600 s. The actual response depends on the electrode geometry, method of enzyme immobilization, rate of stirring and the substrate concentration.

Another advantage is that the sample volume can be small, ca. 20-1000µl (7). This is often desirable when analysing clinical samples. Finally, enzyme electrodes can be made and operated inexpensively and if the device is re-used a number of times the cost per sample is minimised. This can be a major cost benefit over assays based on the use of soluble enzymes where the enzyme is not recovered.

Factors that effect the performance of an enzyme electrode are

summarised in table 1.4.

1.2.1 Amperometric enzyme electrodes

The aim of this work was to develop novel amperometric enzyme electrodes, primarily to monitor metabolites of clinical interest. A diagramatic representation of an amperometric enzyme electrode is shown in figure 1.1. This shows that the immobilised enzyme layer is interposed between the surface of the electrode and the analyte solution. Ideally, the current should be determined only by the chemical reaction and by diffusion through the enzyme layer. This requires that the transducer has a rapid response, the membrane be thin and the bulk solution well stirred. This can not always be achieved in practise and factors such as convection and membrane thickness and permeability can complicate the response.

Figure 1.1, shows that the electrode response to the bulk substrate concentration is determined by a complex set of processes. First, the substrate must be transported from the bulk of the solution to the outside of the membrane; it must then diffuse across the membrane into the enzyme layer where, in the simplest case it will be consumed by the enzyme according to Michaelis-Menten kinetics (29), to give the product, eq 1.3.

$$E + S \underset{}{\overset{k_1}{\rightleftharpoons}} ES \xrightarrow{k_2} E + P \qquad [1.3]$$

Table 1.4 Factors affecting enzyme elctrode performance

Physical Factors:
Stability of base sensor
Mechanical stability of enzyme layer
Mechanical stability of membrane
Chemical Factors:
Enzyme immobilisation method
Co-substrate immobilisation method
Total enzyme activity
Stability of immobilised enzyme
pH
Temperature
Inhibitor concentrations
Storage conditions

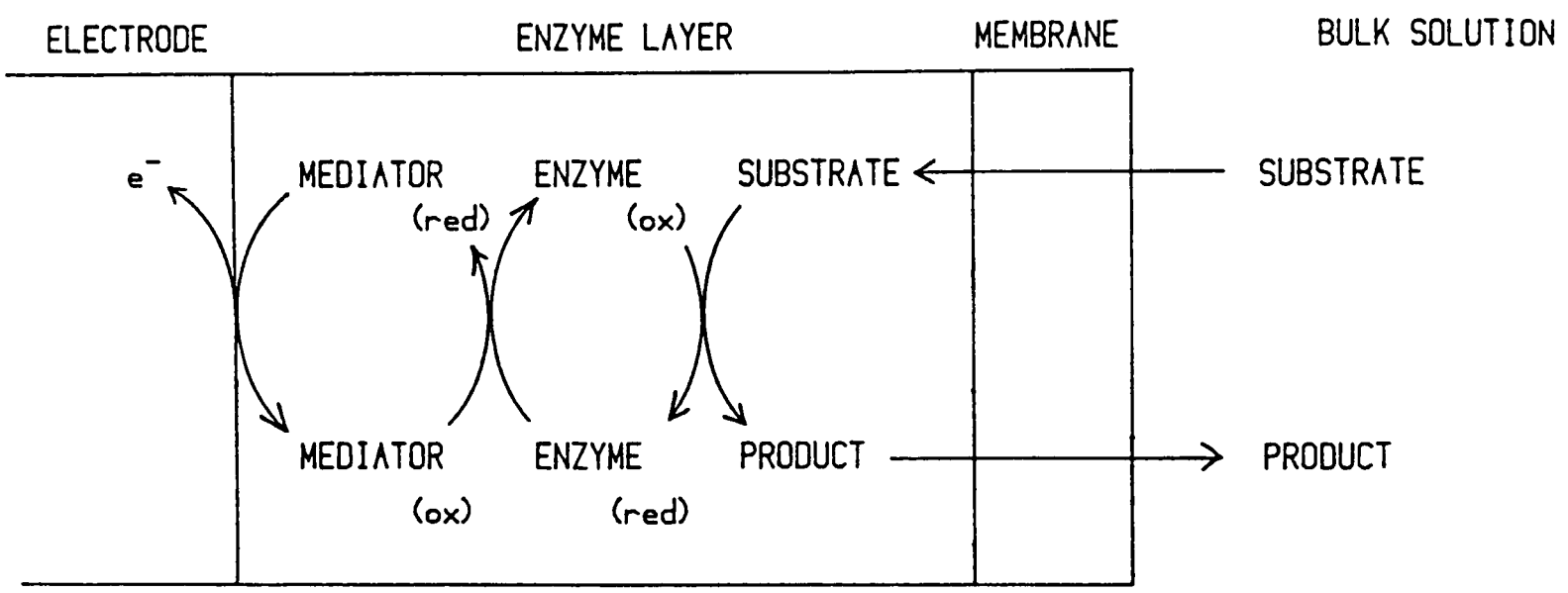

Figure 1.1 Schematic diagram of the sequence of steps that occur at an amperometric enzyme electrode.

Here, E is the enzyme, S is the substrate and ES is the enzyme substrate complex. When an enzyme electrode is operated in an amperometric mode, one of the species involved in the enzymatic reaction must be electrochemically consumed. This is illustrated by considering an enzyme electrode based upon an oxidase which catalyses the oxidation of a substrate and uses oxygen as the electron acceptor, as shown in the following reaction, eq 1.4,

$$S + O_2 \longrightarrow P + H_2O_2 \qquad [1.4]$$

The product of the reaction, hydrogen peroxide, is monitored by oxidation at a platinum electrode. The flux of the product at the electrode (x=0) will be determined by the electrode potential. Maximum sensitivity will be obtained by setting the potential so that the product is completely oxidised, eq 1.5,

$$[P]_{x=0} = 0 \qquad [1.5]$$

The current that is measured will be related by Faraday's law, and Fick's laws of diffusion (30) to the flux of the product at the electrode surface, eq 1.6,

$$i = nFAD_p d[P]/dx_{(x=0)} \qquad [1.6]$$

where, A is the surface area of the electrode, D_p is the diffusion coefficient of the product, n is the number of electrons transferred

and F is Faraday's constant. As a result of the concentration gradient generated by the enzyme, substrate will diffuse to the electrode from the bulk of solution and the reaction will be self-sustaining. In the steady-state, the current will be limited either by the rate of substrate diffusion or by the rate of the enzymatic reaction.

Although the bulk substrate concentration will decrease continuously throughout an experiment, the rate of decrease will be so slow that it will be measureable only when the sample volume is very small, mass transfer is fast, and the total enzyme activity is high.

1.2.2 Theoretical models of amperometric enzyme electrode

Theoretical models, in which the flux of the electro-active species to the electrode is limited by diffusion within the immobilised enzyme layer (31) and by external mass transfer (32), have been developed. The first model applies to electrodes where the enzyme is occluded within a gel matrix. The latter applies to systems in which the enzyme is covalently immobilised at a planar electrode surface. Whilst none of the theoretical models fully characterise the enzyme electrodes developed in subsequent chapters, the external mass transfer model is useful and is discussed further.

1.2.3 External mass transfer model

The external mass transfer model, developed by Mindt and Racine (32), incorporates the effects of enzyme activity, the Michaelis-Menten constant, K_M, of the enzyme for its substrate, and the permeability of the membrane that covers the enzyme electrode. This model assumes that, in the steady-state, the rate of chemical reaction and the rate of mass transfer are the same and that the current is limited by the rate of product formation. The following equation, eq 1.7, relates the current to the bulk substrate concentration.

$$i = nF\phi_s([S]_o - [S]) = nF\phi_s/2.([S]_o + K_M + k_2[E]V^*/\phi_s \quad [1.7]$$

$$+ \sqrt{(K_M - [S]_o + k_2[E]V^*/\phi_s)^2 + 4K_M[S]_o)}$$

Here, ϕ_s is the membrane permeability, [S] and $[S]_o$ are the respective enzyme layer and bulk substrate concentrations, k_2 is the rate of breakdown of the enzyme-substrate complex to form product, [E] is the enzyme concentration within the enzyme layer and V^* is the volume of the enzyme layer. This complex response of the current to the bulk substrate concentration is represented graphically in figure 1.2, and may be analysed in terms of its first order and zero order limits. It is evident that the K_M has an important effect on the linear range of the electrode response. When the bulk substrate concentration is less than the Michaelis-Menten constant, $[S]_o < K_M$,

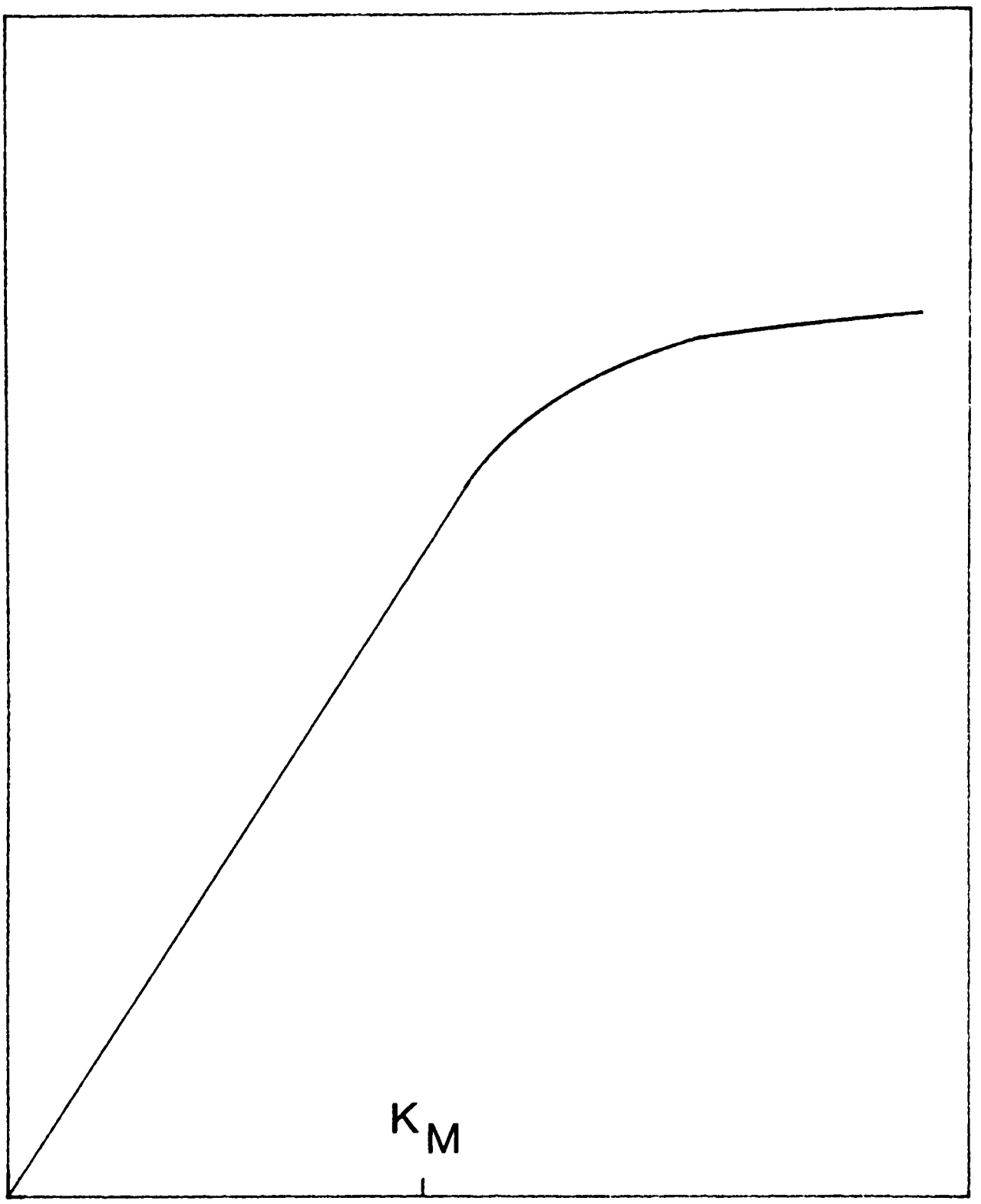

Figure 1.2 Idealised calibration curve for an amperometric enzyme electrode. The current response is linear at bulk substrate concentrations below the K_M of the enzyme, but becomes non-linear above the K_M.

the current response is first order with respect to substrate, eq 1.8.

$$i = nFk_2V^*[S]_o/(K_M + k_2[E]V^*/\phi_s) \qquad [1.8]$$

However, when $[S]_o > K_M$, the current is independent of the bulk substrate concentration, eq 1.9.

$$i = nFk_2[E]V^* \qquad [1.9]$$

The limiting value of the current, figure 1.2, corresponds to the enzyme layer becoming saturated with substrate. From an analytical viewpoint, a high upper limit to the first order response is desirable. Clearly, this will be promoted by a high K_M of the enzyme for its substrate and a low membrane permeability. However, a low membrane permeability will tend to increase the time taken to reach the steady-state.

When the response of the electrode is first order, two further parameters can limit the magnitude of the current. If the enzyme activity within the enzyme layer is insufficient, the magnitude of the current will be limited by the enzymatic reaction, eq 1.10.

$$i = nFV^*k_2[E][S]_o/K_M \qquad [1.10]$$

However, if there is a kinetic excess of enzyme at the electrode the

current becomes predominantly mass transfer limited, eq 1.11.

$$i = nF\phi_s[S]_o \qquad [1.11]$$

From this theoretical model, it is possible to deduce that it is desirable for a practical enzyme electrode to be constructed with a kinetic excess of the enzyme immobilized at the electrode. Whilst this is not always possible to achieve in practice, a kinetic excess of enzyme should reduce the sensitivity of the electrode to factors which affect the rate of the enzymatic reaction, typically changes of pH, temperature, enzyme activity and inhibitor levels.

1.3.1 Outline to thesis

As a prelude to the development of an amperometric enzyme electrode, an analytical technique was required to establish that an enzymatic oxidation (or reduction) reaction could be coupled electrochemically. The theory of stationary electrode D. C. cyclic voltammetry was extended by Nicholson and Shain (33) to systems in which homogeneous chemical reactions are coupled to reversible or irreversible charge transfer at an electrode. This technique gives a qualitative diagnosis of catalytically coupled reactions and can be used to obtain quantitative kinetic data for reactions upon which enzyme electrodes are based. Chapter 2, introduces D. C. cyclic voltammetry and its application to coupled reactions.

Many novel applications of a glucose enzyme electrode may result from the development of a non-oxygen dependent device capable of operating in whole blood and other biological samples. Chapter 4, describes the development of a novel amperometric enzyme electrode for monitoring glucose which may become useful in the control of the disease diabetes mellitus. The electrode uses a substituted ferricinium ion as a mediator of electron transfer between a covalently immobilized enzyme, glucose oxidase, and a graphite electrode.

Chapter 5, describes the use of the glucose enzyme electrode developed in chapter 4, to monitor the rate of comsumption of

glucose by a second enzyme in solution. An assay procedure has been developed for ATP-linked enzymes, termed phosphotransferases or kinases. Creatine kinase was chosen to demonstrate the feasibility of the enzyme electrode monitored assay because of its clinical importance in the diagnosis of acute myocardial infarction.

The identification of a ferrocene derivative as a suitable mediators for incorporation into an enzyme electrode for detecting glucose, suggested the preliminary investigation of the ferricinium ion as an oxidant for a range of enzymes. Chapter 6, describes electrochemically coupled ferrocene-mediated enzymatic oxidation reactions, based on a number of oxido-reductases. These coupled systems form the basis of enzyme electrodes for a range of metabolites including, pyruvate, alcohols, aldehydes, carbon monoxide, sarcosine, NADH, NADPH, isocitrate, lactate and xanthine.

A corollary of an amperometric enzyme electrode is that it forms the basis of an anodic half-cell for a bioelectrochemical fuel cell. Chapter 7, describes the development of a biofuel cell based on the oxidation of methanol to formate by the quino-protein, alcohol dehydrogenase.

References

1. Weetal, H. H. Anal. Chem. 46, 602A, (1974).

2. Guilbault, G. G. Anal. Chem. 42, 334R, (1970).

3. Bowers, L. D. and Carr, P. W. Anal. Chem. 48, 544R, (1976).

4. Weaver, J. C. Biochim. Biophys. Acta. 452, 285, (1976).

5. Bowers, L. D. and Carr, P. W. Immobilised enzymes in analytical chemistry: Chemical Analysis. 56, 197, (1980).

6. Freeman, T. W. and Seitz, W. R. Anal. Chem. 50, 1242, (1978).

7. Bowers, L. D. and Carr, P. W. in: Advances in biochemical engineering; ed Ghose, T. K., 12, 89, (1982).

8. Mosbach, K. ed: Methods in Enzymology, 44, (1976).

9. Zaborsky, O. R. Immobilised enzymes. Cleveland: CRC Press (1973).

10. Weetal, H. H. ed: Immobilised enzymes, antigens, antibodies and peptides. New York: Marcel Dekker (1975).

11. Pye, E. K. and Wingard, L. B. eds: Enzyme engineering. New York: Plenum 2, (1973).

12. Means, G. E. and Feeney, R. E. Chemical modification of proteins. San Francisco: Holden-Day (1971).

13. Chibata, I. ed: Immobilised enzymes. New York: Wiley (1978).

14. Nilsson, H. Biochim. Biophys. Acta. 320, 529, (1973).

15. Cullen, L. F. Anal. Chem. 46, 1955, (1974).

16. Guilbault, G. G. and Hrabaukova, E. Anal. Chem. 42, 1779, (1970).

17. Meyerhoff, M. and Rechnitz, G. A. Anal. Chim. Acta. 85, 277, (1976).

18. Warwo, R. and Rechnitz, G. A. J. Mem. Sci. 1, 143, (1976).

19. Nagy, G. Anal. Chim. Acta. 66, 443, (1973).

20. Notin, M., Guillien, R. and Nabet, P. Ann. Biol. Clin. 30, 193, (1972).

21. Nanjo, M. and Guilbault, G. G. Anal. Chim. Acta. 57, 169, (1975).

22. Nanjo, M. and Guilbault, G. G. Anal. Chim. Acta. 73, 367, (1974).

23. Nanjo, M. and Guilbault, G. G. Anal. Chem. 46, 1769, (1974).

24. Toul, Z. and Macholan, L. Coll. Czech. Chem. Comm. 40, 2208, (1975).

25. Guilbault, G. G. and Lubrano, G. J. Anal. Chim. Acta. 64, 439, (1973).

26. Clark, L. C. Biotech. Bioeng. Symp. 3, 377, (1972).

27. Suzuki, S., Takahashi, F., Satoh, I. and Sonobe, N. Bull. Chem. Soc. Japan, 48, 3246, (1975).

28. Durliat, H., Comtat, M., Mohenc, J. and Baudras, A. J. Electroanal. Chem. 66, 73, (1975).

29. Roberts, D. V. Enzyme kinetics, London: Cambridge Univ. Press (1977).

30. Bard, A. J. and Faulkner, L. R. Electrochemical methods fundamentals and applications. New York: Wiley, 130, (1980).

31. Blaedel, W. J. Anal. Chem. 44, 2030, (1972).

32. Racine, P. and Mindt, W. Experimentia Suppl. 18, 525, (1971).

33. Nicholson, R. S. and Shain, I. Anal Chem. 36, 706, (1964).

CHAPTER 2

ELECTROCHEMICAL THEORY AND BACKGROUND

2.1.1 Direct current cyclic voltammetry

The electrochemical technique of D. C. cyclic voltammetry (1-3) consists of sweeping the potential of a stationary working electrode with time, and with respect to some reference, between two set limits, figure 2.1. The current at the working electrode is recorded continuously throughout the experiment. There are two components to the measured current response to a potential sweep. Firstly, a non-Faradaic component, referred to as the double layer charging current. This results from the re-distribution of species at the electrode. The magnitude of the charging current is proportional to the rate of voltage scan. Secondly, a Faradaic component, which results from electron transfer to and from an electro-active species in solution.

2.1.2 Reversible charge transfer

If the rate of heterogeneous electron transfer between the electrode and the electro-active species is sufficiently fast, the Faradaic current is controlled by the rate of diffusion of the

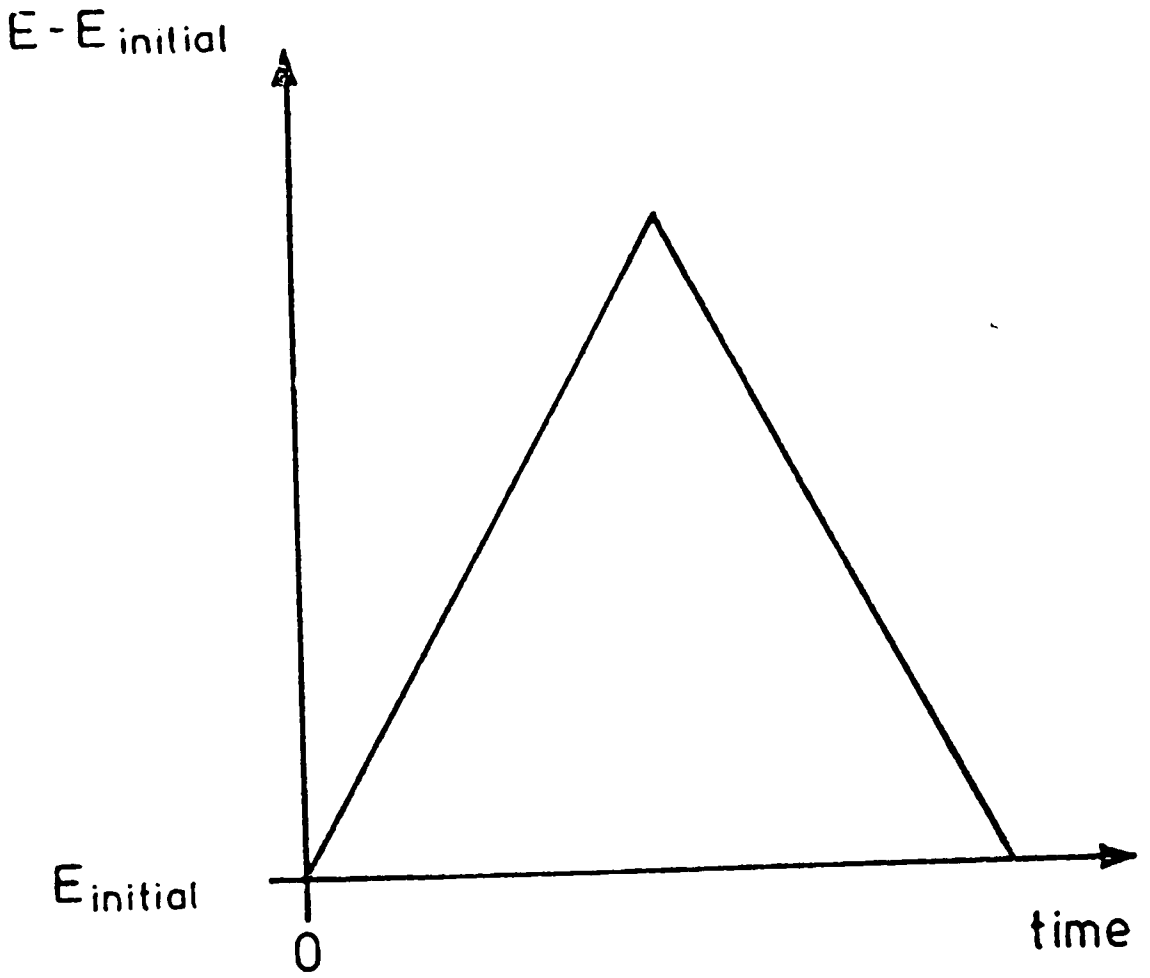

Figure 2.1 Triangular potential wave form for direct current cyclic voltammetry.

electro-active species to the electrode. This behaviour is described as electrochemically reversible electron transfer. For an unstirred solution, the peak current, i_p, is proportional to the square root of the sweep rate, $\nu^{1/2}$. For the reversible redox reduction of the species O, eq 2.1,

$$O + ne^- \rightleftharpoons R \qquad [2.1]$$

with a redox potential E^o, the Faradaic current, i_f, depends on the concentration gradient of O at the electrode surface, eq 2.2.

$$i_f = nFAD_o(d[O]/dx)_{x=0} \qquad [2.2]$$

Where, A is the area of the electrode and D_o is the diffusion coefficient of the oxidised electro-active species. By starting at a positive potential and scanning towards and past E^o, the surface concentration of O will vary in accordance with the Nernst equation, eq 2.3.

$$[O]/[R] = \exp[nF/RT(E-E^o)] \qquad [2.3]$$

As a result of the flow of current, as O is converted to R, there is an increasing concentration gradient at the electrode surface. Consequently, O rapidly becomes depleted within the diffusion layer and the current is not maintained but peaks and decays. By changing the direction of potential scan a peak from the reverse reaction is

obtained. This is illustrated in figure 2.2, which shows a series of voltammograms of ferrocene monocarboxylic at different voltage sweep rates.

For a reversible reaction the maximum cathodic current, i_p, is give by eq 2.4,

$$i_p = 0.4463nFA(D_o a)^{1/2} C_o \qquad [2.4]$$

Where, C_o is the bulk concentration of O and $a=nF\nu/RT$. The peak current occurs at a potential 28.5/n mV cathodic of E^o at 298K and is independent of the rate of potential scan. This means that for a reversible one-electron transfer reaction, voltammograms with a peak separation, ΔE_p = 57mV are obtained. In addition, $i_p/\nu^{1/2}$ = constant, and the ratio of the anodic to cathodic peaks, i_{pa}/i_{pc}, is equal to unity. Voltammograms of ferrocene monocarboxylic acid, shown in figure 2.2 conform to these criteria. The anodic peak current, $i_p a$, is plotted as a function of the square root of the scan rate in figure 2.3, using data from figure 2.2.

2.1.3 Electrochemically coupled reactions

Several of the kinetic systems that can be coupled to a reversible electron transfer have been analysed by Nicholson and Shain (4). They are illustrated by the following schemes which include: a preceeding reversible chemical reaction eq. 2.5; charge

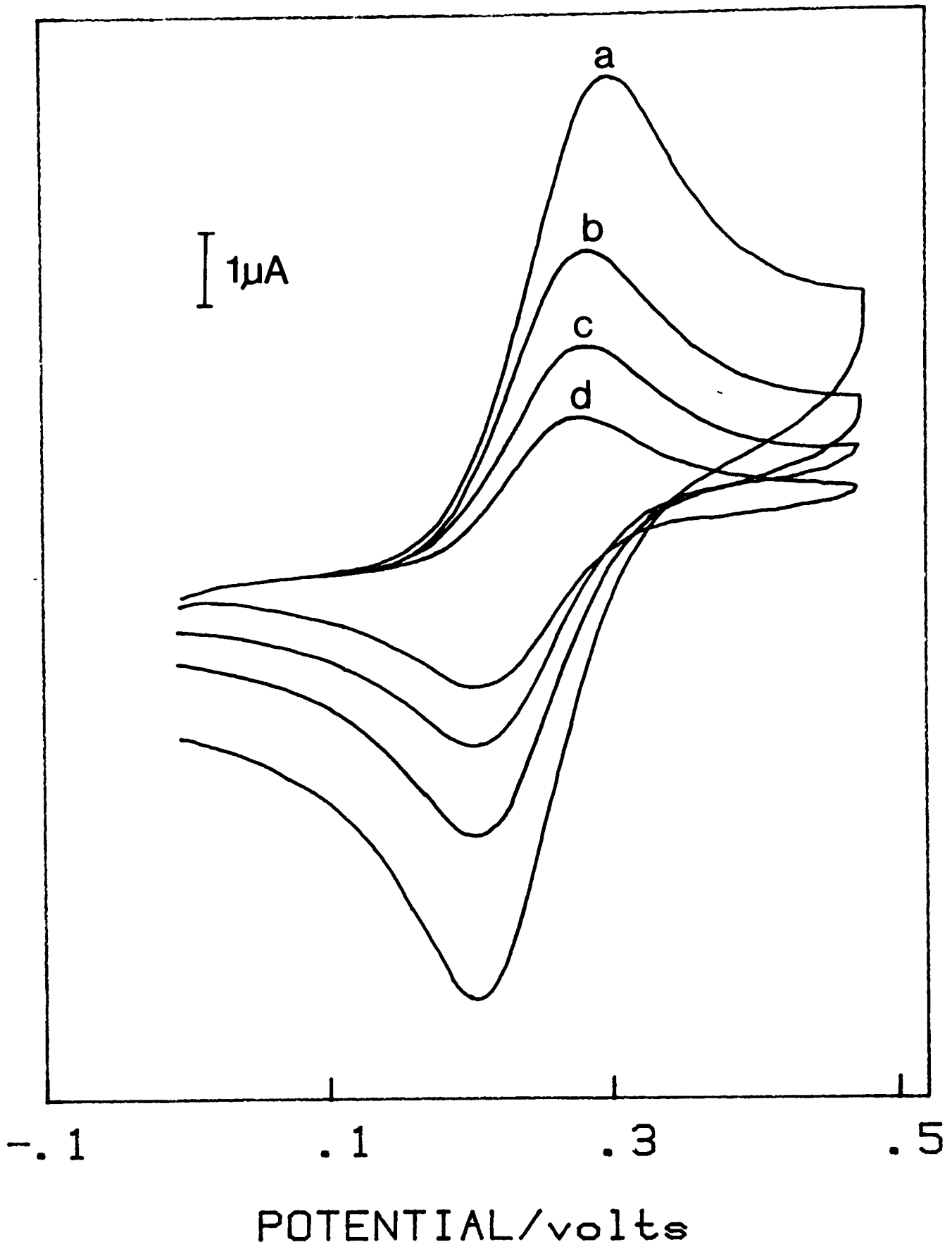

Figure 2.2 D. C. cyclic voltammograms of ferrocene monocarboxylic acid (200μM), in 0.1M $NaClO_4$, 50mM phosphate buffer pH 7.0, at 20°C. The potential range is 0.0 to +0.45V vs SCE at scan rates of (a) 50mVs^{-1}, (b) 20mVs^{-1}, (c) 10mVs^{-1} and (d) 5 mVs^{-1}.

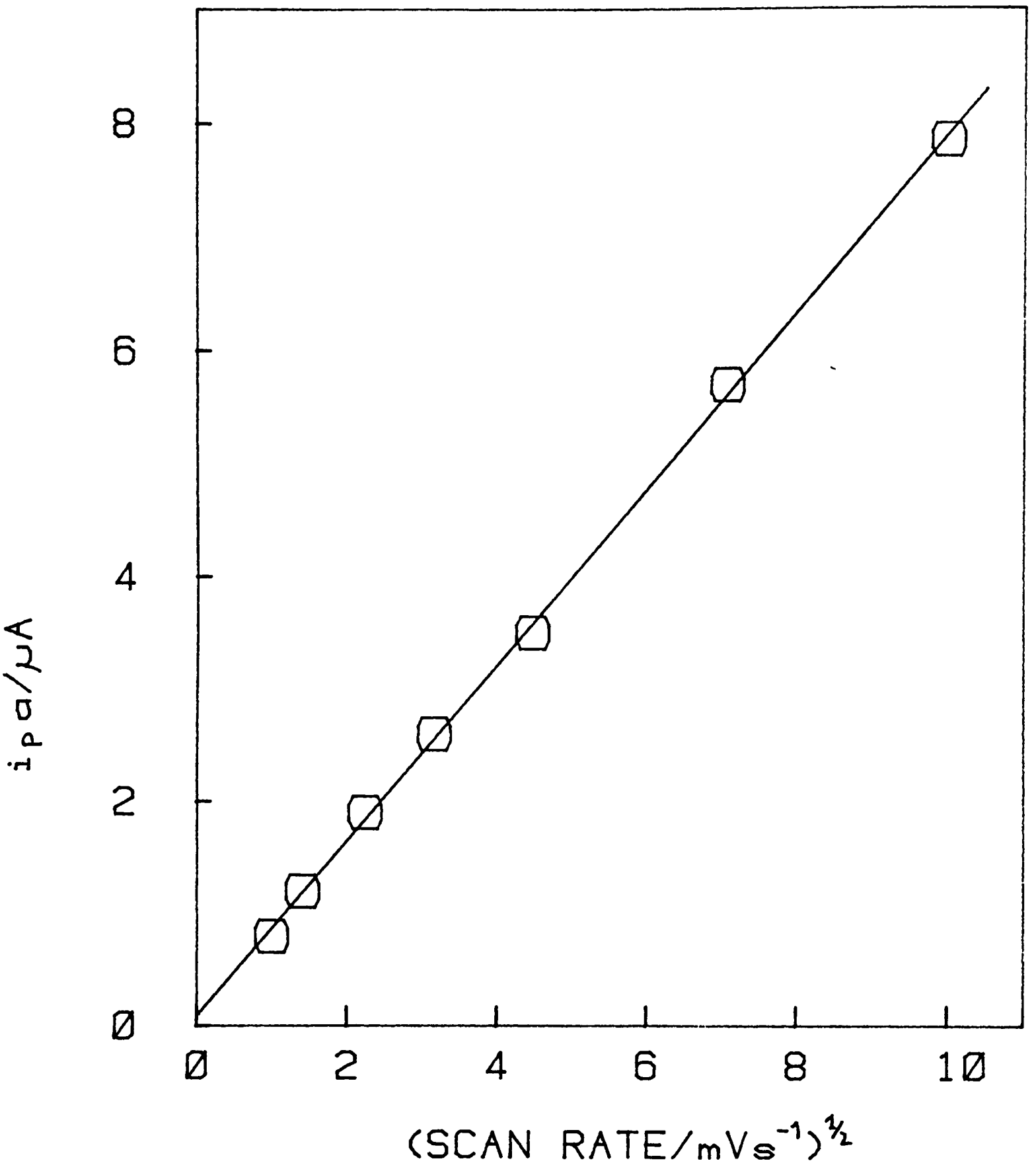

Figure 2.3 Plot of the anodic peak current, i_{pa}, versus the square root of the scan rate, for ferrocene monocarboxylic acid. Conditions are as for figure 2.2.

transfer followed by a reversible chemical reaction eq. 2.6; charge transfer followed by an irreversible chemical reaction eq. 2.7; and a catalytically coupled reaction eq. 2.8.

$$Z \overset{k_f}{\rightleftharpoons} O;\ O + ne^- \rightleftharpoons R \qquad [2.5]$$

$$O + ne^- \rightleftharpoons R;\ R \overset{k_f}{\rightleftharpoons} Z \qquad [2.6]$$

$$O + ne^- \rightleftharpoons R;\ R \xrightarrow{k_f} Z \qquad [2.7]$$

$$O + ne^- \rightleftharpoons R;\ O + Z \xrightarrow{k_f} R \qquad [2.8]$$

Since the scheme shown in eq. 2.8 applies to data presented subsequently it is considered further.

2.1.4 Catalytically coupled reactions

In each of the kinetic schemes, the perturbation that the chemical reaction causes to the voltammogram will depend on its rate, as compared with the time required to perform the electrochemical experiment. For a catalytically coupled reaction, eq 2.8, the component Z would serve to regenerate R at oxidising potentials. Qualitatively, the effect on the voltammogram would be to increase the anodic current and decrease the cathodic current. However, if the pseudo-first order rate constant, k_f, is small, the voltammogram will approximate that of a simple reversible electron

transfer reaction. Alternatively, if k_f is large the current will be directly proportional to $\sqrt{k_f}$ and independent of the rate of voltage scan (4), eq 2.9.

$$i = nFA\sqrt{D_o k_f C_o}/1+\exp[nF/RT(E-E_{1/2})] \qquad [2.9]$$

Under these conditions a limiting, or plateau, current rather than a peak is observed in the voltammogram. Figure 2.4, shows the effect on the voltammogram of different values of the kinetic parameter.

2.1.5 Identifying coupled reactions

By plotting the current function, $i_p/nFA(D_o a)^{1/2}C_o$, against the rate of voltage scan, the effect of scan rate on the diffusional process can be separated from its effect on the kinetics. For a simple reversible charge transfer reaction a horizontal straight line is obtained, figure 2.5(a). However, for a catalytically coupled reaction, the current function only approaches the horizontal line when the voltage scan is sufficiently fast so that the chemical reaction can not proceed significantly before the experiment is complete, figure 2.5(e). Current function plots for each of the coupled reaction eqs 2.5-2.8, are also included in figure 2.5.

Plots such as these are useful diagnostically for identifying different coupled reactions. Experimentally, these correlation plots

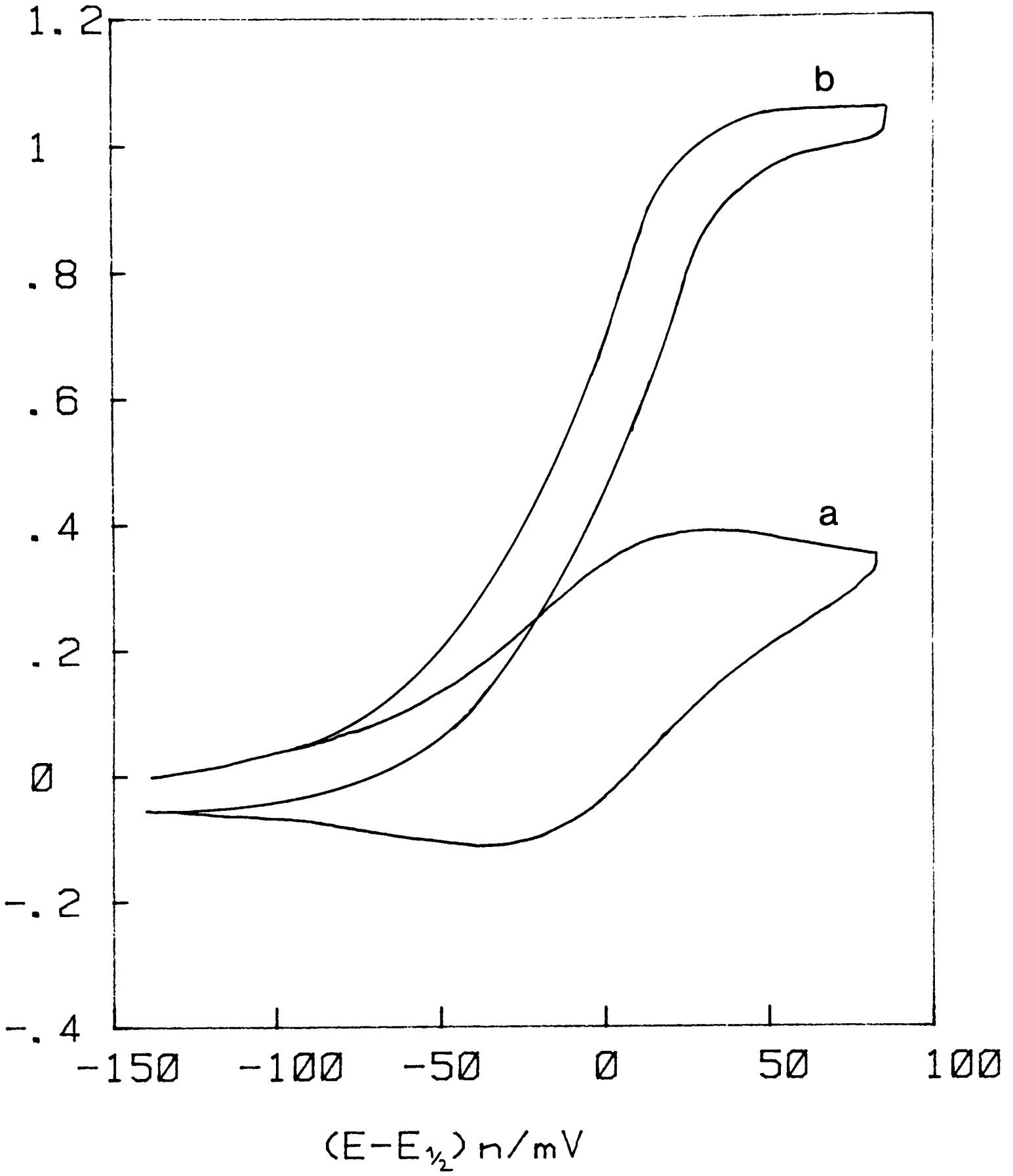

Figure 2.4 D. C. cyclic voltammograms simulated for a catalytic reaction with reversible charge transfer as a function of the kinetic parameter k_f/a, (a)=0.01 and (b)=1.0.

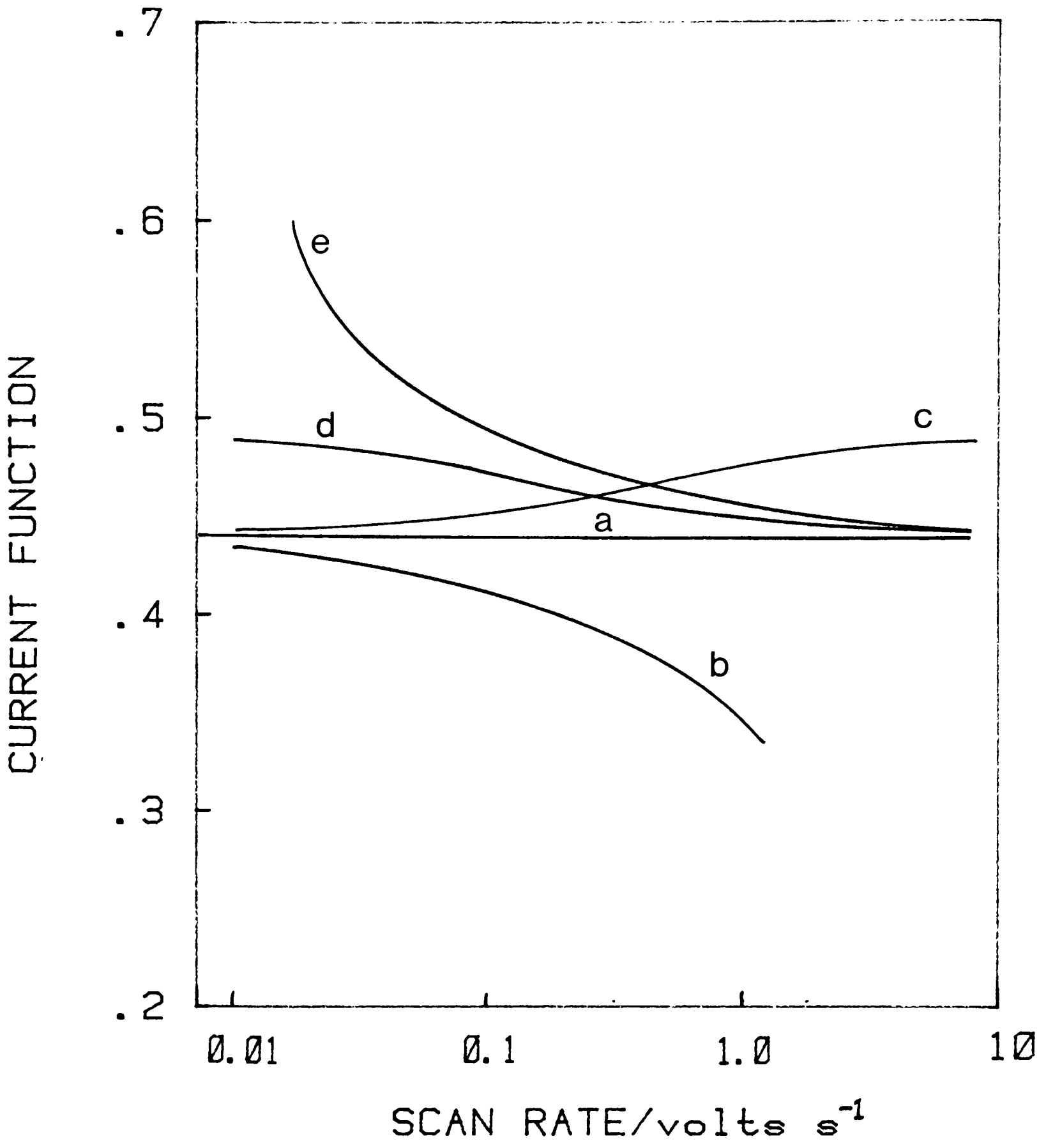

Figure 2.5 Variation of the peak current functions with the rate of voltage scan. Curves (a)-(e) correspond to the coupled reactions shown respectively in eq 2.1 and eqs 2.5-2.8.

are extremely easy to obtain since it is only necessary to plot $i_p/\nu^{1/2}$ (which approximates to the current function) versus $\log_{10}\nu$.

2.1.6 Deriving kinetic information from catalytic systems

The most convenient method of obtaining quantitative kinetic data from experiments is to use a working curve (4), in which the ratio of the kinetically controlled current to the diffusion controlled current, i_k/i_d, is plotted as a function of the kinetic parameter $k_f/a^{1/2}$, figure 2.6. From the ratio, i_k/i_d, measured at different scan rates, a set of values of k_f/a are obtained at a fixed concentration of Z. The effect of scan rate on the kinetic parameter is eliminated by plotting k_f/a versus $1/\nu$. Under pseudo-first order conditions, this gives a straight line passing through the origin with a gradient, $k_f RT/nF$, from which a scan rate independent pseudo-first order rate constant is derived. The second order rate constant for the reaction between O and Z, eq 2.8, is obtained by repeating the experiment at different concentrations of Z and plotting the values of k_f as a function of [Z], eq 2.10.

$$k = k_f\,[Z] \qquad [2.10]$$

2.1.7 Reactions between enzymes and mediators

The theory is suitable for analysing high rates of reaction, with values in the range ca. $k=10^2-10^6$ l mol^{-1} s^{-1}. This encompasses

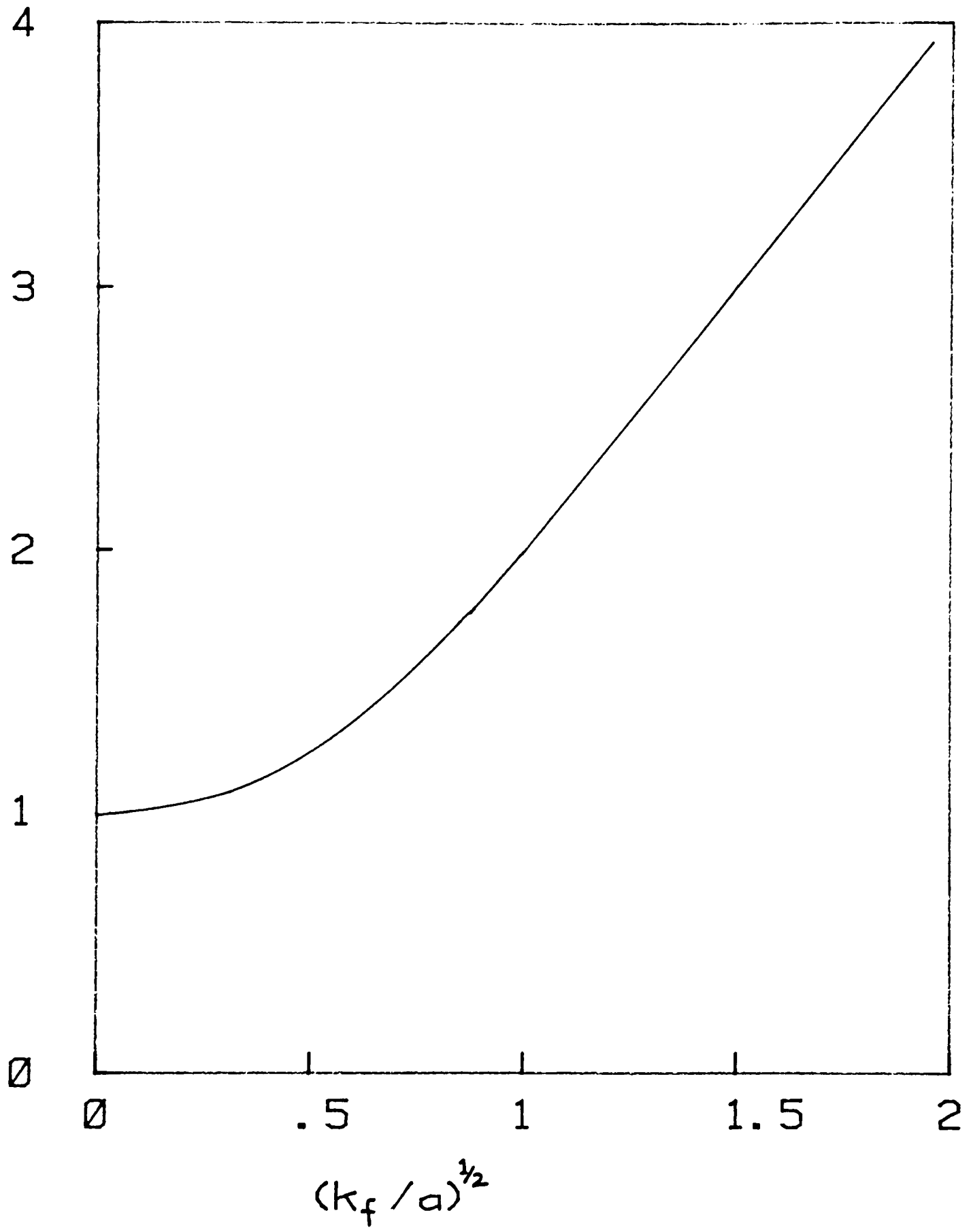

Figure 2.6 Theoretical plot of the ratio of the kinetic peak current to the diffusion-controlled peak current, i_k/i_d, versus the kinetic parameter, $(k_f/a)^{1/2}$.

values typically found for many reactions between oxido-reductases and various redox active compounds. The technique may offer a useful alternative to stopped-flow methods for measuring fast rates of reaction.

References

1. Delahey, P. J. New instrumental methods in electrochemistry. New York: Interscience (1954).

2. Bard, A. J. and Faulkner, L. R. Electrochemical methods fundamentals and applications. New York: Wiley (1980).

3. Sawyer, D. T. and Roberts, J. L. Experimental electrochemistry for chemists. New York: Wiley (1974).

4. Nicholson, R. S. and Shain, I. Anal. Chem. 36, 706, (1964).

CHAPTER 3

EXPERIMENTAL METHODS

3.1.1 Electrochemical instrumentation

D. C. cyclic voltammetry, which is a controlled potential electrochemical method, is based upon the maintenance of the potential of the working electrode (WE) with respect to a reference electrode (RE) by making a current pass between the working and counter electrode (CE). Figure 3.1, shows the circuit that was used which incorporates two operational amplifiers. These were built into an Oxford Electrodes potentiostat. Current-potential curves were recorded with a Bryans X-Y 26000 A3 chart recorder.

A 380Z micro-computer (Research Machines Ltd), interfaced to a potentiostat *via* digital-to-analogue and analogue-to-digital converters, was used for the potential step methods described in section 4.3.15. The potentiostat incorporates a multiplexer which facilitates both switching and monitoring of more than one working electrode, figure 4.19.

3.1.2 Cells and Electrodes

D. C. cyclic voltammetry experiments were performed using a two compartment cell that had a working volume of *ca*. 1ml, figure 3.2.

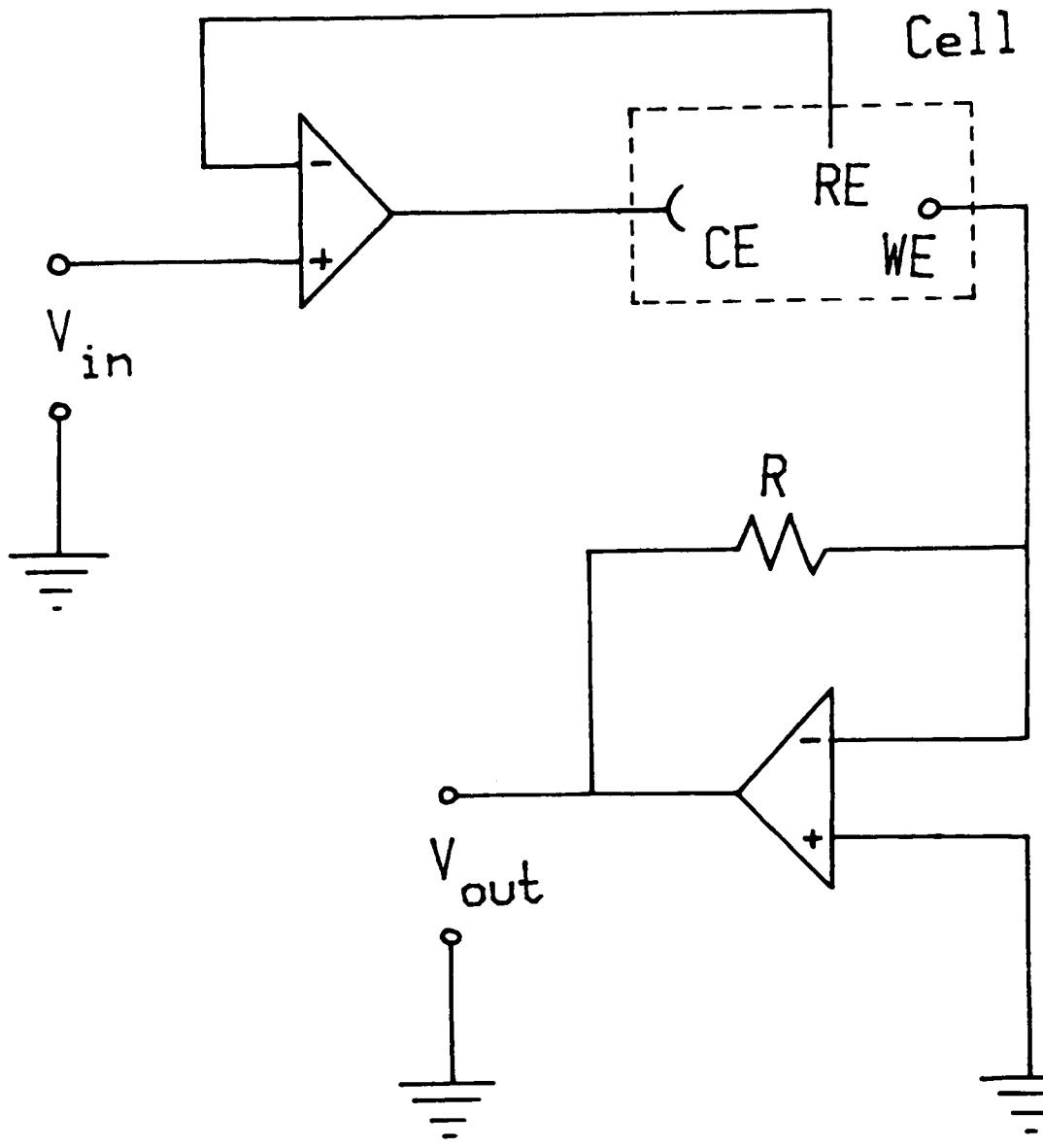

Figure 3.1 Circuit diagram of a simple potentiostat. Applied potential, V_{in}; reference electrode, RE; counter electrode, CE; working electrode, WE; current = V_{out}/R.

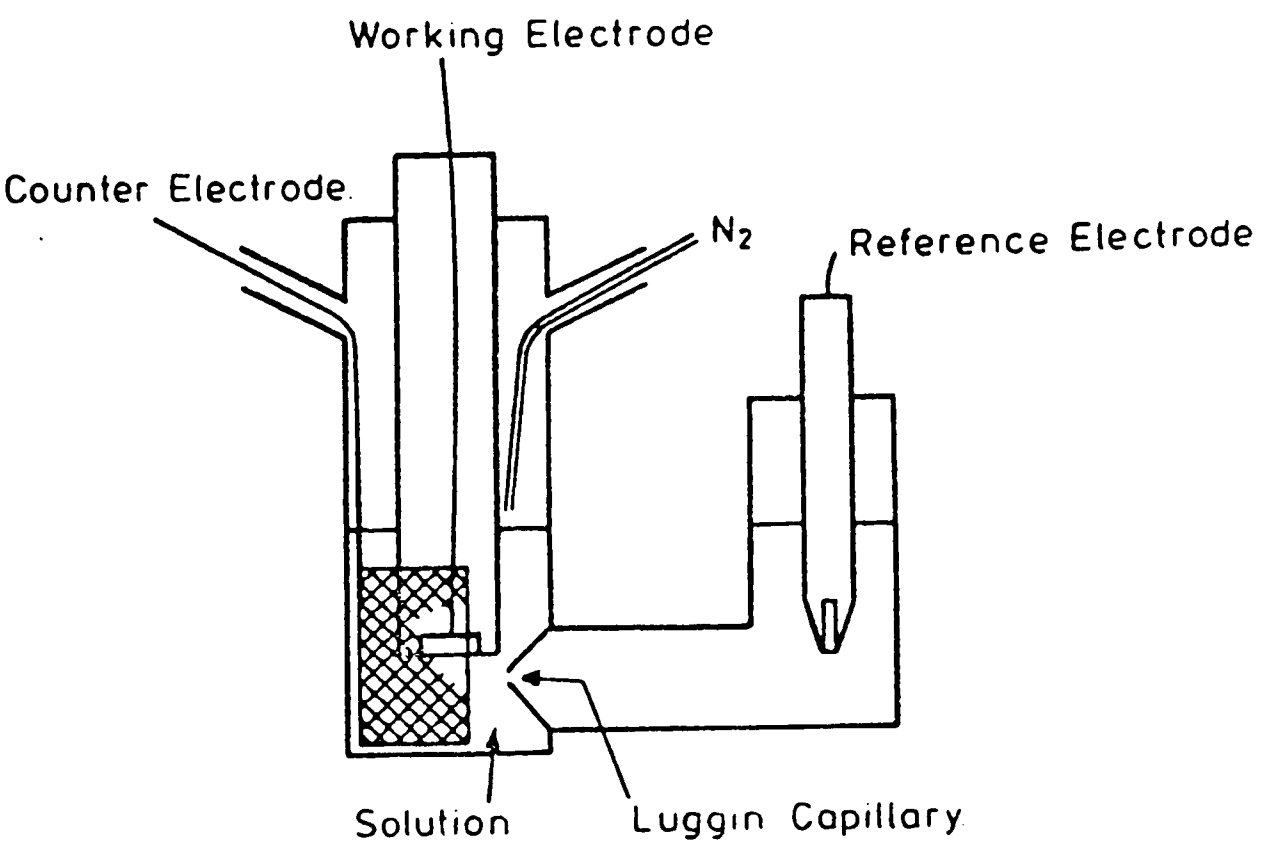

Figure 3.2 Electrochemical cell for stationary electrode voltammetry.

In addition to a 4mm diameter working electrode made of either gold, platinum or pyrolytic graphite, the cell contained a $1cm^2$ platinum gauze counter electrode and a saturated calomel electrode, type K401 (supplied by V. A. Howe Radiometer Electrodes) accurate in the range $-10^{o}C$ to $60^{o}C$, as reference. All potentials are referred to the saturated calomel electrode (SCE), which is +241mV at $20^{o}C$ versus the normal hydrogen electrode (NHE).

Working electrodes were polished before each experiment using an alumina-water paste on cotton wool and then washed with deionised water. Alumina with a particle size ca. 0.3μm, was supplied by BDH.

3.1.3 Temperature control

Electrochemical experiments were performed under thermostatic control by using a Churchill chiller thermocirculator connected to a water bath into which the electrochemical cell was placed.

3.1.4 Spectrophotometric measurements

All optical spectra were recorded with a Pye-Unicam SP8 200 spectrophotometer with the sample and reference solutions in matched quartz micro-cuvettes of path length 1cm.

3.1.5 Water purification

Where possible, all solutions were prepared with water purified by a sequence of reverse osmosis, ion exchange and carbon filtration using a combined Milli-RO4 and Milli-Q system supplied by Millipore Ltd.

3.1.6 Ultrafiltration and diafiltration

Ultrafiltration and diafiltration of proteins were performed by using the appropriately sized Amicon cell with a suitable Diaflo membrane.

3.1.7 Fast protein liquid chromatography

Protein purifications were performed using an FPLC system supplied by Pharmacia. This encorporated two P-500 pumps controlled by a gradient programmer GP-250 operated in conjunction with a single wavelength UV-monitor (λ=260nm) and an automatic fraction collector FRAC-100. Analytical and preparative ion-exchange columns were also supplied by Pharmacia.

CHAPTER 4

DEVELOPMENT OF A NON-OXYGEN MEDIATED GLUCOSE ENZYME ELECTRODE

Introduction

4.1.1. Diabetes mellitus

The best known and one of the most prevalent metabolic defects in humans is diabetes mellitus. Juvenile diabetes occurs in 0.04% of the population, whereas 3% develop the disease by their forties and by their late seventies over 7% of the population are affected (1). The severity of the disease can vary considerably: about 50% of juvenile patients can be treated by dietary restriction whilst the rest require regular injections of insulin. The latter is caused by atrophy of the pancreatic β-cells which naturally secrete this hormone into the blood stream. In non-diabetics, insulin secretion regulates the blood glucose concentration in the range 4-7mM (2). Among diabetic however, blood glucose levels can fluctuate between ca. 1-30mM. Initial diagnosis of the disease usually occurs when the patient becomes hyperglycemic. This results in the appearance of glucose in the urine which is excreted from the body when the renal threshold, of ca. 10mM glucose, is exceeded. The effective management of insulin-dependent diabetes depends on regular assay of blood glucose, usually twice daily, from which the patient's insulin requirement is calculated.

Development of a glucose assay which is rapid, convenient, precise and economical is a clear goal for scientist and clinician alike. To date, a limited range of automatic and semi-automatic glucose analysers, for the clinical chemistry laboratory and disposable enzyme-based test strips for home analyses, have been developed. Looking to the future, there is considerable interest in a minaturised implantable glucose monitor that could be coupled *via* a feedback device to an insulin infusion pump. This would constitute a closed-loop artificial pancreas, figure 4.1. Clinicians hope that the close control of glucose that the latter device may offer will alleviate many of the long-term complications suffered by diabetics, particularly neuropathy, cataracts, microangiopathy, leukocyte and platelet dysfunction, myopathy and cardio-cerebrovascular disease (3).

4.1.2 Methods of glucose analysis

Before the twentieth century, over thirty methods for measuring glucose in biological fluids had been devised (4-9). By the 1960's, the most commonly used methods depended on the ability of glucose to reduce salts of heavy metal atoms or nitro-aromatic acids (10,11). Use of these chemical methods is often complicated by interference attributed to the presence of other non-glucose reducing substances (12,13), common in biological samples. More recently, in order to increase the specificity of the analysis, enzymatic procedures have

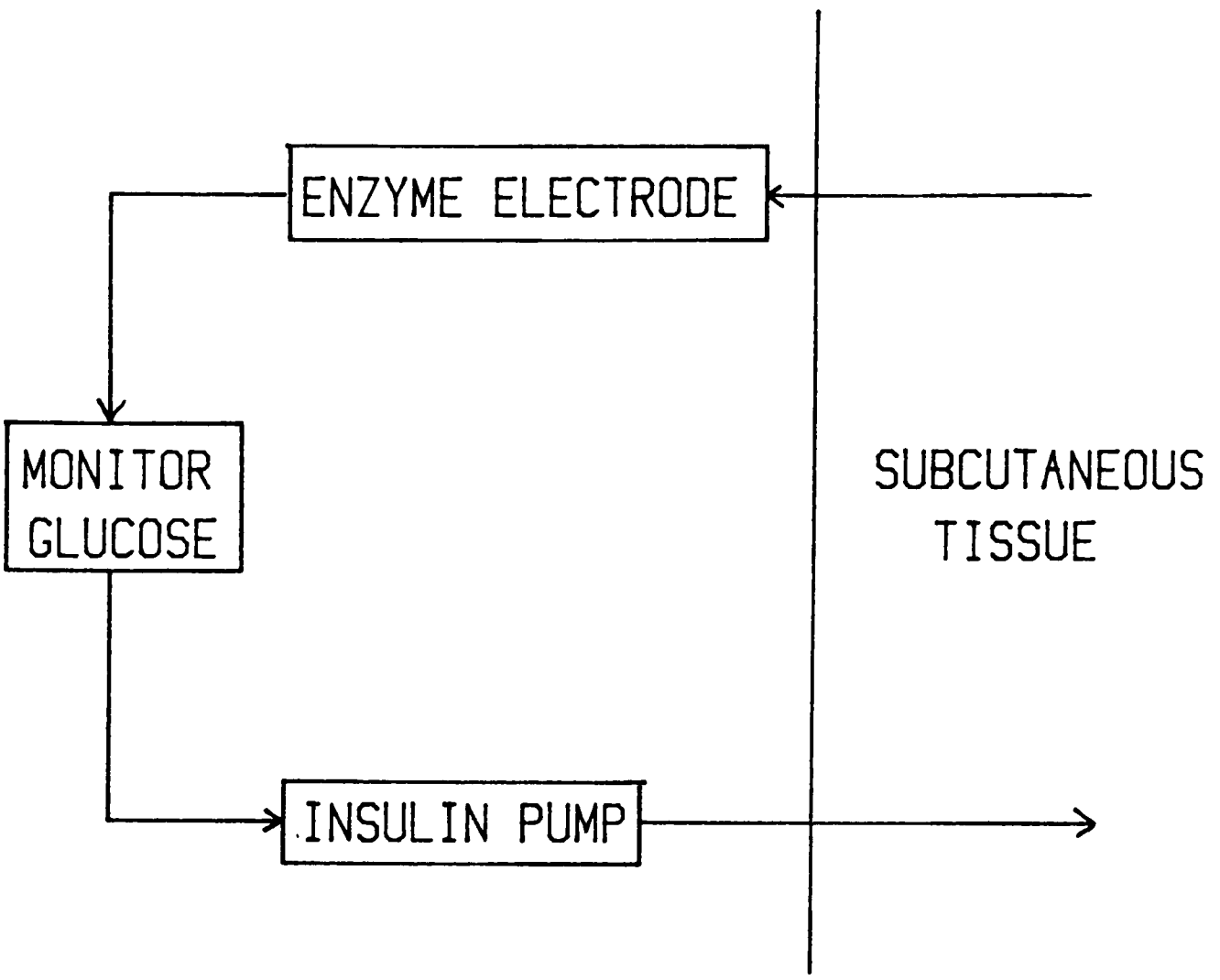

Figure 4.1 Schematic diagram of a closed loop artificial pancreas.

been adopted.

A number of spectrophotometric assays have been devised. The enzyme hexokinase (HK: EC 2.7.1.1) can be used to generate glucose-6-phosphate (G-6-P), eq 4.1, which is the substrate for glucose-6-phosphate dehydrogenase (G-6-PDH: EC 1.1.1.49), eq 4.2. Reduction of NAD^+ is followed at 340nm, from which the glucose concentration is calculated (14).

$$\text{ATP} + \text{glucose} \xrightarrow{\text{HK}} \text{ADP} + \text{G-6-P} \qquad [4.1]$$

$$\text{G-6-P} + \text{NAD}^+ \xrightarrow{\text{G-6-PDH}} \text{gluconolactone-6-P} + \text{NADH} + \text{H}^+ \qquad [4.2]$$

Altenatively, the NAD-linked enzyme glucose dehydrogenase (GDH: EC 1.1.1.118) can be used, to catalyses the following reaction, eq 4.3.

$$\text{glucose} + \text{NAD}^+ \xrightarrow{\text{GDH}} \text{gluconolactone} + \text{NADH} + \text{H}^+ \qquad [4.3]$$

As with the previous assay NADH production is monitored (15).

Glucose can also be assayed with glucose oxidase (GOD: EC 1.1.4.3), eq 4.4, coupled to peroxidase (POD: EC 1.11.1.7)(16). The latter, catalyses the transfer of oxygen from hydrogen peroxide to a chromogenic oxygen acceptor, eq 4.5.

$$\text{glucose} + \text{O}_2 \xrightarrow{\text{GOD}} \text{gluconolactone} + \text{H}_2\text{O}_2 \qquad [4.4]$$

$$\text{chromogenic acceptor} + H_2O_2 \xrightarrow{POD} \text{chromogen} + H_2O \qquad [4.5]$$

Chromophores that have been used include, o-toluidine (17), 3,3′-dimethoxybenzidine(18), 4-hydroxy-3-methoxyphenylacetic acid (19) and 2,6-dichlorobenzenone indophenol (20).

A disposable test strip based on this method, using N,N′-dimethyl(4,4′-diaminobiphenyl)hydrochloride as the chromophore, is commercially available from Miles Laboratories Ltd. A gradual colour change from yellow to purple corresponds to glucose concentrations in the range 0-14mM. Personal use of these test strips by diabetics gives a rough value of their whole-blood glucose level, from which their daily insulin requirement is estimated.

4.1.3 Enzyme electrodes for glucose analysis

The trend towards automation and simplification of glucose analysis, in addition to problems of sample turbidity when working with many biological fluids, has promoted interest in enzyme-linked electrochemical methods. The most common enzyme used is the fungal flavoprotein, glucose oxidase. The enzymes properties and specificity are shown in tables 4.1 and 4.2. Glucose oxidase catalyses the oxidation of β-D-glucose to D-δ-gluconolactone which, in aqueous solution, is rapidly hydrolysed to gluconic acid. Figure 4.2(a), shows the α- and β- anomers and the free aldehyde form of D-glucose. The oxidised and reduced forms of the prosthetic group of

Table 4.1 Properties of glucose oxidase

Source:	Aspergillus niger
RMM:	186 000
Co-factor:	2FAD
Co-substrate:	Oxygen
Optimum pH:	5.6
K_M glucose:	3.0mM

Table 4.2 Glucose oxidase substrate specificity

Substrate	Relative rate
β-D-glucose	100
2-deoxy-D-glucose	25
6-methyl-D-glucose	2
D-mannose	1
α-D-glucose	0.6

(a)

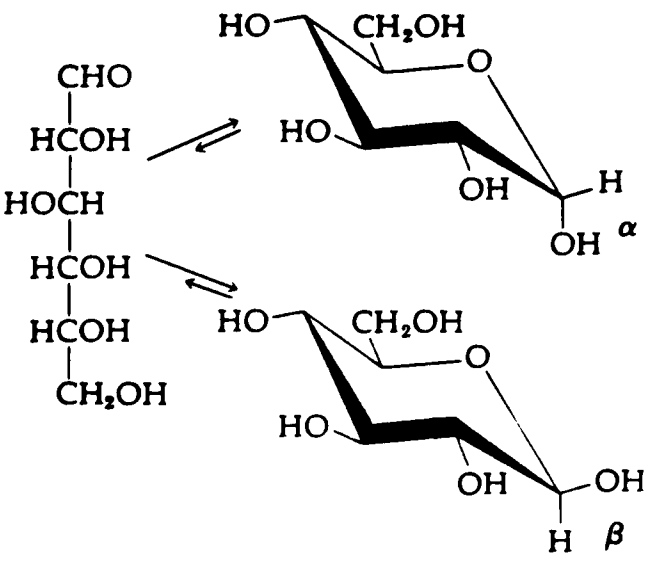

(b)

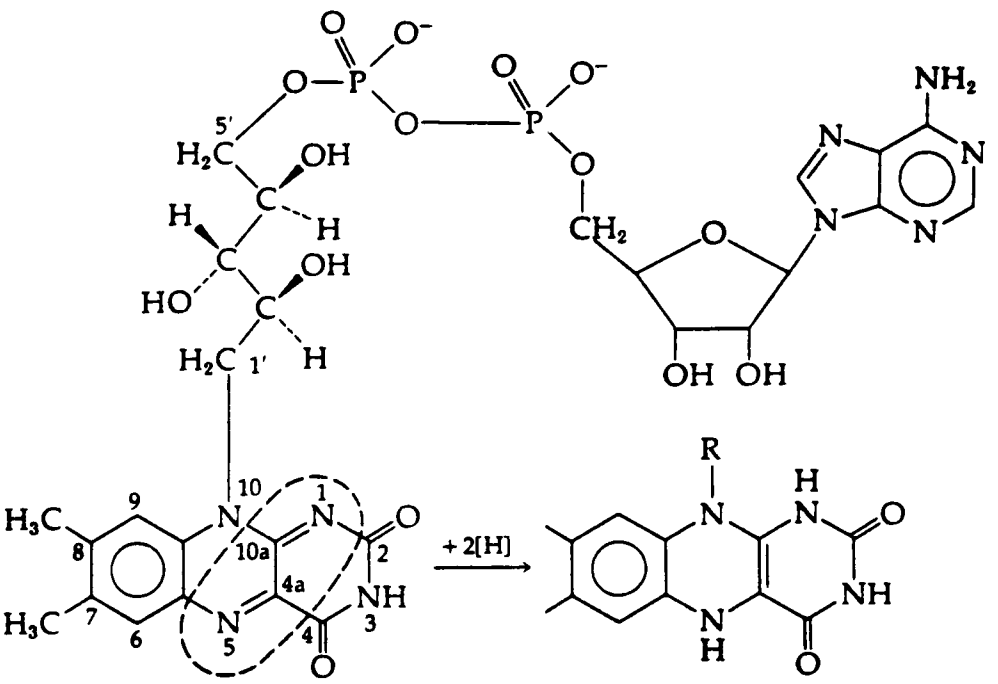

Figure 4.2 (a) Structures of the anomers of D-glucose, showing the α-, β- and free aldehyde forms. (b) Structure of the coenzyme of glucose oxidase, flavin adenine dinucleotide. The dotted line enclose the region that is altered upon reduction.

the enzyme, flavin adenine dinucleotide (FAD), are shown in figure 4.2(b). The natural electron acceptor for the reduced flavoprotein is molecular oxygen which is reduced to hydrogen peroxide, eq 4.4.

By using electrochemical methods, it is possible to deduce the glucose concentration indirectly from each of the other three reaction components: gluconic acid by a pH electrode; oxygen by electrochemical reduction; and hydrogen peroxide by electrochemical oxidation.

Clark (21) described the measurement of glucose using soluble glucose oxidase retained behind a membrane on a pH electrode. The method could not be widely adopted since it was found to be unsuitable for samples with variable buffer capacity.

In 1967, Updike (22), developed the first operational glucose electrode based on the amperometric measurement of the amount of oxygen depletion within a polyacrylamide gel containing glucose oxidase. It was necessary to operate this system in a dual electrode mode to compensate for non-enzymatic utilisation of oxygen e. g., its reaction with uric acid and ascorbic acid. Notin (23) reported an enzyme electrode in which glucose oxidase was immobilized on to a cellulose acetate membrane directly on the platinum tip of an oxygen electrode. The electrode was stable during three days of operation and gave a linear current response to glucose in the range 0.1-1mM.

Several glucose electrodes have been formulated which measure hydrogen peroxide production. Clark (24) devised an electrode in which H_2O_2 is measured amperometrically by oxidation at a platinum electrode poised at 700mV vs. SCE. The enzyme is entrapped on a polycarbonate membrane. A commercial desk-top analyser based on this electrode, is available from Yellow Springs Instruments Co. The instrument gives a linear current response to glucose in the range 0.1-3mM. The device is operated under thermostatic control at $37^{o}C$ and is reported to be insensitive to normal plasma concentrations of ascorbic acid, uric acid, reduced glutathione and cysteine (24,25). The instrument is designed to operate with plasma samples of 25µl which are pre-diluted into 1ml of air-saturated buffer.

The detection of glucose via hydrogen peroxide can also be achieved using a coupled reaction, eq 4.6.

$$2H^{+} + H_2O_2 + 2I^{-} \longrightarrow 2H_2O + I_2 \qquad [4.6]$$

The change in the iodide concentration can be measured potentiometrically with an iodide selective electrode (26) or amperometrically, by reduction of iodine (27,28).

A general problem associated with systems relying on the detection of hydrogen peroxide is the non-electrochemical decomposition, catalysed by impurities retained in the glucose oxidase preparation, the most common of which is the enzyme catalase

(CAT: EC 1.11.1.6) (29) which catalyses the following reaction, eq 4.7.

$$H_2O_2 \xrightarrow{CAT} H_2O + 1/_2O_2 \qquad [4.7]$$

Considering these various methods, there are a number of disadvantages in using an oxygen-dependent assay in biological samples. In the analysis of whole-blood from diabetics, the oxygen tension and consequently the electrode response can be affected by the oxyhemoglobin concentration (30). In addition, at low oxygen tensions, the enzymatic reaction may become oxygen limited. This results in a reduction of the upper limit of the linear response of the electrode. The general approach to solving these problems is to assay the sample as plasma pre-diluted into an oxygenated buffer. A corollary of this sample preparation, which requires centrifugation of the whole-blood, is that it restricts the use of the enzyme electrode to hospital analysers.

The potential problems associated with the use of an oxygen-mediated enzyme electrode are also apparent when considering application to continuous automatic in vivo monitoring of glucose. The subcutaneous tissue is the favoured site for implantation since it is used already for continuous insulin infusion (31) and avoids the risks of thrombosis and infection associated with intra-venous implantation. However, poor perfusion of the subcutaneous tissue, during diabetic ketoacidosis, often causes a fall in the tissue

oxygen tension (31). This is likely to adversely affect the performance of an implantable oxygen-mediated glucose enzyme electrode.

To circumvent these problems an alternative amperometric detection method, which is not dependent on oxygen as the mediator of electron transfer and does not require pre-preparation or dilution of the sample was sought. The aim was to develop an amperometric enzyme electrode suitable for *in vitro* testing of whole blood, which can then be adapted to an application *in vivo*.

4.1.4 Non-physiological electron acceptors for glucose oxidase

A number of non-physiological electron acceptors for glucose oxidase have been reported including hexacyanoferrate(111) (32) and a range of organic dyes, table 4.3, including, phenazine methosulphate, N,N,N′,N′-tetramethyl-4-phenylenediamine, benzoquinone, o-chloranil and 2,6-dichlorophenol indophenol (33). However, there are a number of reasons why these molecules are unsuitable for incorporation into a conventional enzyme electrode design. Firstly, high solubility in aqueous solution means that they are not readily entrapped within an enzyme electrode (unless attached directly to either the enzyme or the electrode). Secondly, many of the organic dyes have unsuitable properties including rapid autoxidation, cyto-toxicity, instablity in the reduced form and pH-dependent redox potentials. To be a viable alternative to oxygen,

Table 4.3 Electron acceptors for glucose oxidase

Acceptors	E^{o} pH-dependent	Soluble(aq)	Autoxidisable
Ferricyanide	x	✓	x
Phenazonium ions	✓	✓	✓
Phenylene diamines	x✓	✓	✓
Benzoquinones	✓	x	✓
Ferrocenes	x	x✓	x

a mediator was required that combined the well behaved electrochemistry of hexacyanoferrate with the variations available through structural modification of the organic dyes without the other disadvantages.

4.1.5 Ferrocenes

The unique structure and properties of ferrocene (bis η^5cyclopentadienyliron: $Fecp_2$) and its derivatives has resulted in a considerable amount of theoretical and experimental studies. First synthesised (34) in 1951, ferrocene was the earliest example of the now well-known metallocene compounds (35-37).

Whilst ferrocenes, table 4.4, had been found of limited value in spectrophotometric assays (37) as a result of their poor solubility in aqueous solution and low extinction coefficients, they appeared to be more suited to a bio-electrochemical system. Interest in ferrocenes resulted from: the wide range of redox potentials accessible through substitution of the cyclopentadienyl rings which can be functionalised (35); the electrochemically reversible one-electron redox properties, eq 4.8; the pH-independent redox potential and the slow autoxidation of the reduced form.

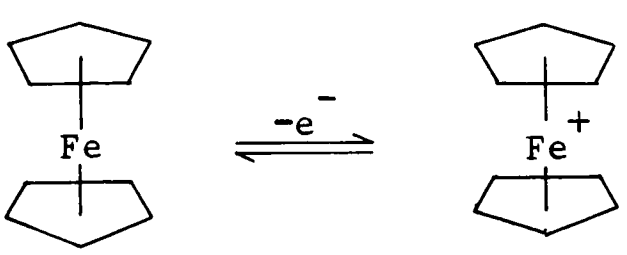

[4.8]

The E^{o} values of various ferrocenes in phosphate buffer at pH 7.0 , given in table 4.4 , span a range of potentials, E^{o} = 100 to 400mV vs SCE. The trend in E^{o} values is in agreement with that expected on the basis of substituent effects (38). In general electron-donating groups stabilize the positive charge and hence promote oxidation more so than electron withdrawing groups (39).

4.1.6 Ferrocene modified electrodes

Ferrocene-modified electrodes can be prepared by a number of different techniques. The simplest procedure is to dope hydrophobic derivatives e. g. ferrocene, vinylferrocene and 1,1′-dimethylferrocene on to a platinum or graphite surface by evaporation from a solution in an organic solvent (40). Alternatively, substituted derivatives can be covalently attached to hydroxyl functions on either carbon or platinum (41), eq 4.9.

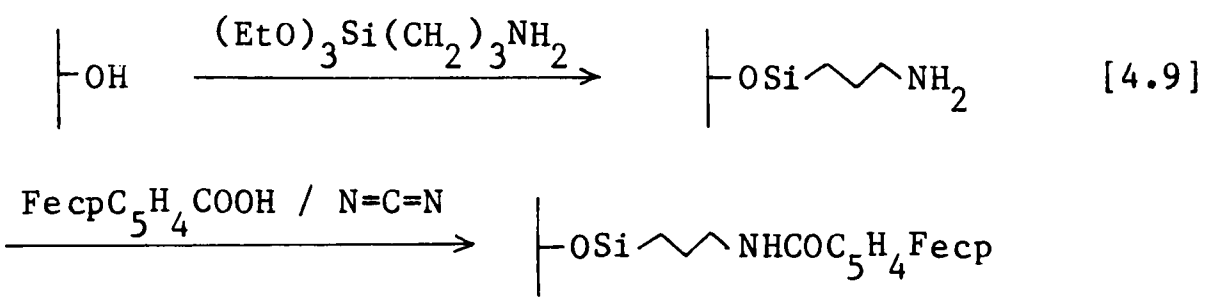

[4.9]

Electrode surfaces may also be coated with a functionalised polymer, polytyramine (41) for example, to which substituted ferrocenes are covalently attached, eq 4.10.

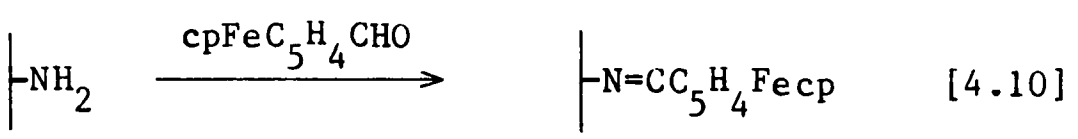

[4.10]

Table 4.4 Electrochemical and optical properties of ferrocenes

Ferrocene derivative	E^{o}(mV vs SCE)	Solubility	ε (cm^{-1} M^{-1})
1,1′-dimethyl	100	I,D	-
acetic acid	124	S	370
hydroxyethyl	161	S	-
ferrocene	165	I,D	335
1,1′bis(hydroxymethyl)	224	S	385
monocarboxylic acid	275	S	420
1,1′-dicarboxylic acid	285	S	-
chloro	345	I,D	-
methyl trimethylamino	400	S	-

S indicates water solubility; I,D means insoluble and detergent solubilised in 3% Tween-20.

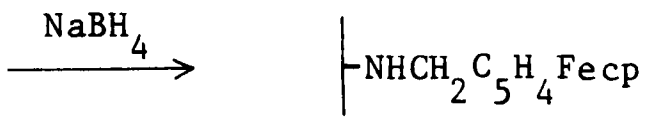

Alternatively, vinylferrocene can be polymerised to give poly(vinylferrocene), eq 4.11, which can be coated on to an electrode either by solvent evaporation or by electro-deposition (40).

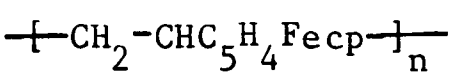

[4.11]

4.1.7 Outline of research

The initial priority was to investigate the propensity of ferrocenes in the oxidised, ferricinium ion form, to act as electron acceptors for glucose oxidase, by using D. C. cyclic voltammetry. Since the construction of an efficient enzyme electrode would depend on the effective retention of the redox mediator at the electrode surface, methods of achieving this whilst retaining catalytic activity with the enzyme were investigated. Once this had been achieved an amperometric enzyme electrode device was developed.

Experimental

4.2.1 Reagents

Glucose oxidase type 2, from Aspergillus niger mol wt 186 000, was supplied by Boehringer Mannheim with an activity of 274 IU mg^{-1}. The purity of glucose oxidase (as supplied) was investigated by fast protein liquid chromatography (FPLC). The enzyme at a concentration of 1.0 mg ml^{-1} in 25mM Tris-HCl pH 7.0 (buffer A) was loaded on to a Mono-Q analytical column (Pharmacia). The protein was eluted by a linear ionic strength gradient using buffer B (A + 1.0M NaCl). Glucose oxidase activity eluted as a single peak at an ionic strength equivalent to 35% buffer B, figure 4.3.

In electrochemical experiments, the concentration of glucose oxidase is expressed in terms of the amount of catalytically active flavin adenine dinucleotide (FAD). Active flavin was determined spectrophotometrically using a molar extinction coefficient of 1.31×10^{4} l mol^{-1} cm^{-1}, at 450nm (42). D-glucose (AnalaR) was from BDH; ferrocene and its derivatives, listed in table 4.5, were from Strem Chem. Co. The supporting electrolyte was 50mM K_2HPO_4 adjusted to the required pH with $HClO_4$. Glucose solutions were stored overnight to equilibrate the α- and β-anomers.

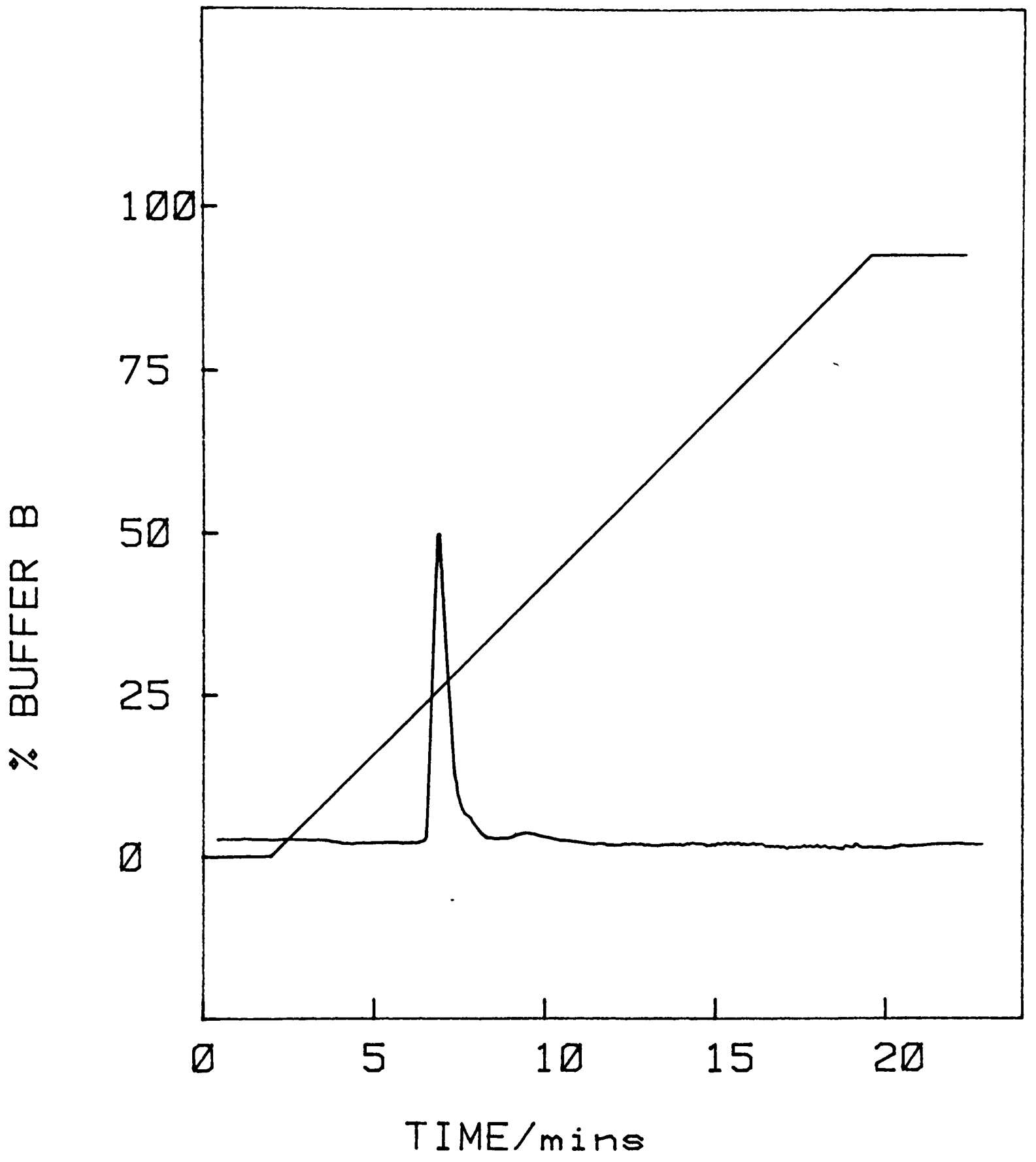

Figure 4.3 FPLC elution profile of glucose oxidase.

4.2.2 Ferrocene modified electrodes

Polyvinylferrocene (40) and polytyramine (41) were synthesised and deposited on to platinum and pyrolytic graphite electrodes according to literature methods.

4.2.3 Biological samples

Heparinised whole blood and plasma samples from human diabetics were supplied by the Metabolic Unit, Guy's Hospital, London. Plasma samples were analysed at Guy's hospital with a Yellow Springs Instruments, Ohio., glucose analyser. The pH of each plasma sample was measured. All samples were within the range pH 6.8-8.2.

4.2.4 Electrochemical experiments

D. C. cyclic voltammetry experiments were performed as described in section 3.2.2., using a 4mm pyrolytic graphite disc working electrode.

Potentiostatically-controlled steady-state current measurements were made using three different cells of similar design incorporating separate compartments for the counter and reference electrodes. Cells had a working volume of 1, 5 and 100ml, the latter used for experiments described in 4.3.15 was able to accomodate up to seven enzyme electrodes. The working compartment was stirred

during operation with a magnetic stirrer bar. Current-time curves were recorded with a Bryans Y-t BS-271 recorder. The temperature of the electrochemical cells during experiments was controlled to within $\mp 0.5^{o}C$.

4.2.5 First prototype enzyme electrode

Graphite foil 1mm thick, supplied by Union Carbide, was the base sensor. Electrodes were constructed by cutting the graphite into 4mm diameter discs and sealing into glass rods with epoxy resin, figure 4.4(a). The electrodes were then heated at $200^{o}C$ in air for 40 hours and allowed to cool. Then 15µl of 1,1'dimethylferrocene (0.1M in toluene) was deposited on to the surface of the electrode and air-dried. Covalent attachment of the glucose oxidase to the oxidised graphite surface was achieved by a method similar to that described by Bourdillon (43). The electrodes were placed in 1ml of a solution of water-soluble 1-cyclohexyl-3-(2-morpholino ethyl)carbodiimide metho-p-toluene sulphonate from Sigma Chem. Co. (0.15M in 0.1M acetate, pH 4.5), for 80 mins at $20^{o}C$, washed with water and then placed in a stirred solution of acetate buffer (0.1M, pH 9.5) containing glucose oxidase (12.5 mg ml^{-1}) for 90 mins at $20^{o}C$. After washing, the electrodes were covered with a polycarbonate membrane (Nucleopore, 0.03µm) and stored frozen in buffer at $-20^{o}C$.

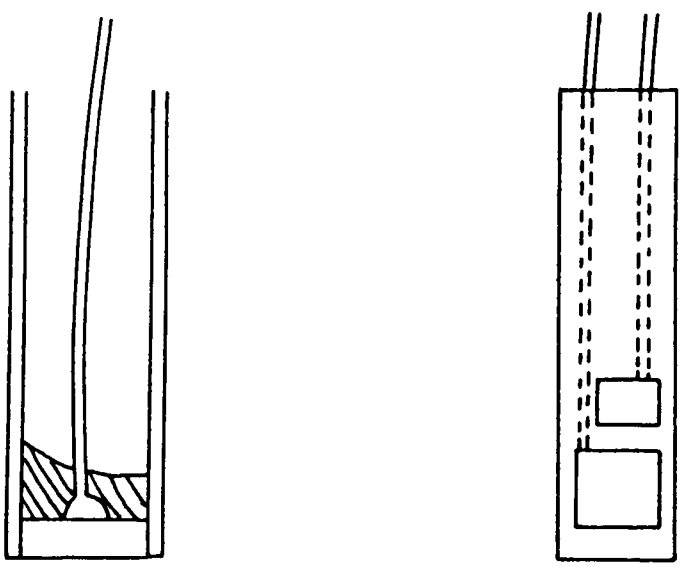

a b

Figure 4.4 (a) First proto-type glucose enzyme electrode, showing a 4mm diameter graphite foil disc secured into a glass tube with epoxy resin. A connecting wire is attached to the reverse side of the electrode by silver araldite. (b) Second proto-type glucose enzyme electrode. A 4mm square graphite foil electrode and a 3mm square silver electrode are attached to a rectangular piece of circuit board (1cm x 5cm) with external connectors on the reverse side.

4.2.6 Second prototype enzyme electrode

The preparation of the second prototype glucose enzyme electrode was the same as the first with the exception that a silver reference electrode coated with silver chloride was included on to the test strip, figure 4.4(b). Test strips were operated at 205mV vs Ag/AgCl (equivalent to 160mV vs SCE) with a portable mini-potentiostat, designed and supplied by Genetics International, Inc.

Results and discussion

4.3.1 Ferricinium ion as an oxidant for glucose oxidase

A number of ferrocene derivatives, table 4.5, with a range of redox potentials, -50 to 400mV vs SCE, were investigated by D. C. cyclic voltammetry, as possible oxidants for glucose oxidase. Under the experimental conditions used, and over the complete range of potential scan (-200 to 600mV) and range of potential scan rates (ν =1-100mVs^{-1}), ferrocene and its derivatives gave voltammograms (of the type shown in figure 2.2) consistent with a reversible one-electron redox agent at a pyrolytic graphite electrode, ΔEp~60mV at 298K; $i_p/\nu^{1/2}$=constant, $D_o \sim 3\times10^{-6}$ cm^2 s^{-1}. Under the same conditions neither glucose nor glucose oxidase (GOD) exhibited any observable electrochemistry.

Figure 4.5(a), shows a voltammogram of ferrocene monocarboxylic acid ($Fecp_2R$) in the presence of glucose alone. Upon addition of glucose oxidase to the solution a striking change in the voltammogram occurs, figure 4.5(b). No peak is observed and a large current flows at oxidising potentials. This behaviour is particularly apparent at the slower scan rates, figure 4.6, and is indicative of the catalytic regeneration ferrocene from the ferricinium ion by reduced glucose oxidase. The diagnostic plot, figure 4.7 of $i_{pa}/\nu^{1/2}$ ($=i_k/i_d$) versus $\log_{10}\nu$, which is similar to that shown in figure 2.5(e) indicates that the experimental results

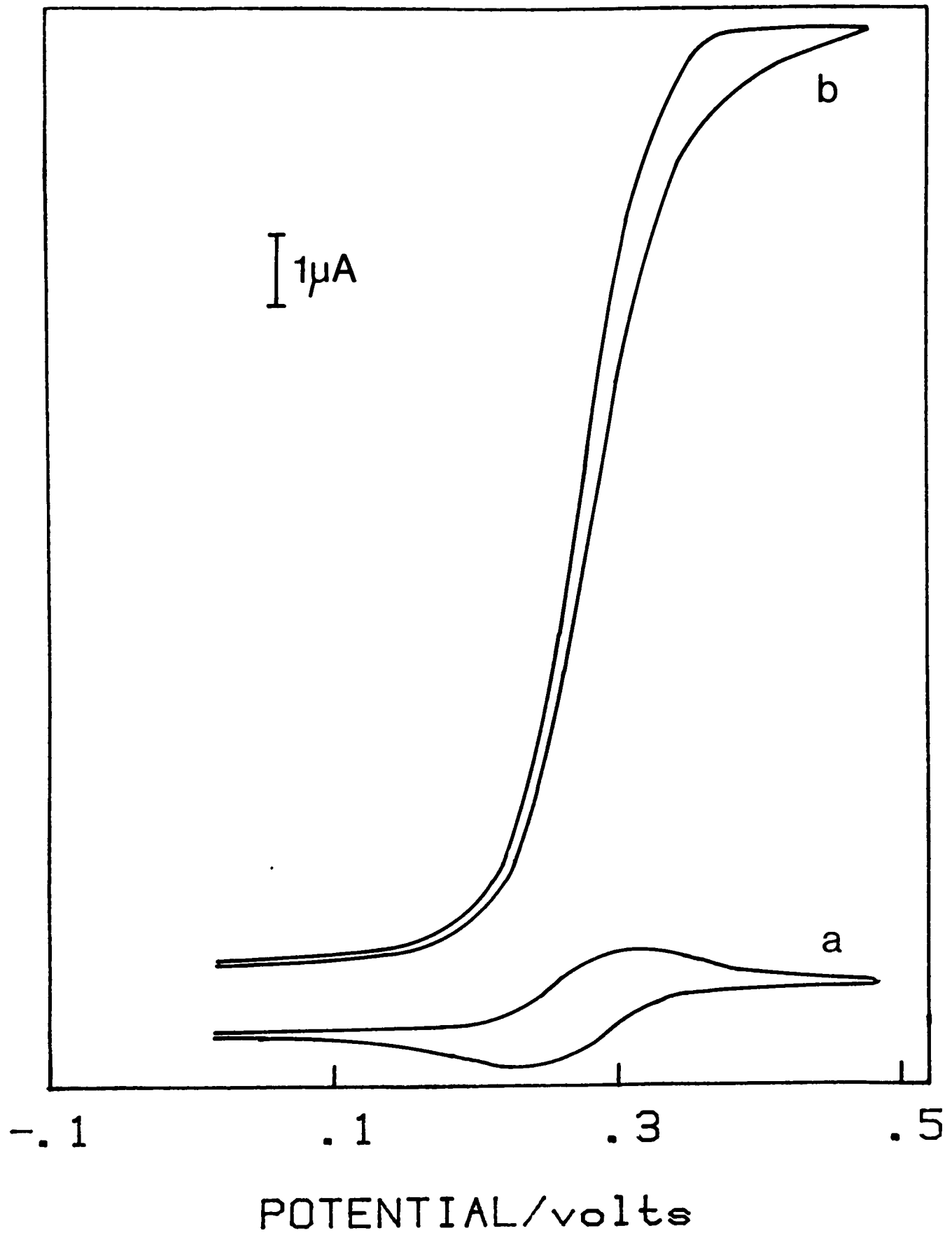

Figure 4.5 (a) D. C. cyclic voltammogram of ferrocene monocarboxylic acid 200μM in 50mM phosphate-perchlorate pH 7.0 at 20°C, in the presence of D-glucose 50mM at a scan rate of $1mVs^{-1}$. (b) as for (a), but with the addition of glucose oxidase 10.9μM.

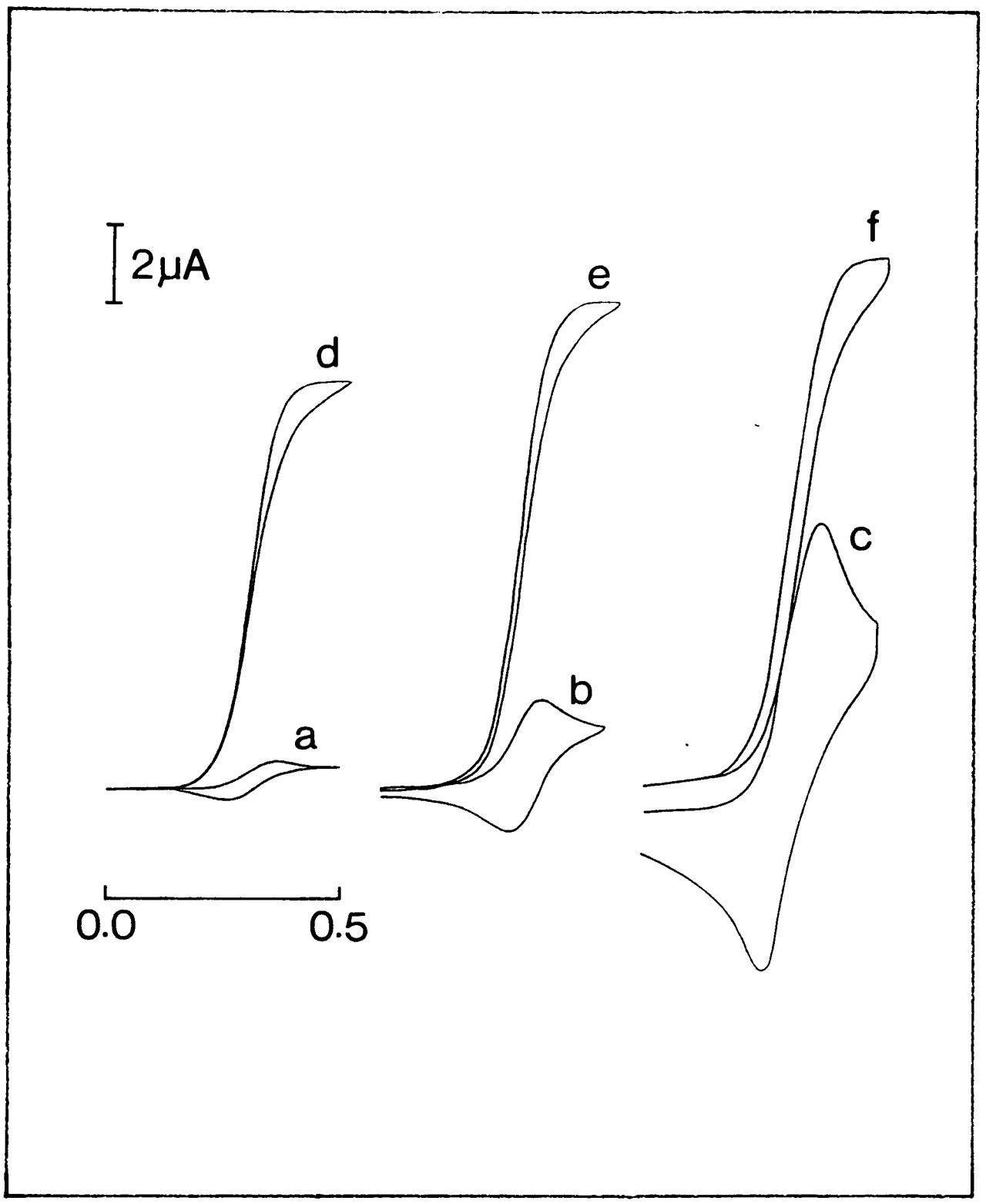

Figure 4.6 (a)-(c) D. C. cyclic voltammograms of ferrocene monocarboxylic acid with condition described in figure 4.5(a), at scan rates of 1, 10 and 100mVs^{-1}, respectively. (d)-(f) as for (a)-(c), but with the addition of glucose oxidase 10.9μM.

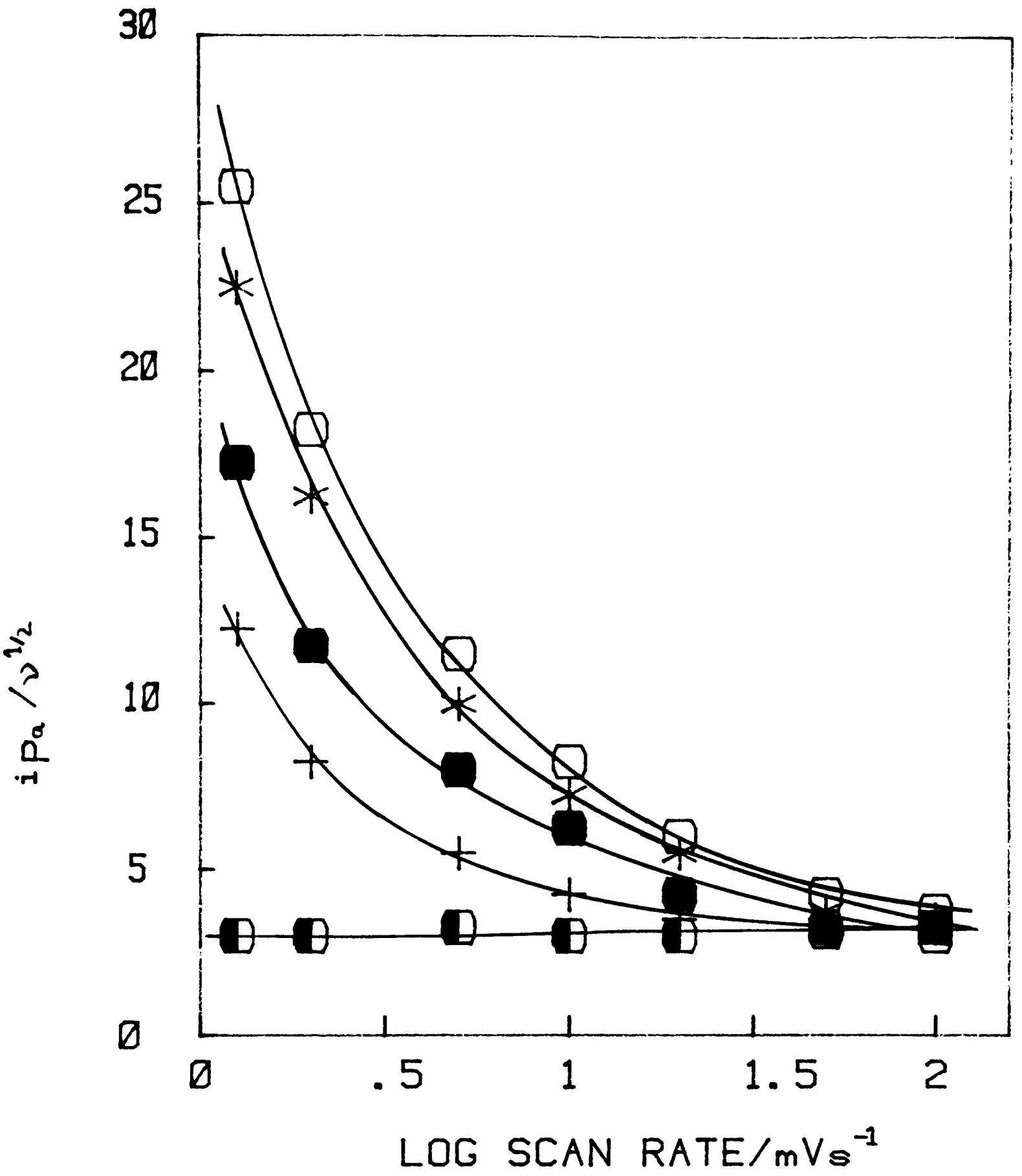

Figure 4.7 Diagnostic plots of the peak current function $i_{pa}/\nu^{1/2}$ at glucose oxidase concentrations, ◐ zero; + 10.9μM; ● 20.64μM; * 29.3μM; O 37.2μM. Other conditions as for figure 4.5(a).

conform to the theoretical model for a catalytically coupled reaction, eq 4.11.

$$O + Z \longrightarrow R;\ R - e^- \rightleftharpoons O. \qquad [4.11]$$

The following scheme describes the reaction sequence, eq 4.12-4.14.

$$\text{glucose} + GOD_{(ox)} \longrightarrow \text{gluconolactone} + GOD_{(red)} \qquad [4.12]$$

$$GOD_{(red)} + 2Fecp_2R^+ \longrightarrow GOD_{(ox)} + 2Fecp_2R + 2H^+ \qquad [4.13]$$

$$2Fecp_2R \rightleftharpoons 2Fecp_2R^+ + 2e^- \qquad [4.14]$$

The rate of reaction between the reduced form of the enzyme and the oxidised ferrocene, eq 4.13, can be derived from an analysis of the cyclic voltammograms, section 2.1.5, provided that: the heterogeneous electron transfer reaction, eq 4.14, is fast (diffusion-controlled) compared to the rate of the homogeneous reaction between ferricinium ion and glucose oxidase, and that there is a sufficient excess of substrate to ensure that the enzyme is essentially fully reduced, eq 4.12.

To obtain quantitative kinetic information, the data were analysed making use of the working curve, figure 2.6, which equates the experimentally derived parameter, i_k/i_d (the ratio of the kinetic to diffusion-controlled current), to the kinetic parameter

$(k_f/a)^{1/2}$. The data are re-plotted for a series of glucose oxidase concentrations as k_f/a against $1/\nu$ (ν=1-20mVs^{-1}) figure 4.8, which is linear under pseudo-first order conditions.

A sample tabulation for one glucose oxidase concentration is presented in table 4.5 to show more clearly the way the data are processed. Table 4.5(a) shows values for the anodic peak current under conditions described in figure 4.5(a). The effect of added enzyme as in figure 4.5(b), is presented in table 4.5(b). The value of i_d is the mean value of $i_{pa}/\nu^{1/2}$ in the absence of the enzyme.

From the slope of each curve in figure 4.8, which equals $k_f nF/RT$, a scan-rate independent pseudo-first order rate constant is obtained for each glucose oxidase concentration. Figure 4.9, plots the pseudo-first order rate constant as a function of glucose oxidase concentration. From the slope, $k=k_f/[GOD]$, the second order homogeneous rate constant for the reaction between ferricinium monocarboxylic acid and glucose oxidase, eq 4.13, was obtained $k=2.01\times10^5$ l mol^{-1} s^{-1} (pH 7.0, 20^{o}C).

Kinetic data obtained using this analysis, presented in table 4.6, show that most ferrocene derivates investigated act as rapid oxidants for the enzyme glucose oxidase. These rates are lower than that for the reaction between reduced glucose oxidase and its natural redox partner, dioxygen. Using a stopped-flow method a value for this reaction was obtained, $k=1.5\times10^6$ l mol^{-1} s^{-1}, (pH 7.0,

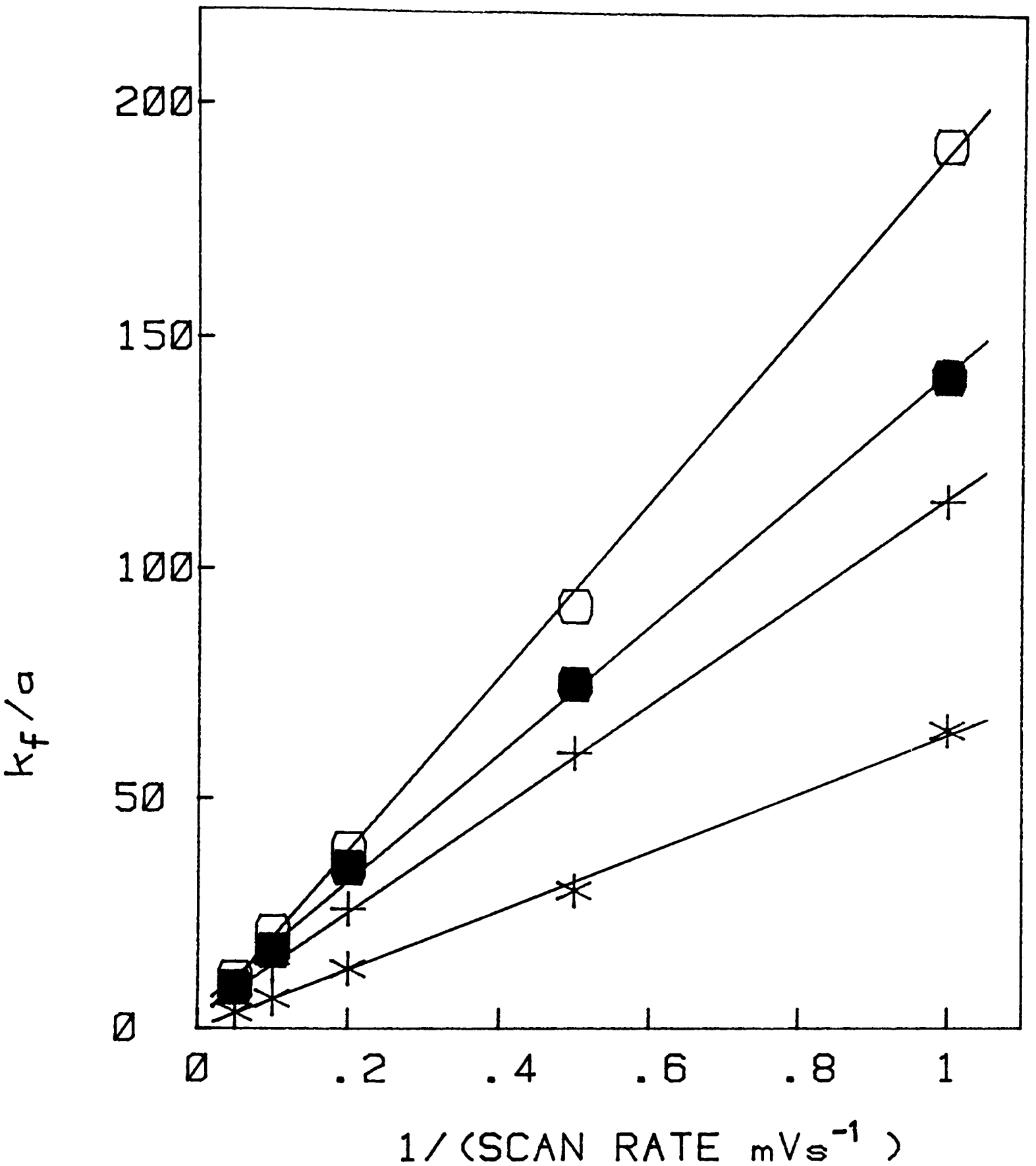

Figure 4.8 Plot of kinetic parameter k_f/a as a function of $1/\nu$ at glucose oxidase concentrations, * 10.9μM; + 20.64μM; ● 29.3μM; o 37.2μM.

Table 4.5 Derivation of kinetic data

ν	$\nu^{1/2}$	$i_p a$	$i_p/\nu^{1/2}$	$\log \nu$	i_k/i_d	$(k_f/a)^{1/2}$	k_f/a	$1/\nu$
(a) 200μM ferrocene monocarboxylic acid plus 50mM glucose.								
1	1.00	1.0	1.0		0.1			
2	1.41	1.2	0.85		0.3			
5	2.24	2.2	0.98		0.7			
10	3.16	2.8	0.89		1.0			
20	4.47	4.4	0.98		1.3			
50	7.07	6.6	0.93		1.7			
100	10.00	9.7	0.97		2.0			
(b) as for (a) but with the addition of 20.68μM glucose oxidase.								
1		19.4	19.40		23.15	10.85	117.7	1.00
2		19.7	14.00		16.70	7.80	60.8	0.50
5		20.8	9.28		11.07	5.17	26.7	0.20
10		21.9	6.93		8.27	3.85	14.8	0.10
20		22.6	5.06		6.03	2.80	7.8	0.05
50		23.2	3.28		3.91	1.79	3.2	0.02
100		23.6	2.36		2.82	1.27	1.6	0.01

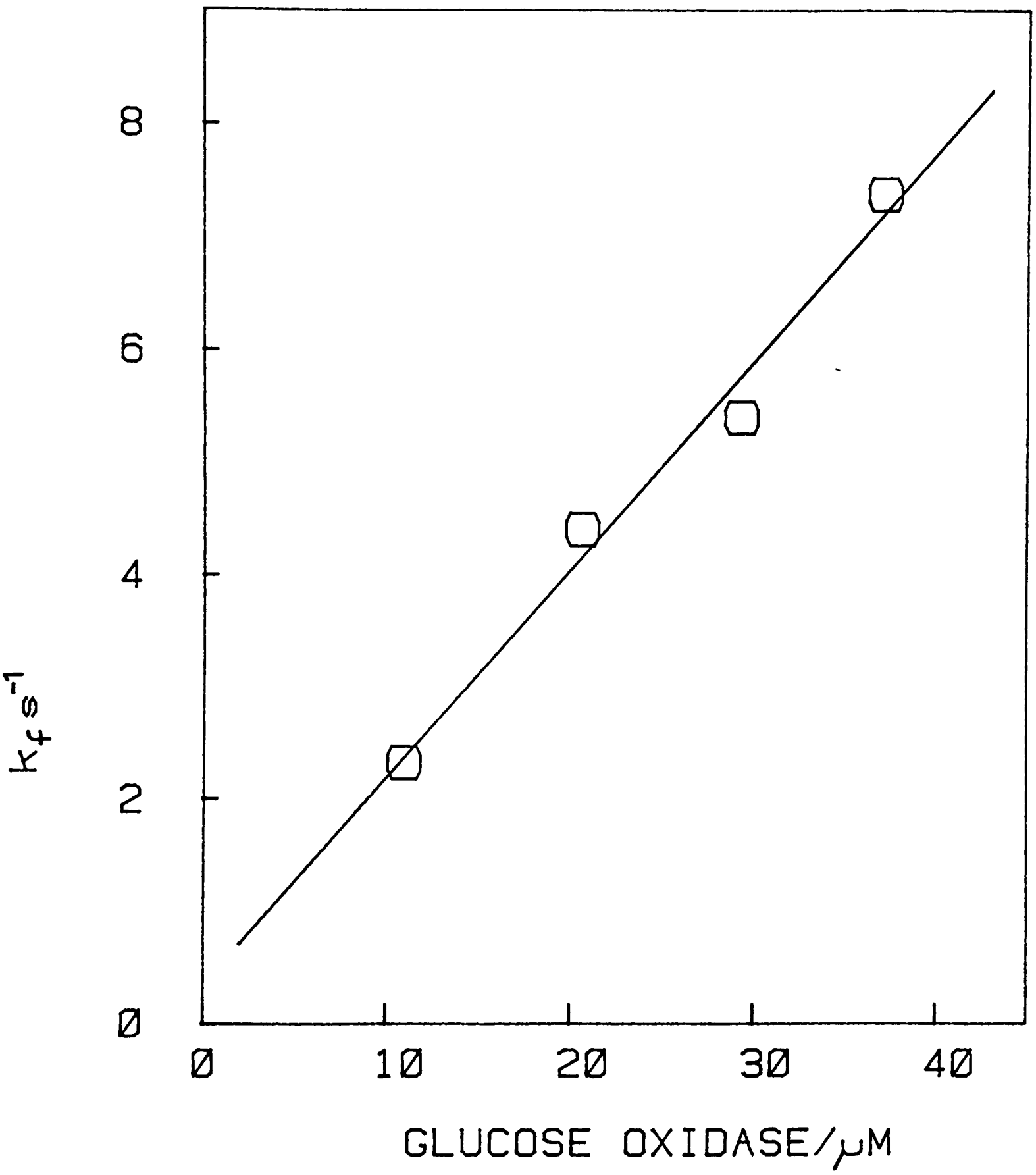

Figure 4.9 Pseudo-first order rate constants plotted as a function of glucose oxidase concentration.

Table 4.6 Rates of glucose oxidase oxidation

Ferrocene derivative	E^{o} mV vs SCE	$k_s \times 10^{-5}$ l mol^{-1} s^{-1}
decamethyl	-50	-
1,1′-dimethyl	100	0.77
ferrocene	165	0.26
bis(indenyl)	220	-
vinyl	250	0.30
monocarboxylic acid	275	2.01
1,1′-dicarboxylic acid	285	0.26
methyl trimethylamino	400	5.25

All rates determined at pH 7.0 and 20^{o}C.

25°C) (44).

4.3.2 Effect of pH on the kinetics

Glucose oxidase, with oxygen as the electron acceptor, has optimum activity at pH 5.6, whereas with non-physiological acceptors, a broad maximum around pH 7.5 is observed (33). The effect of pH on the electrochemically determined second-order rate constants for the ferrocene derivatives was investigated over the range pH 6.0-9.0. Figure 4.10 shows values of k for the reaction of glucose oxidase with ferricinium monocarboxylic acid, plotted versus pH. All of the ferrocenes shown in table 4.5, which act as oxidants for glucose oxidase, exhibit rate constants which are essentially independent of pH. These results were important in relation to the development of a glucose enzyme electrode, since it indicated that its performance was likely to be independent of pH changes over the physiologically relevant range.

In plasma, it was found that variations in pH occur within the limits pH 6.8-8.2, section 4.2.3. This probably results from either the addition of an anti-coagulating agent, usually heparin, which acts by binding calcium ions thus liberating protons, or through the loss of dissolved carbon dioxide (31).

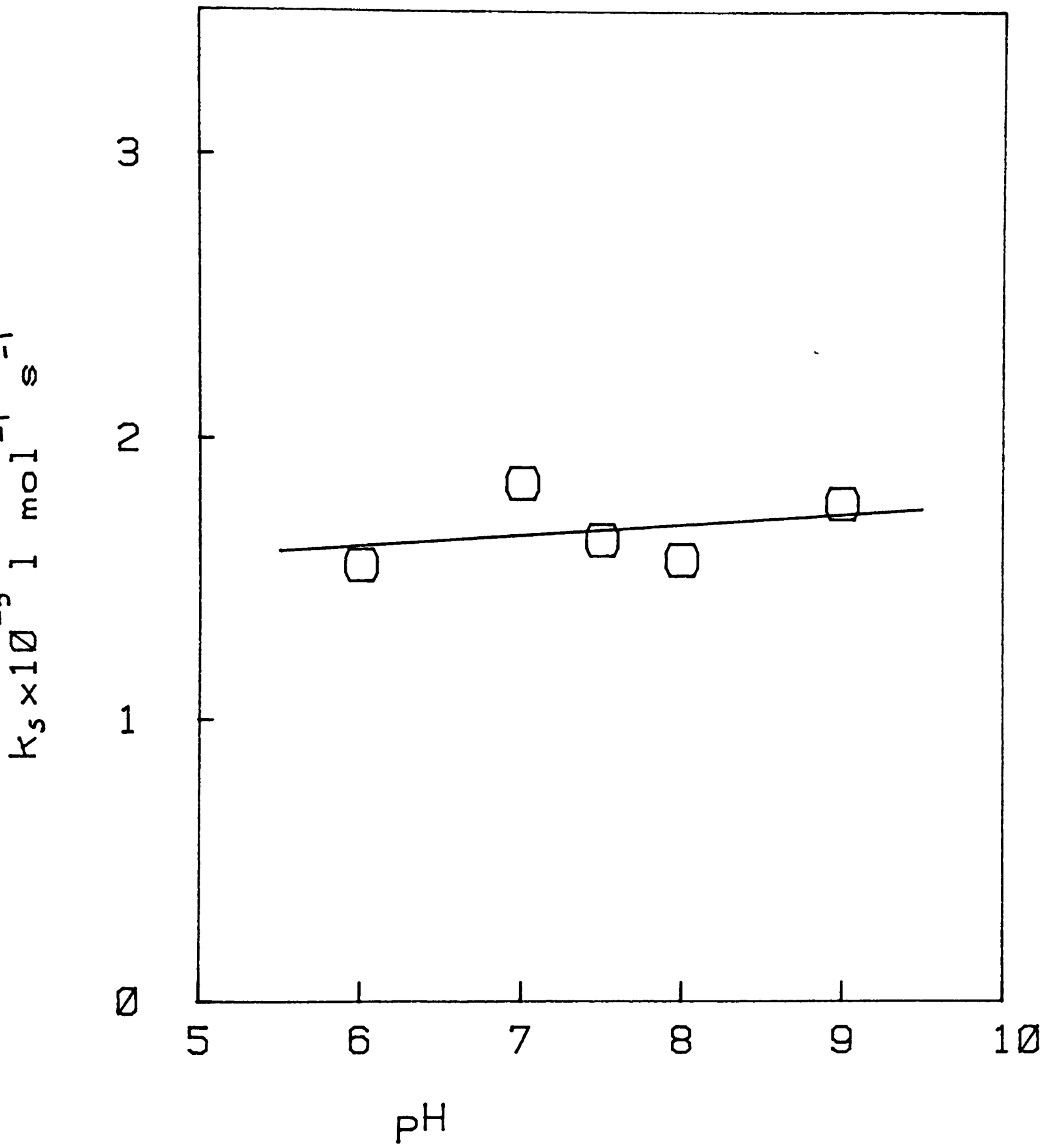

Figure 4.10 Effect of pH on the second order rate constant for the reaction between glucose oxidase and ferrocene monocarboxylic acid, at 20°C.

4.3.3 Effect of temperature on the kinetics

To determine the temperature dependence of the reaction between ferricinium ion and reduced glucose oxidase, the variation in the catalytic current, measured by cyclic voltammetry, was recorded in the range 5-50^{o}C. The temperature range was limited for two reasons: firstly thermal inactivation of the enzyme occurs above 50^{o}C (41); in addition the saturated calomel reference electrode is reliable only in the range -10^{o} to 60^{o}C. Since the diffusion coefficient of the mediator is dependent upon temperature, a correction was made in the calculation of the rate constant (45). Figure 4.11 shows a plot of $\log_e k$ versus 1/T(K). The slope of the plot is unchanged, indicating that the activation energy for the reaction is unaltered over the temperature range investigated. From the Arrhenius expression, $k=A\exp(-E_a/RT)$ an activation energy was calculated, E_a = 50 KJ mol^{-1}.

4.3.4 Ferrocene-modified electrodes

Most of the ferrocenes derivatives shown in table 4.6, lead to the effective electrochemical oxidation of glucose via glucose oxidase. However, in designing a practical enzyme electrode, other criteria were also important. The major problem was to confine the mediator within the enzyme layer, as shown in figure 1.1. Various methods of preparing a ferrocene modified electrodes were investigated and the diagnostic technique of cyclic voltammetry used

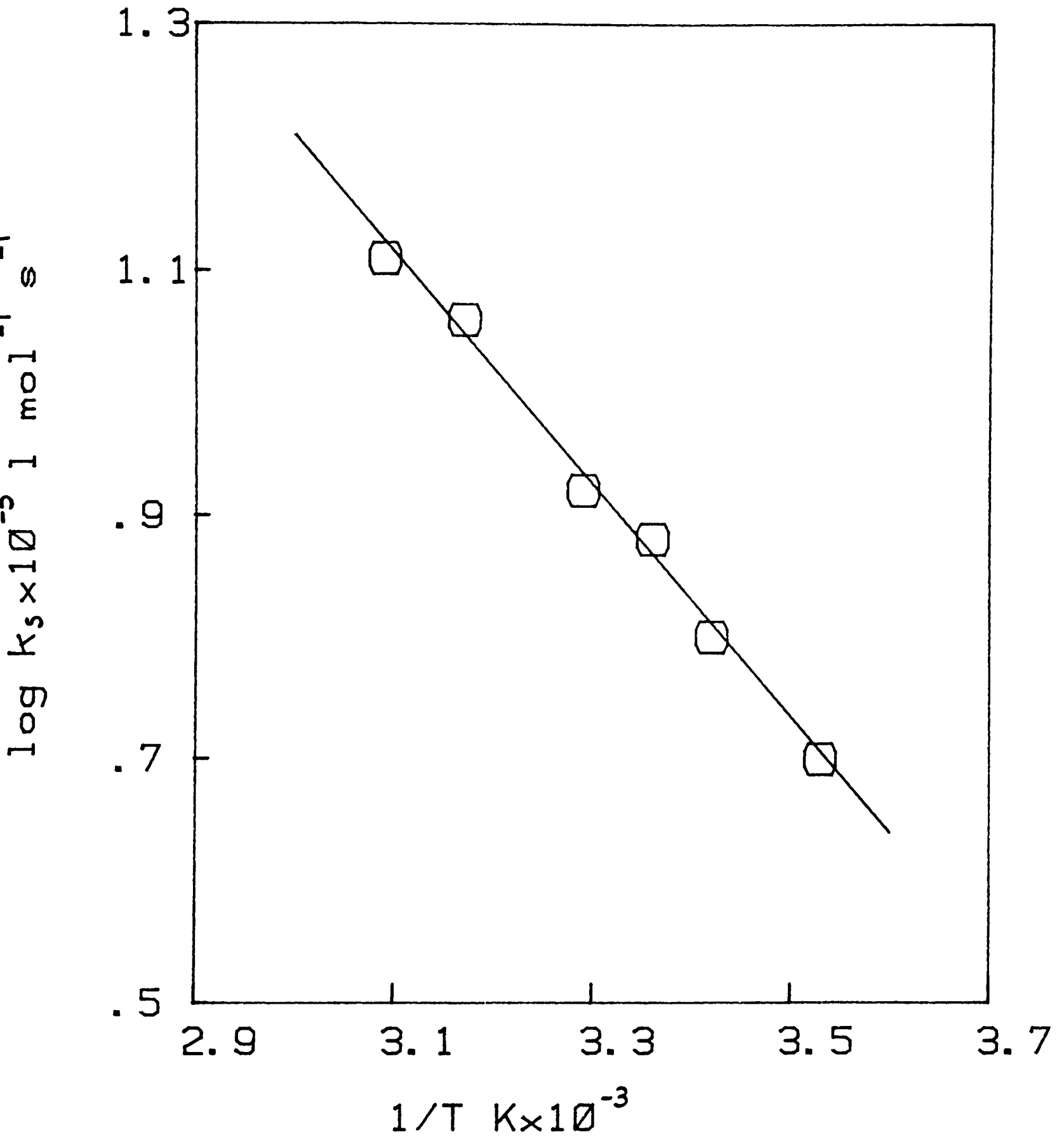

Figure 4.11 Arrhenius plot, showing the effect of temperature upon the second order rate constant for the reaction between glucose oxidase and ferrocene monocarboxylic acid. Conditions as for figure 4.5(b).

as a probe for cataltytic activity with glucose oxidase.

The simplest approach was to dope ferrocenes, with low solubility in aqueous solution, directly on to the electrode surface. 1,1′-Dimethylferrocene was doped on to a pyrolytic graphite electrode from a solution in toluene. Once the solvent had evaporated the electrode was placed into aqueous buffer and after continuous scanning between -200 and 400mV for ca. 100 cycles, a stable voltammogram was obtained. Integration of the faradaic current indicated a surface coverage of ca. $5x10^{-9}$ mol cm^{-2}(geometric area) which is of the order of a monolayer (46). Figure 4.12(a), shows a voltammogram of the 1,1′-dimethylferrocene doped electrode in the presence of glucose. Upon addition of glucose oxidase to the solution, figure 4.12(b), a characteristic catalytic current at oxidising potentials was observed. Similiar results to those shown in figure 4.12, were also obtained with ferrocene and vinylferrocene doped electrodes.

Polyvinylferrocene (PVF) synthesised from vinylferrocene, eq 4.11, was coated (by poising the electrode at 600mV vs SCE) on to a pyrolytic graphite disc electrode from a solution in acetonitrile containing t-butylammonium perchlorate as the electrolyte (40). The electrochemistry of PVF coated electrodes were examined by cyclic voltammetry and found to be consistent with reversible electron transfer to an immobilised species, i_p/ν =constant; $\Delta E_p \sim 0$mV; E^o= 450mV vs. SCE. This was consistent with data obtained previously for

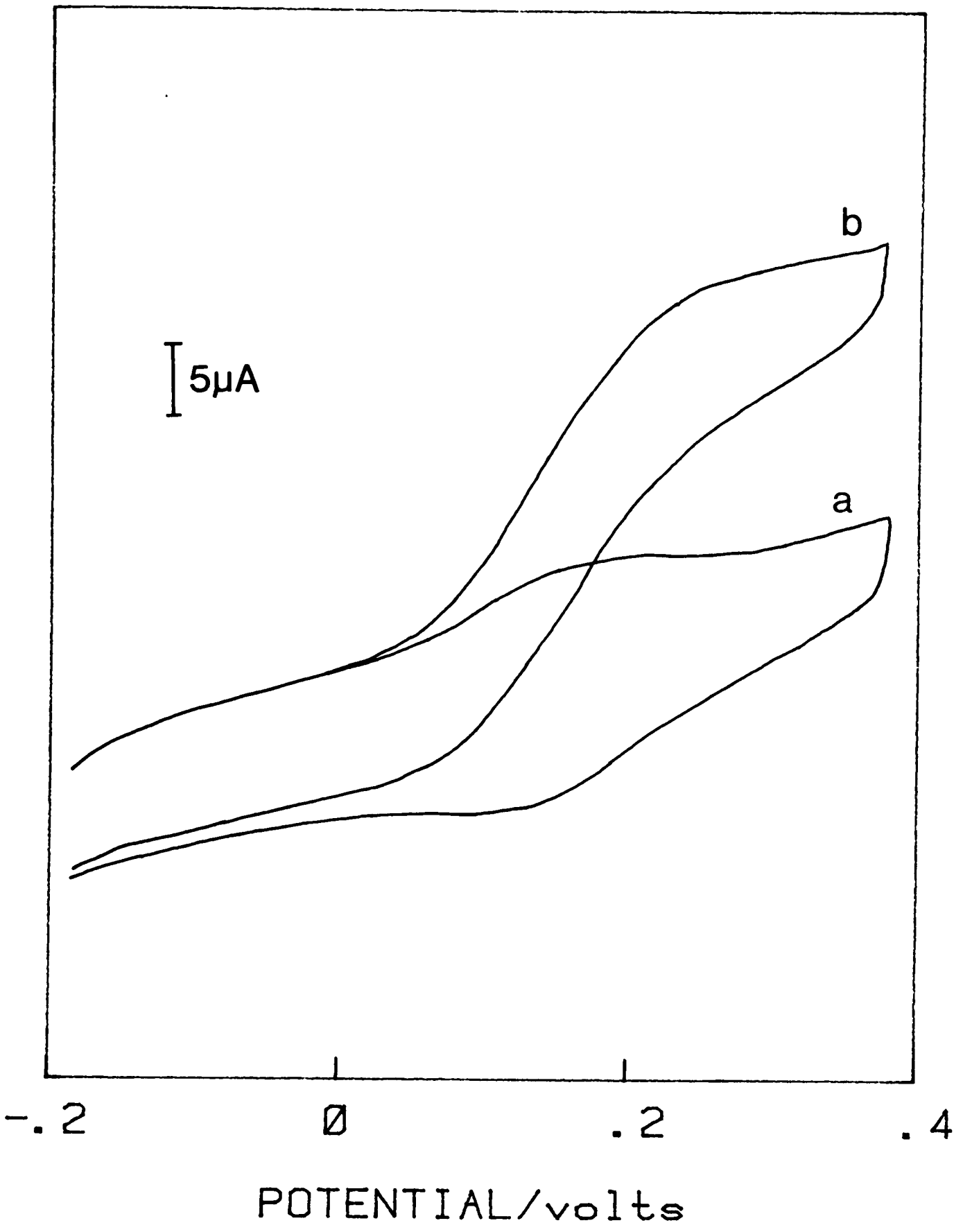

Figure 4.12 (a) D. C. cyclic voltammogram of 1,1′-dimethylferrocene doped on to a 4mm diameter pyrolytic graphite electrode at pH 7.0 and 20°C in the presence of 50mM glucose and at a scan rate of $10mVs^{-1}$. (b) as for (a), but with the addition of 20μM glucose oxidase to the solution.

polymers of molecular weight ca. 16 000 (40). Similar results were obtained in aqueous solution (phosphate-perchlorate pH 7.0). However, voltammograms of PVF were not changed discernibly upon addition of glucose and glucose oxidase. The lack of a catalytic current at oxidizing potentials, indicated that unlike the monomeric form, polyvinylferrocene did not couple to glucose oxidase. The same result was found when PVF was coated on to a pyrolytic graphite electrode from a solution in chloroform (40).

A ferrocene-modified polytyramine-coated pyrolytic graphite electrode, eq 4.10, prepared according to the method of Dubois (41), also proved to be catalytically inactive towards glucose oxidase.

Lack of catalytic behaviour of the enzyme with these polymer modified electrodes may be interpreted in terms of steric hinderence, where the prosthetic group of the enzyme is prevented from approaching the modified electrode surface in such a way as to enable a significant rate of electron transfer. These experiments led to the conclusion that doping a monomeric ferrocene on to an electrode provided the best method of confinement or immobilisation, whilst maintaining catalytic activity. With this method, the greater solubility of the ferricinium ion probably allows diffusion away from the electrode to the enzyme, thus facilitating efficient electron transfer.

4.3.5 Factors in designing the glucose enzyme electrode

A number of criteria were considered to be important in designing a practical prototype glucose enzyme electrode. With respect to the mediator, 1,1′-dimethylferrocene doped on to the electrode was preferred for three reasons: its stability at physiological pH; its higher rate of reaction with the enzyme; its low redox potential. This latter point is particularly important when considering possible interference from electroactive substances present in biological samples, section 4.3.14. With respect to the base sensor, in addition to its ability to adsorb 1,1′-dimethylferrocene, it should possess functional groups suitable for covalent attachment of the enzyme. This favoured the use of an oxidised graphite material. Papyex foil, made from exfoliated graphite compressed into a flexible paper ca. 1mm thick, had the best properties and possesses a sufficient surface concentration of carboxyl functions to allow glucose oxidase to be immobilized using a carbodiimide coupling method (43) as in eq. 1.2.

4.3.6 First prototype glucose enzyme electrode

The method used to construct a prototype glucose enzyme electrode is described in section 4.2.5, and shown schematically in figure 4.13. The design of the base sensor is show in figure 4.4(a).

4.3.7 Calibration and range

Figure 4.14 shows the dependence of the steady-state current on the applied potential at the enzyme electrode, in the presence and absence of glucose. Clearly, a current flows only when the electrode is poised sufficiently positive to generate the ferricinium ion. Since a limiting current occurred at potentials more positive than ca. 160mV, this potential was chosen to measure glucose dependent calibration curves for the electrodes. A typical steady-state current calibration curve, determined on gravimetrically prepared buffered glucose solutions (saturated with argon), is shown in figure 4.15. The background current at the electrode in the absence of glucose was measured, i_o=1.0μA, and subtracted from the data in figure 4.15. Electrodes gave a linear current response in the range 1-30mM glucose and finally saturated at approximately 70mM glucose.

4.3.8 Response time and flow dependence

In the linear region of the calibration curve, electrodes showed a rapid response reaching 90% of the final steady-state

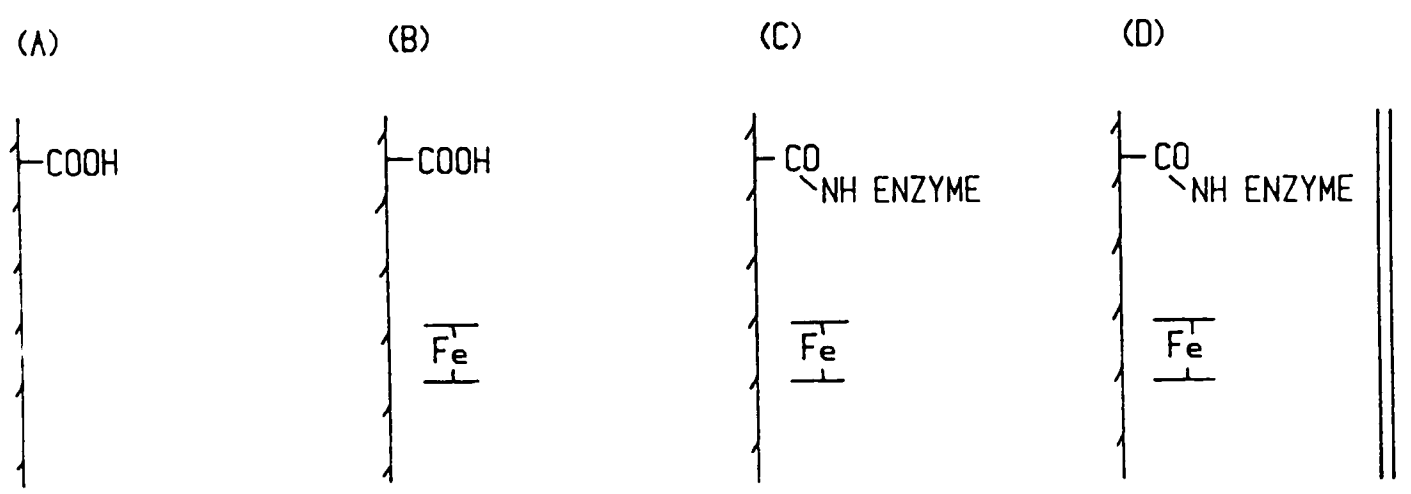

Figure 4.13 Schematic representation of the method of preparation of the proto-type glucose enzyme electrode. The graphite foil is heated to 200^{o}C for a period of 40h (A). The electrode is then doped with 1,1′-dimethylferrocene (B). Glucose oxidase is then attached to the electrode via 1-cyclohexyl-3-(2-morpholine ethyl)carbodiimide metho-4-toluene sulphonate (C). Finally, the electrode is covered with a polycarbonate membrane (D).

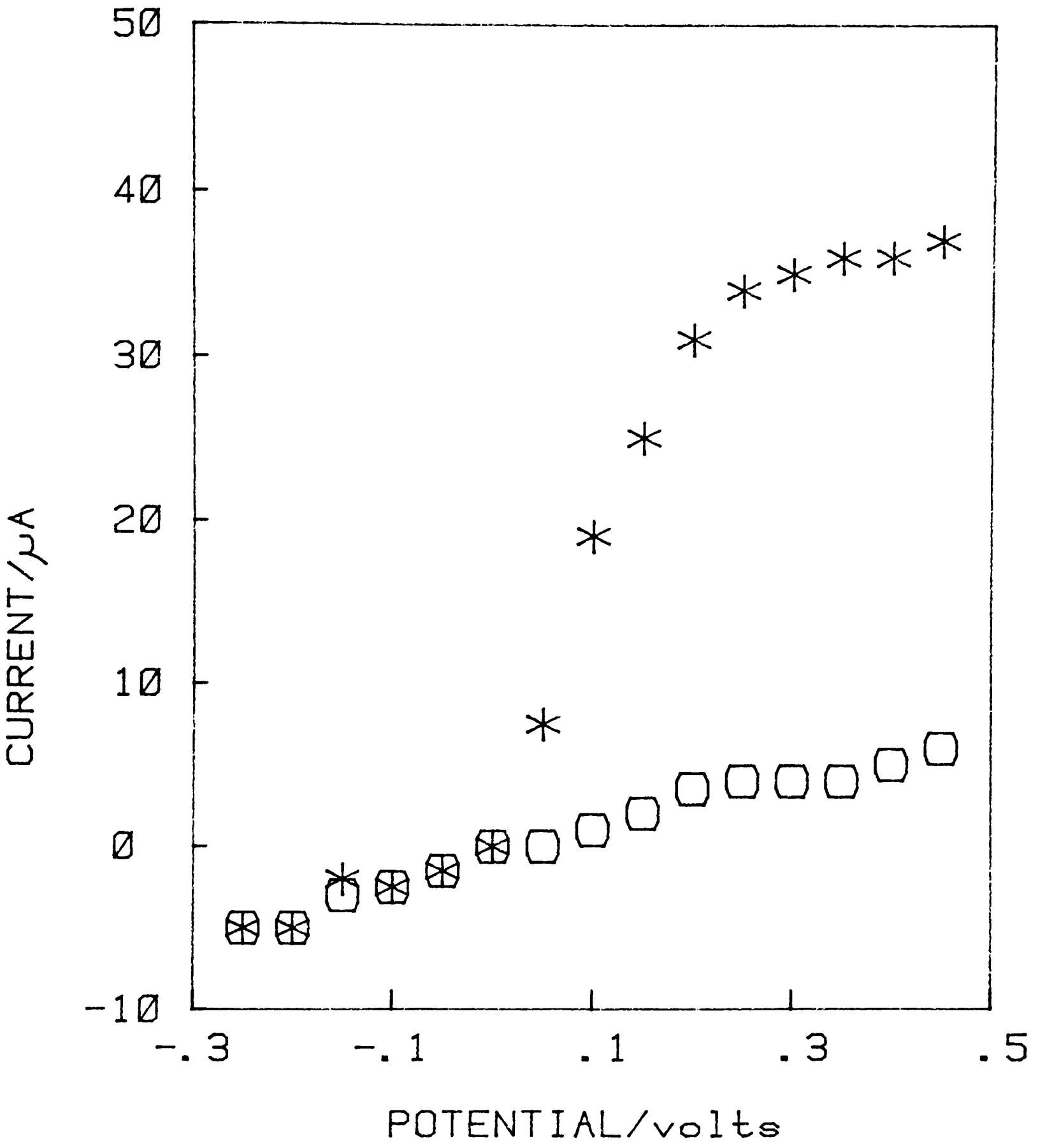

Figure 4.14 Plot of the steady-state current at the proto-type glucose enzyme electrode as a function of potential in the absense (O) and presence (*) of 100mM glucose. Data were obtained in quiescent solutions at pH 7.0 and at 20°C.

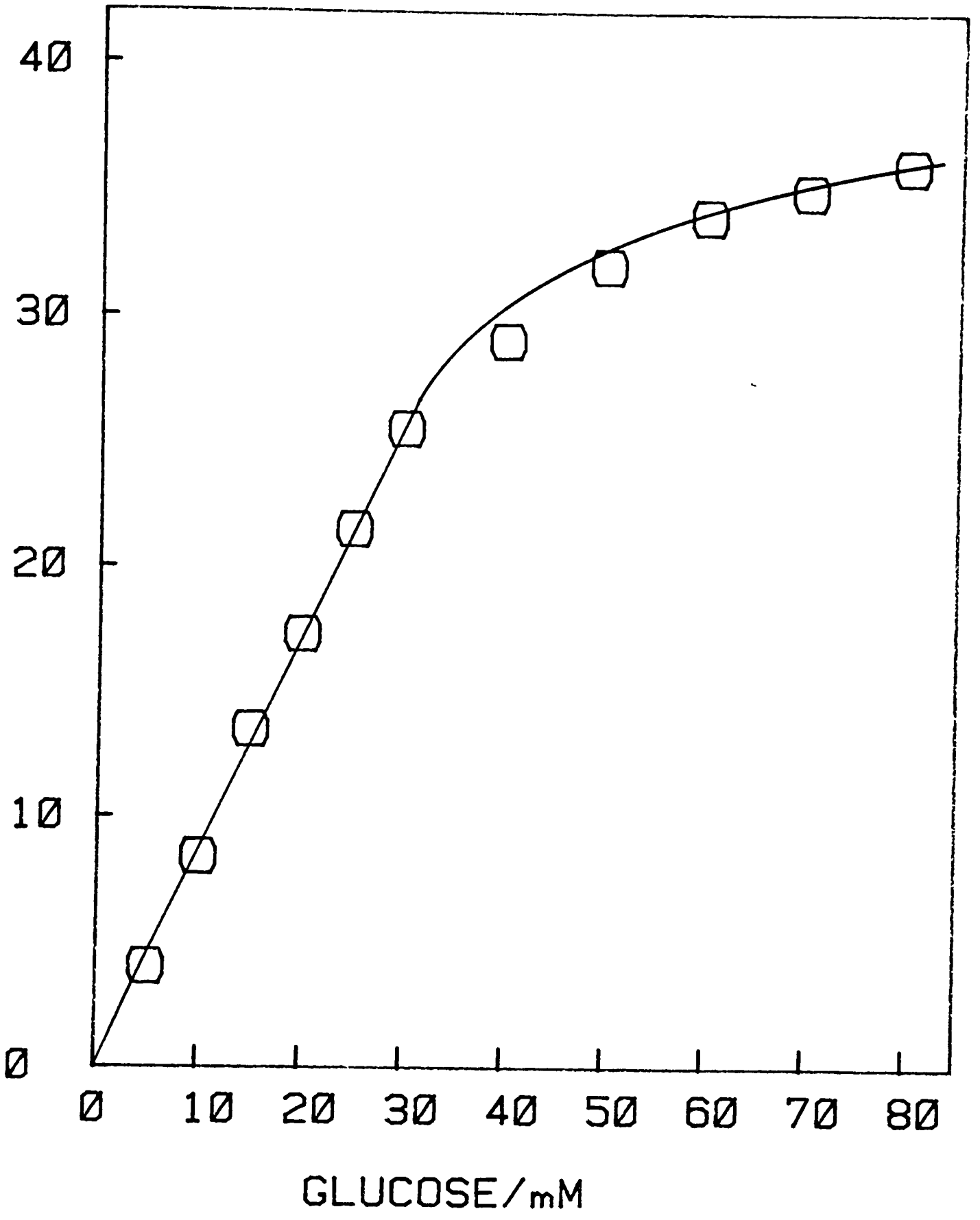

Figure 4.15 Steady-state current calibration curve for glucose enzyme electrode poised at a potential of 160mV vs SCE in argon-saturated buffer pH 7.0 at 20°C. The background current of 1.0μA is subtracted from the data.

current within 60-90 s. This was not dependent on whether the electrode was covered with a Nucleopore membrane.

The current response of the electrode was investigated in both quiescent and stirred solutions of 8mM glucose. An increase in the steady-state current of ca. 10% was observed upon changing from quiescent to rapid stirring. All subsequent experiments were performed in stirred solutions.

4.3.9 Models of enzyme electrodes

The limits of the linear range of this glucose enzyme electrode, figure 4.15, are relevant to the analysis of undiluted plasma samples from diabetics since changes in the patients blood glucose concentration (between hypo- and hyper-glycemia) are generally within this range.

Considering the theoretical models of enzyme electrodes outlined previously, the upper limit of linearity is higher than might be expected if the electrode response depended solely on the kinetics of the soluble enzyme, which has a Michaelis-Menten constant for glucose of 3.0mM (42). If this value was pertinent (or pertained to) the immobilized enzyme, the device would be expected to give a non-linear current response above this concentration. The upper limit does not however, appear to be limited solely by diffusion across the outer membrane, section 4.3.8. Two possible

explanations for the high upper limit remain: either the method by which the enzyme is immobilised on to the graphite foil reduces its affinity (increases its K_M) for glucose, or there is a diffusional limitation within the enzyme layer. The response of this enzyme electrode does not fit the theoretical models described previously, which assume a planar surface as the base sensor. Rather than being a planar surface, the electrode is a loosely compressed material throughout which the enzyme and mediator are dispersed.

4.3.10 Reproduciblity of electrode construction

The reproducibility of the electrode construction protocol was investigated by measuring the steady-state current for each electrode in 10mM glucose. A batch of twenty-four prototype electrodes gave a mean current response of 7.9μA with a standard deviation of 2.8μA. This was fair for a non-automated construction procedure. All electrodes gave a linear response over the clinically relevant range.

4.3.11 Effect of oxygen on enzyme electrode

Figure 4.16 shows glucose calibration curves for the enzyme electrode in buffer saturated with argon, air and oxygen. Whilst some interference from oxygen is expected (since in the presence of oxygen there is competition between the ferricinium ion and oxygen for reduced enzyme), the decrease in the steady-state current occurs

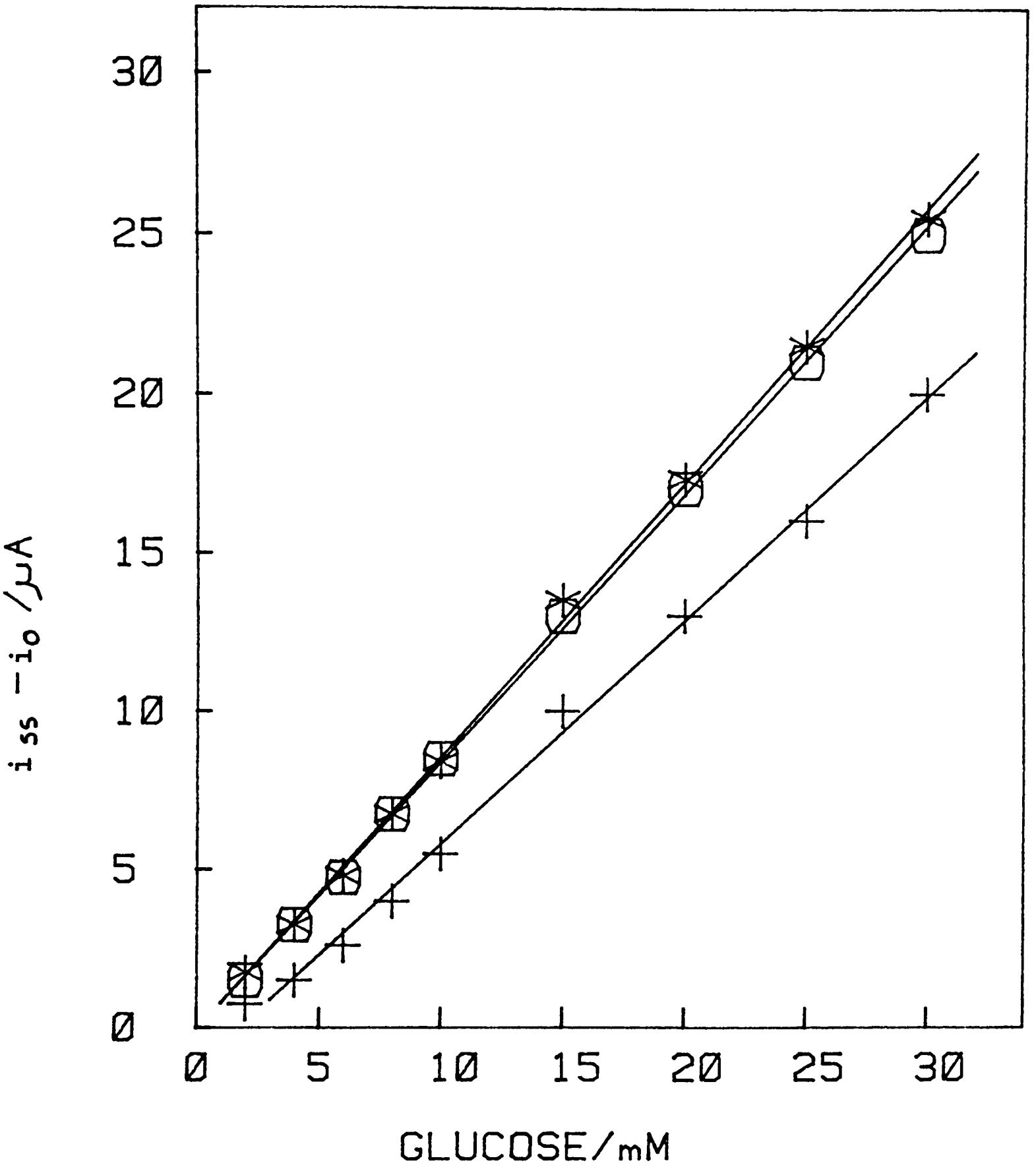

Figure 4.16 Steady-state calibration curves in argon (*), air (0) and oxygen-saturated (+) buffer. Other conditions as for figure 4.15.

as the base sensor is not poised sufficiently positive to re-oxidise any hydrogen peroxide that is generated by the enzyme, eq 1.5. Operation at a potential sufficiently positive (700mV vs SCE), to re-oxidise the hydrogen peroxide led to increased interference from other metabolites found in blood samples, particularly ascorbate section 4.3.14.

At normal blood glucose concentrations (4-7mM), the decrease in current upon air-saturation (equivalent to an oxygen concentration of ca. 260μM), of previously argon-saturated buffer is ca. 4.0%. The concentration of oxygen in whole venous blood and plasma is usually less than 200μM (47), suggesting that interference from oxygen, when assaying authentic undiluted clinical samples may be no greater than that observed in air-saturated buffer. This is clinically acceptable. All subsequent experiments were performed in solutions which had not been de-oxygenated.

4.3.12 Effect of pH on enzyme electrode

The effect of pH on the response of the glucose enzyme electrode was investigated over the physiologically relevant range, pH 6.0-9.0. Figure 4.17 shows that the steady-state current of a typical prototype electrode, in buffer containing 10mM glucose, is essentially independent of pH. This desirable feature of a non-pH dependent response contrasts with data obtained for a typical oxygen-mediated glucose enzyme electrode (48) which exhibits a

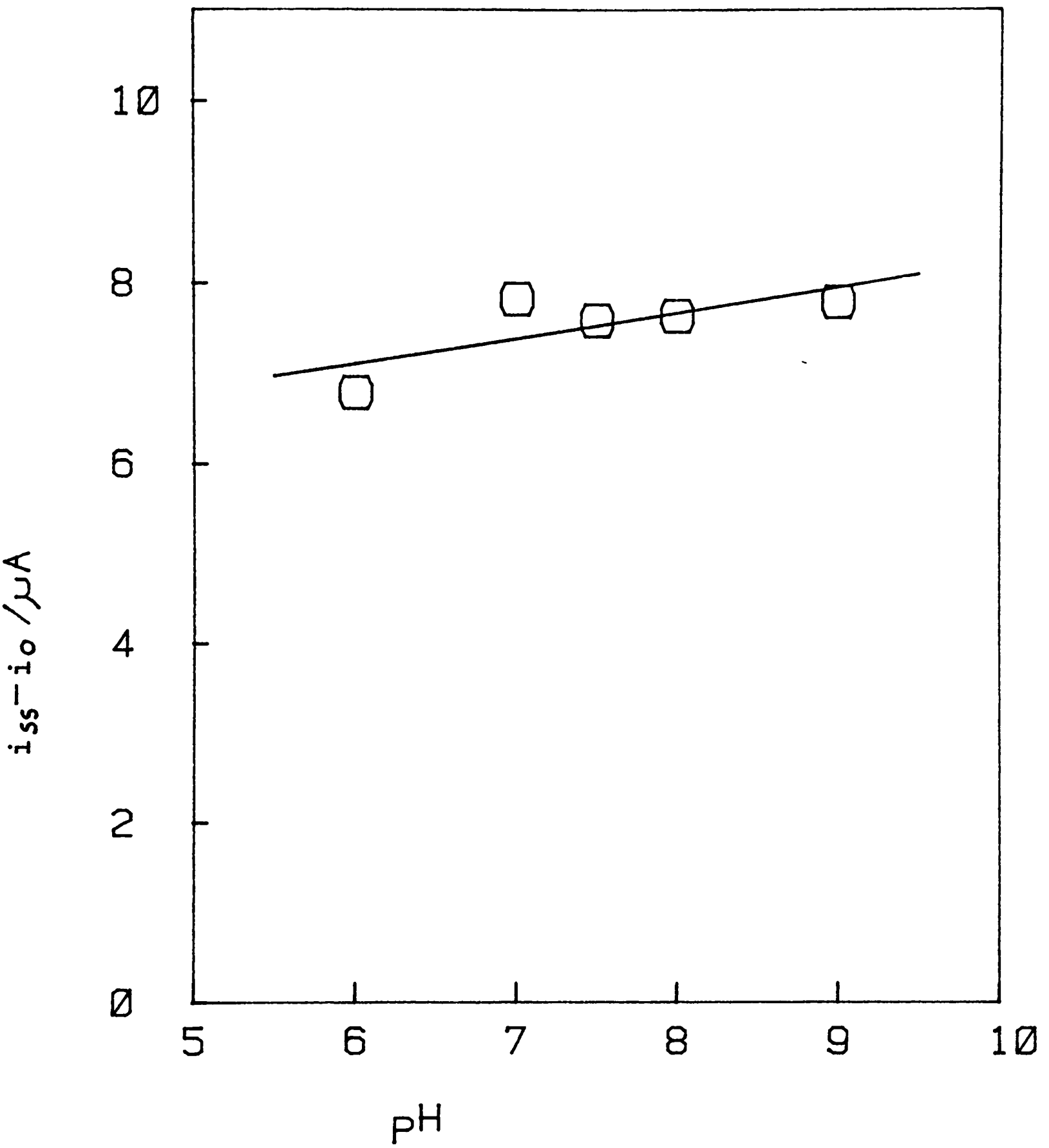

Figure 4.17 Plot of Steady-state current, i_{ss}, minus background current, i_o, as a function of pH, in the presence of 10mM glucose at 20°C.

marked pH dependence in the current response, with a maximum value occurring at pH 6.5. This difference in behaviour may result from the fact that, unlike oxygen, no proton transfer is involved in the reduction of ferricinium ion.

4.3.13 Effect of temperature on enzyme electrode

The effect of temperature on the electrode response was studied over the range 10-50^{o}C in buffer containing 10mM glucose. Figure 4.18, shows the increase in steady-state current with increasing temperature, ca. 4%/^{o}C. This emphasised the importance of performing the glucose assays under thermostatic control.

4.3.14 Effect of interfering substances

The effect of substances commonly found in blood which might interfere with the response of the electrode, either through direct electrode oxidation, reaction with 1,1´-dimethylferrocene or inhibition of glucose oxidase, were examined. Analyses of buffered solutions containing 8mM glucose, to which metabolites were added to give the normal physiological concentration in blood, were carried out, table 4.7. Though L-ascorbate increased the current by ca. 4.0%, addition of uric acid, L-cysteine, reduced glutathione, sodium formate, D-xylose, α-galactose and α-mannose did not cause any observable interference to the electrode response. It was apparent that the low operating potential of the device obviated significant

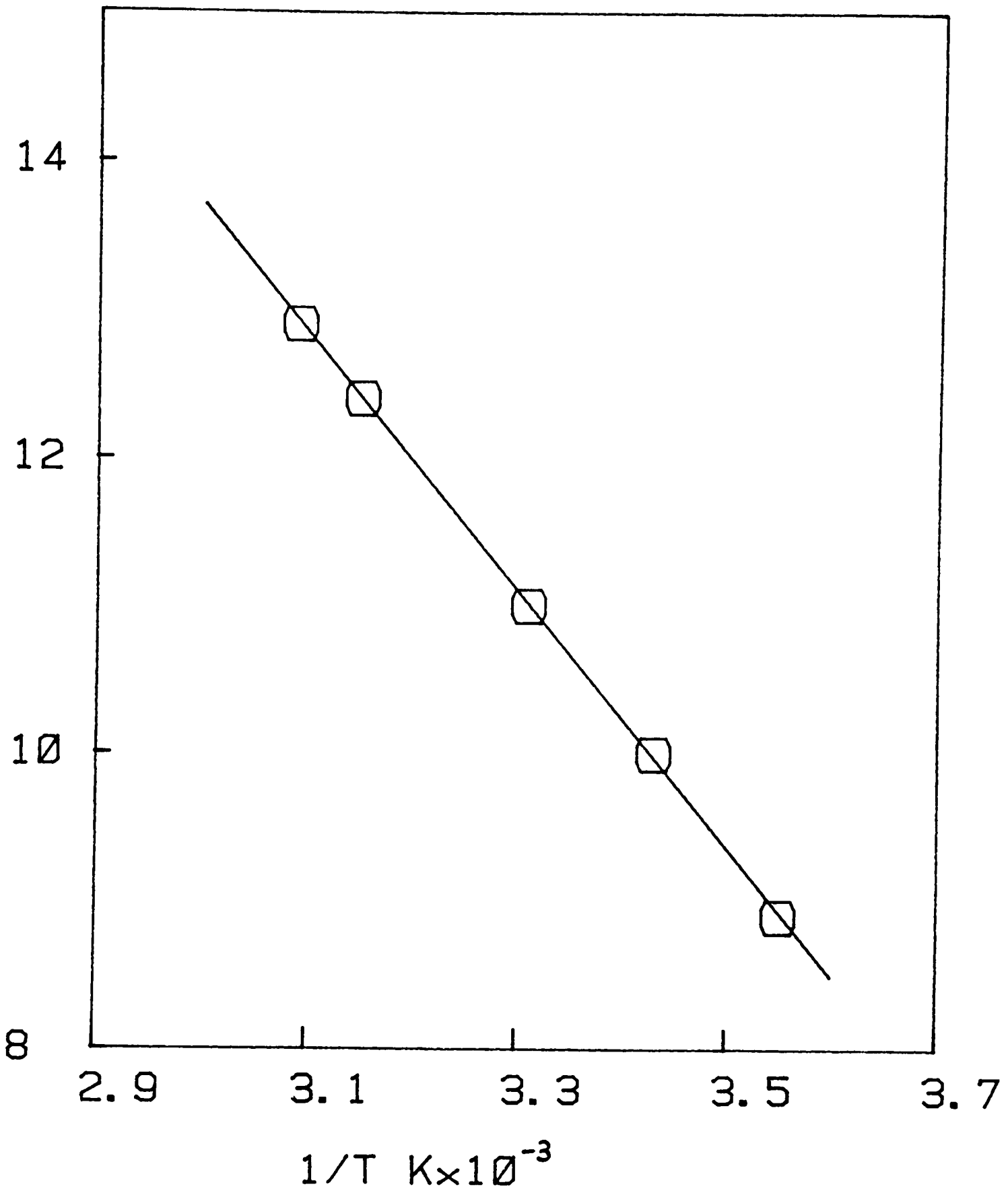

Figure 4.18 Arrhenius plot shows the effect of temperature on the steady-state current, in the presence of 10mM glucose at pH 7.0.

Table 4.7 Interfering substances

Metabolite	Concentration/mM	Percentage change in current
L-ascorbate	0.13	+4.0%
uric acid	0.42	-
L-cysteine	0.88	-
reduced glutathione	0.5	-
sodium formate	7.5	-
D-xylose	8.0	-
galactose	8.0	-
mannose	8.0	-
oxygen	0.26	-4.0%

interference from the electro-active metabolites, table 4.7.

Niether heparin or potassium oxalate, at concentrations required to prevent coagulation of whole-blood samples, caused any interference with the electrode response.

4.3.15 Operational stability

To investigate the operational stability of the enzyme electrode, a method for testing electrodes in batches was required. By using a potentiostat equipped with a multiplexer under computer control, section 3.1.1, a set of five electrodes could be activated in sequence, figure 4.19. Initially, each electrode was poised at 0mV (switched off), to each electrode in turn the potential was then stepped to 160mV (switched on) and the current measured after 60s. A total cycle time of six minutes was used, giving ten measurements per hour.

Figure 4.20 shows an experimental current decay curve for an electrode at a fixed glucose concentration and at constant temperature over a 24h period. Experiments on batches of five electrodes were conducted at saturating and non-saturating glucose concentrations, 10mM and 100mM respectively, and at 20^{o}C and 37^{o}C. The mean values for the residual current, expressed as a percentage of the initial current, after 24h continuous operation are presented in table 4.8.

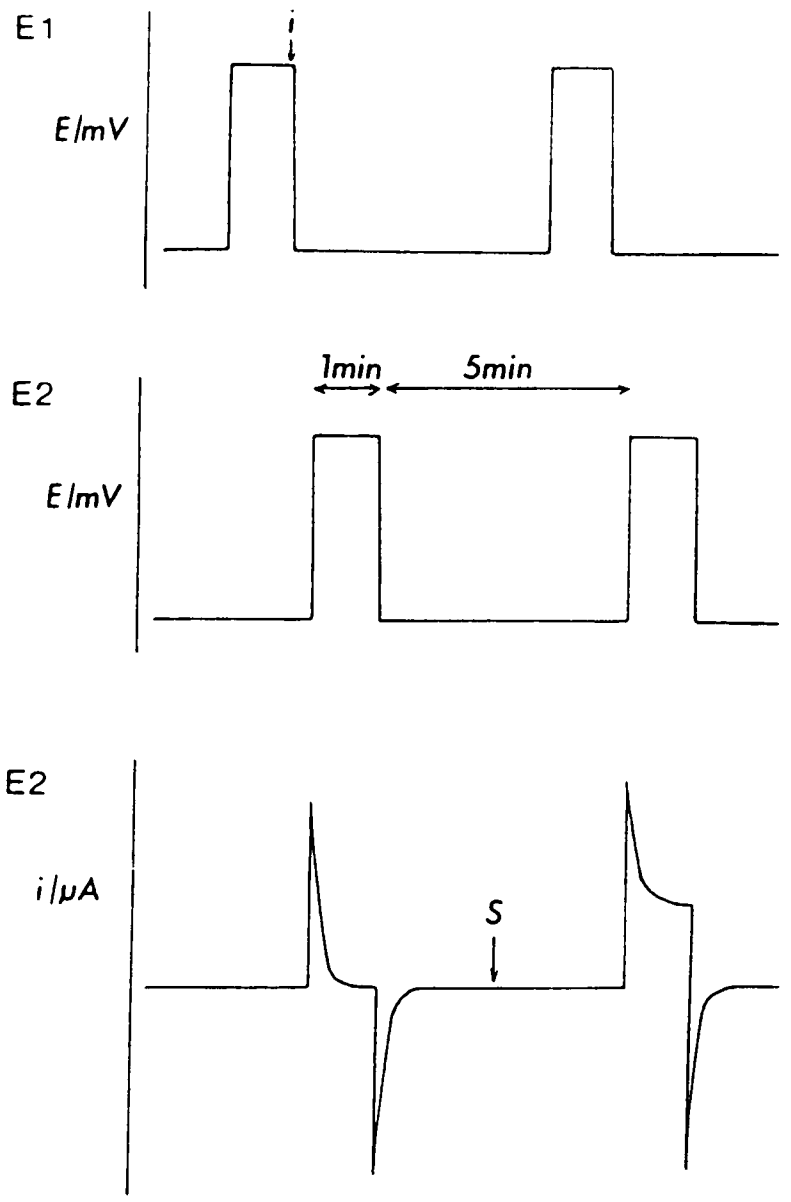

Figure 4.19 The potential pulse sequence for an electrode is shown in E1. A rest potential of 0mV with a pulse height of 160mV was used, with the current, i, being measured at the end of each pulse. The pulse duration and rest period are shown in E2. The transient current response is shown for E2 before and after the addition of substrate, S.

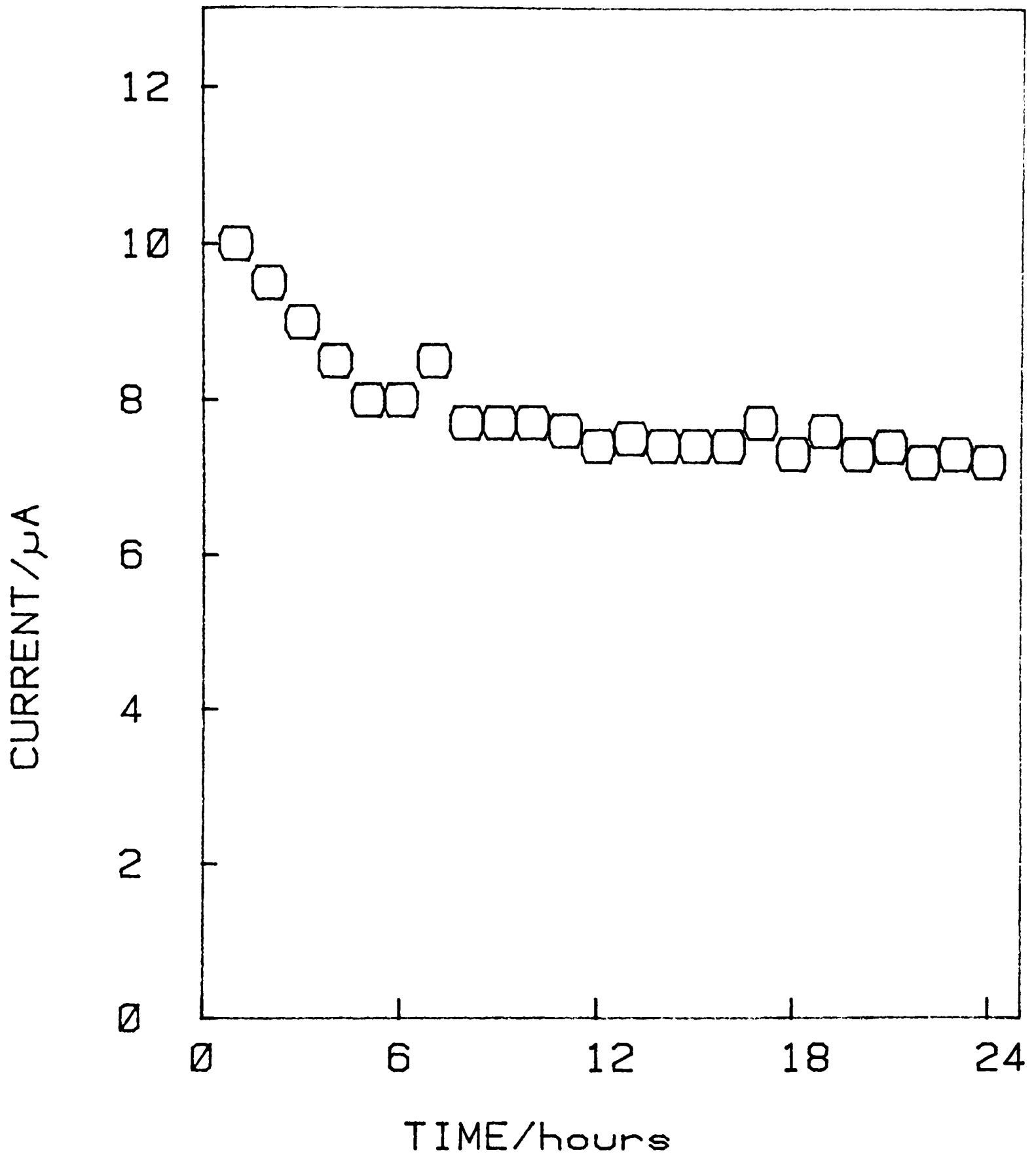

Figure 4.20 Plot of the current decay of the glucose enzyme electrode during a period of 24h at 20°C in the presence of 10mM glucose. Every tenth data point is plotted.

Table 4.8 Stability of glucose enzyme electrodes

Glucose/mM	Temperature/^{o}C	Mean percentage of initial current after 24 hours operation
10	20	70% +5
100	20	80% +5
10	37	50% +5
100	37	75% +5

means are for batches of five electrodes

In 'normal' use and with intermittant re-calibration, electrodes could be used to perform glucose assays for about 3-4 days.

4.3.16 Assay of diabetic plasma

Experiments were carried out to test the performance of the ferrocene-based enzyme electrode against a standard clinical method in the analysis of authentic clinical samples.

Fresh plasma samples, taken from human diabetics, were first analysed with a Yellow Springs Instruments (YSI) glucose analyser, in daily use on the Metabolic ward at Guy's Hospital, London. This device incorporates glucose oxidase immobilized on to a cellulose acetate membrane and is based on the amperometric detection of hydrogen peroxide. As the plasma sample is injected into the analyser it is automatically diluted into aerated buffer. By this method, the samples were found to have concentrations of glucose in the range 2-20mM.

The same samples, in an undiluted form, were re-assayed with a ferrocene-based glucose enzyme electrode using a three compartment cell with a working volume of 1ml. Figure 4.21 shows a correlation plot for the two methods from which a correlation coefficient of 0.98 was calculated, n=23, $y=0.951\mp0.18$. Both the YSI analyser and

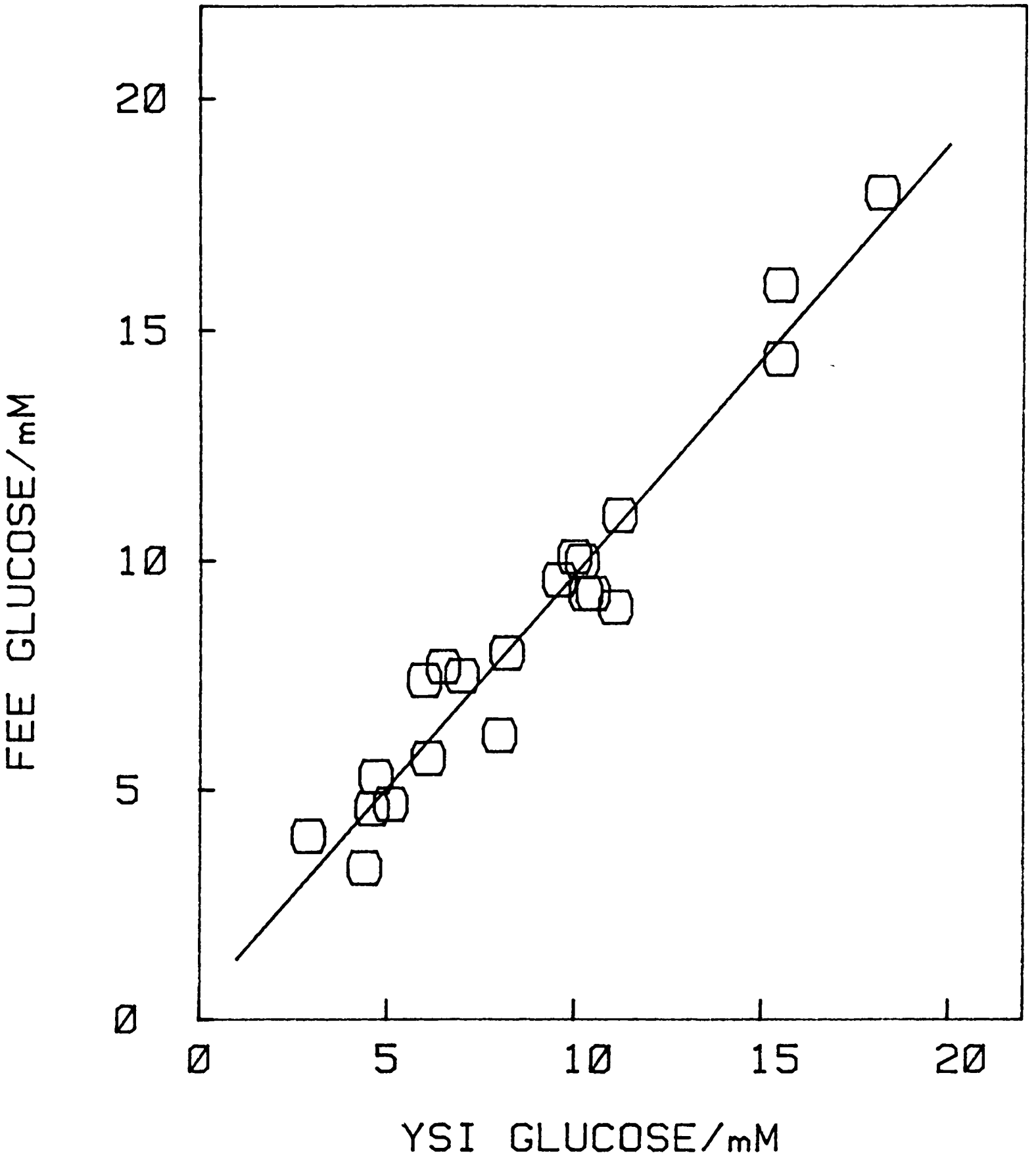

Figure 4.21 Correlation plot for plasma samples assayed with a Yellow Springs Instruments (YSI) glucose analyser and with the ferrocene-based glucose enzyme electrode. The latter assays were performed at 20°C.

the ferrocene-based electrode were calibrated with the same solutions, 0mM and 10mM glucose. The background current, measured by the ferrocene-based electrode in plasma from which glucose was removed enzymatically (49) by the addition of hexokinase and ATP, section 5.3.2, was i_o=1.2μA. This was similar to the value obtained in buffer, section 4.3.7.

4.3.17 Second prototype glucose enzyme electrode

Whilst the first prototype enzyme electrode demonstrated that it was possible to determine glucose concentrations in plasma samples with a non-oxygen mediated enzyme electrode, two related deficiencies made the assay procedure unsuitable as a practical device. Clearly, the plasma sample volume of ca. 1ml required for the electrochemical cell was unnecessarily large. The enzyme electrode required re-designing to work on a sample of ca. 100μl (a volume of blood that can easily be milked from a thumb prick).

A simple solution to this problem was to have the electrodes mounted on to a single horizontal strip on to which a small sample could be pipetted. In addition, simpler electronics, incorporated into a hand-held mini-potentiostat, 3.2.6, could be used if the enzyme electrode was operated in a two electrode mode using a Ag/AgCl reference electrode. (A third, auxillary electrode is used in many electrochemical techniques to compensate for an iR drop between the working and reference electrode (50). However, passing a

current of ca. 10μA in an aqueous medium like plasma, which has a conductivity of ca. 100 $\Omega\,cm^{-1}$ results in an iR drop of ca. 1mV. This was acceptable in this type of potentiostatic measurement).

The enzyme electrode was re-designed to incorporate these two features, figure 4.4(b). This second prototype glucose enzyme electrode gave similiar performance charateristics to the first design when operated at 205mV vs Ag/AgCl, equivalent to 160mV vs SCE, in buffer.

4.3.18 Assay of whole-blood versus plasma

The second prototype enzyme electrode was used to assess the applicability of the assay system to heparinised whole-blood, in addition to plasma. Blood samples, ca. 3ml, were taken from diabetic patients and after the addition of heparin an aliquot of 100μl was pipetted on to the strip so as to cover the enzyme electrode and the reference. The steady-state current was measured after 60s. This procedure was repeated after the original samples had been converted to plasma by centrifugation. A correlation plot for plasma versus whole-blood is shown in figure 4.22. From the data, a correlation coefficient of 0.99 was calculated, n=10, $y=1.079\mp0.86$. The electrode was calibrated with 0mM and 10mM glucose solutions.

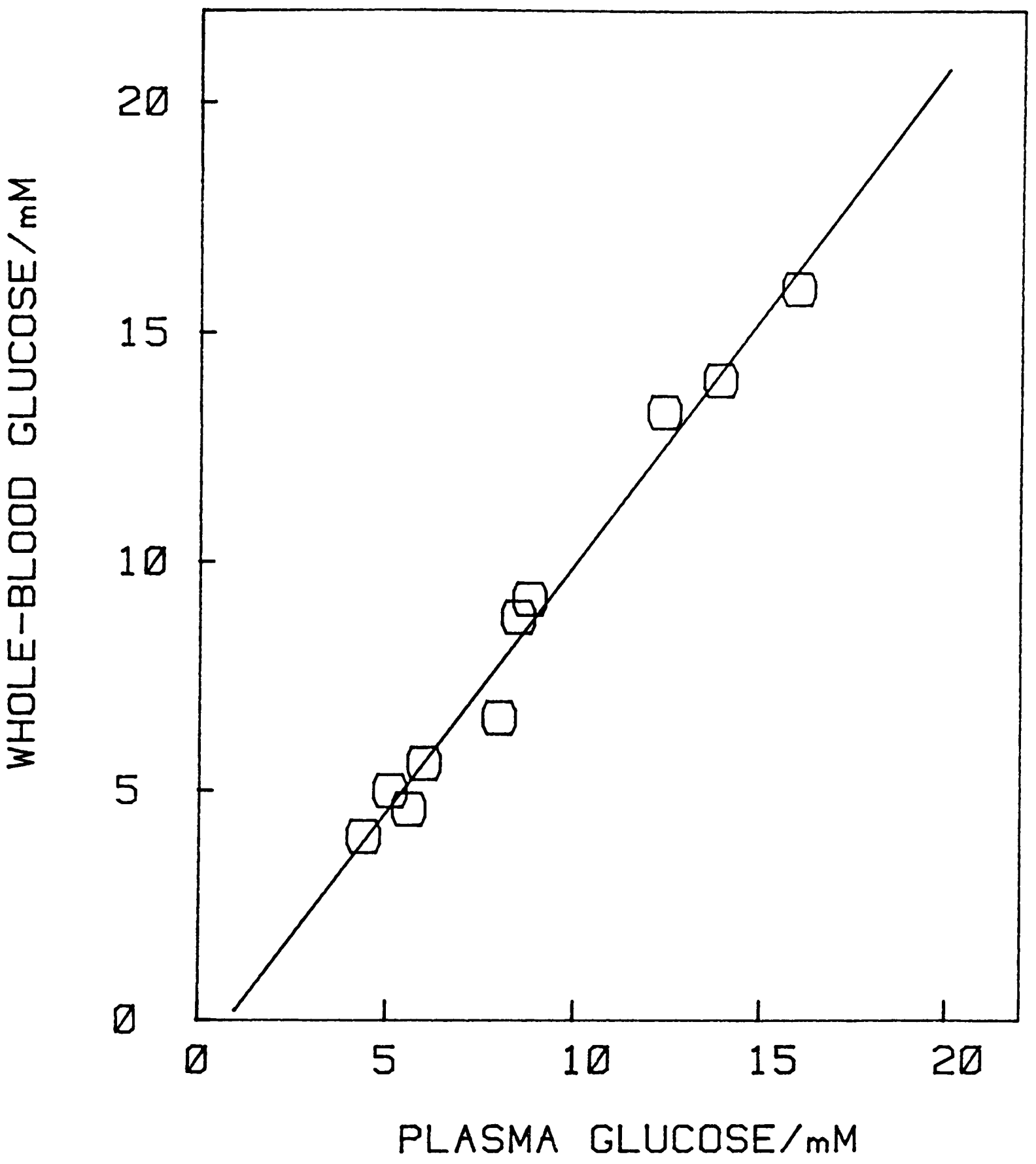

Figure 4.22 Correlation plot for diabetic samples assayed as both plasma and whole-blood using the ferrocene-based glucose enzyme electrode. All assays were performed at 20°C.

4.4.1 Conclusions

The electrode has many of the features required for the analysis of clinical glucose samples. The performance apparently depends on a number of features: the rapid rate of electron transfer between reduced enzyme and the ferricinium ion, and the subsequent rapid electrochemical oxidation of the ferrocene. The low solubility of the ferrocene presumably results in its effective confinement to the electrode surface, though the finite solubility allows the ferricinium ion to diffuse between the immobilized enzyme and the electrode surface. Whilst a fuller understanding of the mechanism of action is required, this has not prevented the application of this novel electrode to the *in vitro* analysis of clinically relevant samples.

At present, the electrode could be further adapted in two ways, either by incorpoation into a clinical analyser for whole-blood glucose assays, or as an alternative to chromogen-based test strips. Future work on this system should concentrate on miniturising the device for *in vivo* glucose monitoring.

References

1. Apgar, V. and Beck, J. Is my baby alright ? New York: Trident (1972).

2. Maugh, T. H. Science 193, 220, (1976).

3. Walton, D. Clin. Prod. 5, 42, (1983).

4. Sanderman, F. W., MacFate, R. P. and Evans, G. T. Amer. J. Clin. Path. 21, 901, (1951).

5. Martinek, R. G. J. Amer. Med. Tech. 31, 530, (1969).

6. Henry, C. J. Clinical chemistry principles and techniques. New York: Hoeber (1964).

7. Fales, F. W., Russell, J. A. and Fain, J. N. Clin. Chem. 7, 289, (1964).

8. Watson, D. and Stevenson, M. E. K. Aust. J. Exp. Biol. Med. Sci. 41, 211, (1963).

9. Bryant, D. NZ J. Med. Lab. Tech. 20, 52, (1966).

10. Guilbault, G. G. and Lubrano, G. J. Anal. Chim. Acta. 64, 439, (1973).

11. Pilegyi, V. J. and Szustkiewicz, C. P. in: Carbohydrates in clinical chemistry. Henry, R. J. ed. New York: Harpers and Row (1974).

12. Giampietro, O., Pilo, A. and Boni, C. Clin. Chem. 28, 2405, (1982).

13. Mager, M. and Farese, G. Amer. J. Clin. Path. 44, 104, (1965).

14. Schmidt, F. H. Klin. Wochenschr. 39, 1244, (1961).

15. Hu, A. S. and Cline, A. L. Biochim. Biophys. Acta. 93, 237, (1964).

16. Kadish, A. H., Little, R. L. and Sternberg, J. C. Clin. Chem. 14, 116, (1969).

17. Blaedel, W. J. and Hicks, G. P. Anal. Chem. 32, 388, (1960).

18. Malmstadt, H. V. and Hicks, G. P. Anal. Chem. 32, 394, (1960).

19. Guilbualt, G. G., Brignac, P. and Zimmer, M. Anal. Chem. 40, 190, (1968).

20. Dobrick, L. A. J. Biol. Chem. 231, 403, (1958).

21. Clark, L. C. and Lyons, C. Ann. N. Y. Acad. Sci. 102, 39, (1962).

22. Updike, S. J. and Hicks, G. P. Nature 214, 986, (1967).

23. Notin, M., Guillien, R. and Nabet, P. Ann. Biol. Chem. 30, 193, (1972).

24. Clark, L. C. US Patent 3539455 (1970).

25. Clark, L. C. and Sachs, G. Ann. N. Y. Acad. Sci. 48, 133, (1968).

26. Nagy, G., Storp, H. and Guilbault, G. G. Anal. Chim. Acta. 66, 443, (1973).

27. Mell, L. D. and Maloy, J. T. Anal. Chem. 47, 299, (1975).

28. Mell, L. D. and Maloy, J. T. Anal. Chem. 48, 1579, (1976).

29. Herbert, D. and Pinsent, J. Biochem. J. 43, 193, (1948).

30. Clark, L. C. Biotech. Bioeng. Symp. 3, 377, (1972).

31. Pickup, J. C. Brit. Med. J. 285, 49, (1982).

32. Schlapfer, P., Mindt, W. and Racine, P. Clin. Chim. Acta. 57, 283, (1974).

33. Aleksandrovskii, Y. A., Bezhikina, L. V. and Rodinov, Y. V. 46, 708, (1981).

34. Kealy, T. J. and Paulson, P. L. Nature 168, 1039, (1951).

35. Deeming, A. J. in: Comprehensive organometallic chemistry. eds Wilkinson, G. et al. Oxford: Pergammon (1982).

36. Marr, G. and Rockett, B. W. J. Organometal. Chem. 227, 373, (1982).

37. Szentrimay, R., Yeh, P. and Kuwana, T. Amer. Chem. Soc. Symp. 38, 143, (1977).

38. Hennig, H. and Gurtler, O. J. Organometal. Chem. 11, 307, (1968).

39. Mason, J. G. and Rosenblum, M. J. Amer. Chem. Soc. 82, 4206, (1960).

40. Murray, R. W. J. Amer. Chem. Soc. 103, 1, (1980).

41. Dubios, J-E., Lacaze, P-C. Pham, M. C. J. Electroanal. Chem. 117, 233, (1981).

42. Weibel. M. K., Duke, R. F., Page, D. S., Bulgrin, V. G. and Luthy, J. J. Amer. Chem. Soc. 91, 3904, (1969).

43. Bourdillion, C., Borgeois, J-P. and Thomas, D. J. Amer. Chem. Soc. 102, 4231, (1980).

44. Weibel, M. K. and Bright, H. J. J. Biol. Chem. 246, 2734, (1971).

45. Lingane, J. J. Anal. Chim. Acta. 44, 411, (1969).

46. Evans, J. F., Kuwana, T., Henne, M. T. and Royer, G. P. J. Electroanal. Chem. 80, 409, (1977).

47. CIBA Physifax daignostic handbook. London: Morrison (1981).

48. Ianniello, R. M. and Yacynych, A. M. Anal. Chem. 53, 2090, (1981).

49. Thomas, L. C. and Christian, G. D. Anal. Chim. Acta. 77, 153, (1975).

50. Bard, A. J. and Faulkner, L. R. Electrochemical methods fundamentals and applications. New York: Wiley (1980).

CHAPTER 5

CREATINE KINASE ASSAY USING THE GLUCOSE ENZYME ELECTRODE

Introduction

5.1.1 Acute myocardial infarction

The sudden and complete occlusion of the coronary artery by a thrombosis cuts the blood supply to a zone of myocardial tissue depriving it of oxygen and glucose. Damage to the affected muscle leads to a release of cardiac enzymes into the blood circulation. The enzyme creatine kinase, (ATP:creatine N-phosphotransferase[EC 2.7.3.2]) abbreviated to CK, constitutes ca. 20% of the soluble sarcoplasmic protein of heart muscle (1). Consequently, the occurance of elevated levels of CK in the blood often results in the diagnosis of acute myocardial infarction (AMI). Figure 5.1, shows the mean activity of CK present in plasma samples taken from post-AMI patients, subsequent to the infarction (1).

Several methods for measuring CK activity in plasma have been devised and are in daily use in clinical biochemistry laboratories (2). Many are in the form of commercially available test kits. These are used to perform over 30 million determinations throughout the

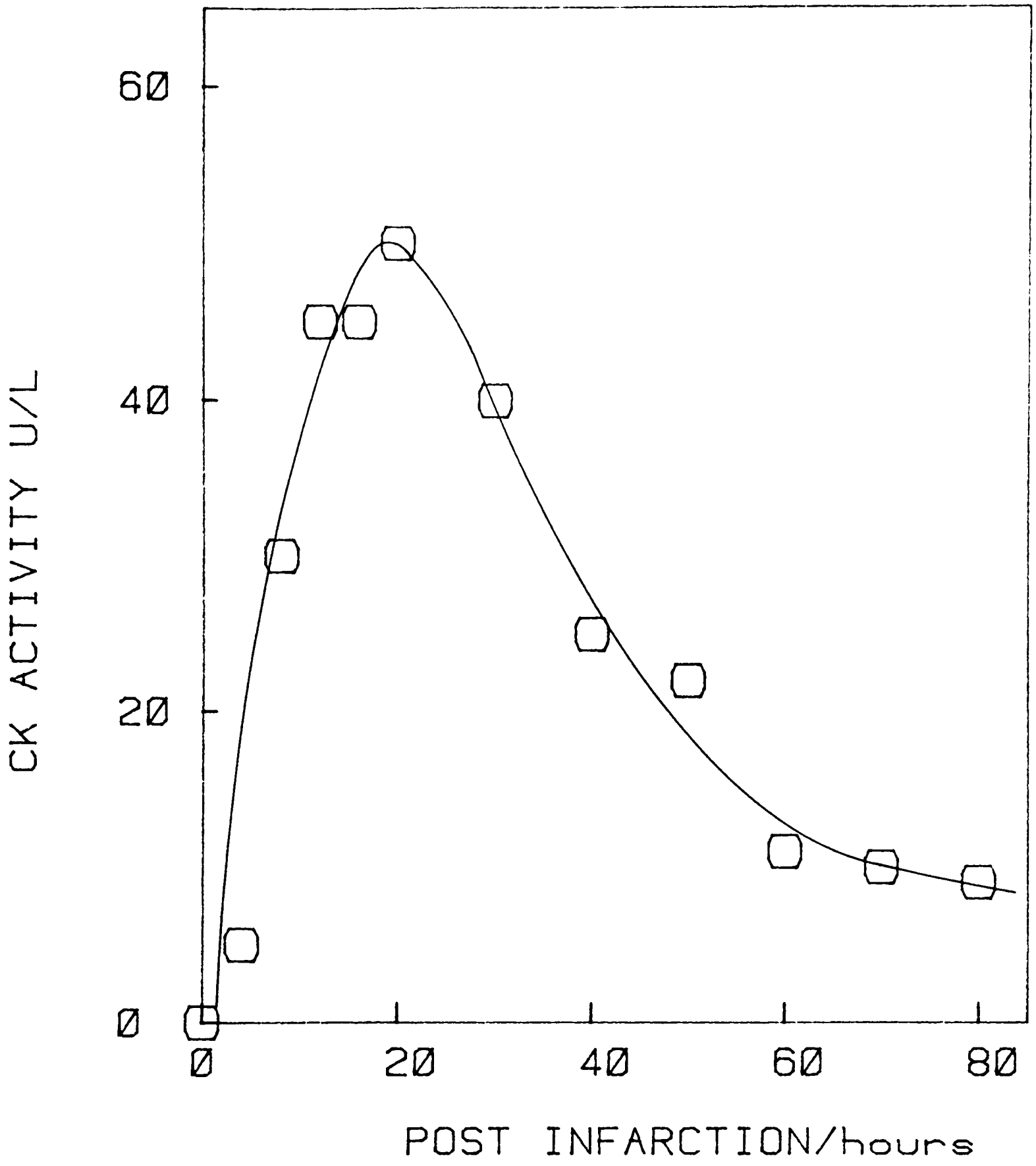

Figure 5.1 Mean activity of CK-MB in plasma after myocardial infarction.

world each year.

5.1.2 Creatine kinase

Creatine kinase catalyses the reversible transfer of a phosphate residue from adenosine-5′-triphosphate (ATP) to creatine, eq 5.1.

$$H_2NC(=NH)N(CH_3)CH_2CO_2H + ATP \overset{CK}{\rightleftharpoons} PO_3^{2-}NHC(=NH)N(CH_3)CH_2CO_2H + ADP \quad [5.1]$$

The reaction product, creatine phosphate, represents an essential energy store for contraction, relaxation and transport of substances within muscle cells. Catalysis of the reverse reaction has a pH optimum of 6.8, whereas the forward reaction is optimum at pH 9.0 (2,3). This is shown in, Figure 5.2, which depicts the pH profiles for the forward and reverse reactions. The enzyme is activated by magnesium ions, and is inhibited by zinc, copper and mercuric ions (3). Thiols, such as glutathione, dithioerythritol and cysteine also have a stabilising effect on the enzyme (3). It is necessary to add of one of these reagents to plasma samples, during storage, to stabilise the enzyme as CK possesses two labile thiol groups which are important for activity (3).

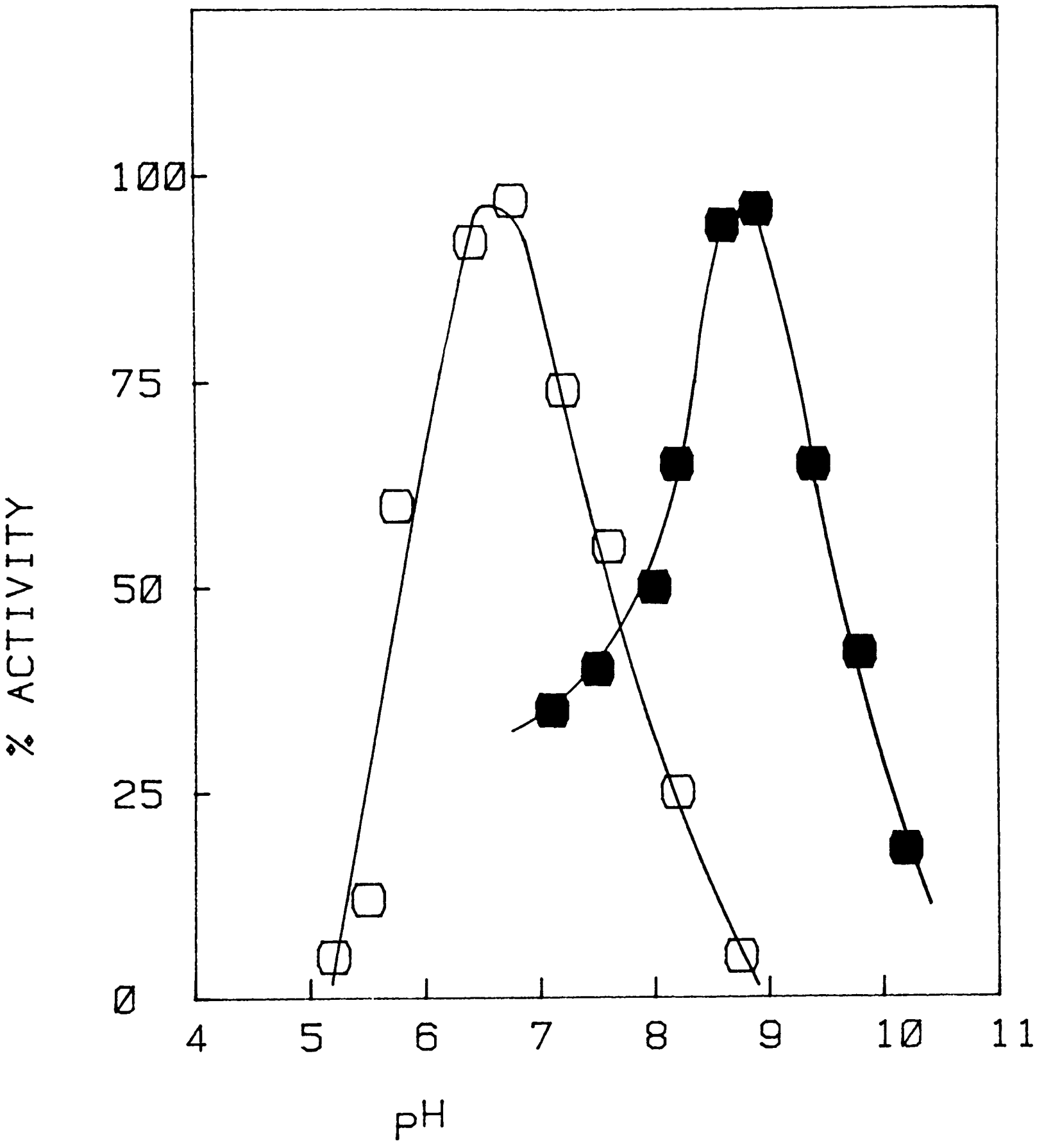

Figure 5.2 Activity profile for the forward (●) and reverse (O) reaction catalysed by creatine kinase as a function of pH.

5.1.3 Creatine kinase isoenzymes

Creatine kinase is a dimeric enzyme, molecular weight 82 000, constituted of two subunits weighing 41 000 (3). In human tissue two different types of subunits exist, designated M (muscle) and B (brain). The dimeric enzyme can have the following forms: CK-MM skeletal muscle type, CK-BB brain type and CK-MB myocardial type. These isoenzymes can be separated by electrophoretic techniques (3), or by an immuno-inhibition method based on the use of goat anti-human CK-MB antibody (4). Methods of separating the different isoenzymes are of clinical importance, since elevated isoenzyme levels in plasma have been detected and found to be associated with causes other than AMI e. g. surgery, muscular dystrophy and muscular injury, and strenuous exercise. These are listed in table 5.1 (1). Whilst this may appear to negate the significance of a total plasma CK assay to AMI, in practise the assay remains of great value since other clinical factors are also taken into account before a diagnosis is made.

5.1.4 Creatine kinase assays

Since the equilibrium , eq 5.1, at physiological pH favours the reverse reaction, most assays for CK activity utilise this reaction. A number of methods have been developed for assaying CK and are extensively reviewed by Hegler (5). The preferred spectrophotometric method first outlined by Oliver (6), and improved by Rosalki (7) and

Table 5.1 Causes of increase in plasma creatine kinase

Condition	Total CK activity U/L	CK-MB activity U/L
Acute myocardial infarction	30-1970	6-232
Cardiogenic shock	90-860	5-114
Polytrauma with myocardial injury	110-2640	8-196
Cardiogenic defibrillation	180-580	9-41
Duchenne muscular dystrophy	400-4550	31-280
Delerium tremens	88-13510	4-830
Orthopaedic operations	15-630	0-18
Head injury	153-380	0-18
Neurosurgical operations	63-610	0-88
Weight lifters	110-740	0-10
Polytrauma without myocardial injury	76-6220	0-230

others (8,9), is based on the following reaction sequence:

$$\text{creatine phosphate} + \text{ADP} \xrightarrow{\text{CK}} \text{creatine} + \text{ATP} \qquad [5.2]$$

$$\text{glucose} + \text{ATP} \xrightarrow{\text{HK}} \text{G-6-P} + \text{ADP} \qquad [5.3]$$

$$\text{G-6-P} + \text{NADP}^{+} \xrightarrow{\text{G-6-PDH}} \text{gluconolactone-6-P} + \text{NADPH} + \text{H}^{+} \qquad [5.4]$$

The ATP formed, eq 5.2, reacts with glucose in the presence of hexokinase (HK: EC 2.7.1.1), eq 5.3, the glucose-6-phosphate (G-6-P) that is produced then reacts with the NADP-linked enzyme glucose-6-phosphate dehydrogenase (G-6-PDH: EC 1.1.1.49), eq 5.4. The rate of reduction of $NADP^{+}$, is monitored by the increase in absorbance at 340nm, from which the CK activity is calculated. Several methodological modifications have been elaborated in order to adapt this measurement of CK activity to different auto-analyser systems (10,11).

5.1.5 Electrochemical assays for creatine kinase

A novel electrochemical method of determining creatine kinase actitiviy in plasma has been developed by Guilbault (12). A platinum electrode is used to couple the NADPH generated, eq 5.4, to hexacyanoferrate (III) reduction via a diaphorase eqs 5.5 and 5.6. The steady-state current from electrochemical re-oxidation of

$Fe(CN)_6^{4-}$, monitored at a platinum electrode poised at 360mV vs SCE, is proportional to the CK activity in the range 10-1000 IU l^{-1}.

$$NADPH + 2Fe(CN)_6^{3-} \xrightarrow{\text{diaphorase}} NADP^+ + 2Fe(CN)_6^{4-} + H^+ \quad [5.5]$$

$$2Fe(CN)_6^{4-} \rightleftharpoons 2Fe(CN)_6^{3-} + 2e^- \quad [5.6]$$

5.1.6 Glucose enzyme electrode-based assay for creatine kinase

The rapid response time of the ferrocene-based glucose enzyme electrode, developed in chapter 4, suggested that in addition to monitoring bulk glucose concentration, the device could be used to monitor rates of change in bulk glucose concentration. It was proposed that CK activity could be determined using the coupled reactions sequence shown in eqs 5.2 and 5.3, with the glucose enzyme electrode monitoring the rate of consumption of glucose. Under optimised conditions the rate of decrease in the electrode current should be proportional to the rate of consumption of glucose, which in turn would be proportional to the rate of consumption of creatine phosphate, from which the activity of CK can be estimated. The coupled reaction sequence is shown in figure 5.3.

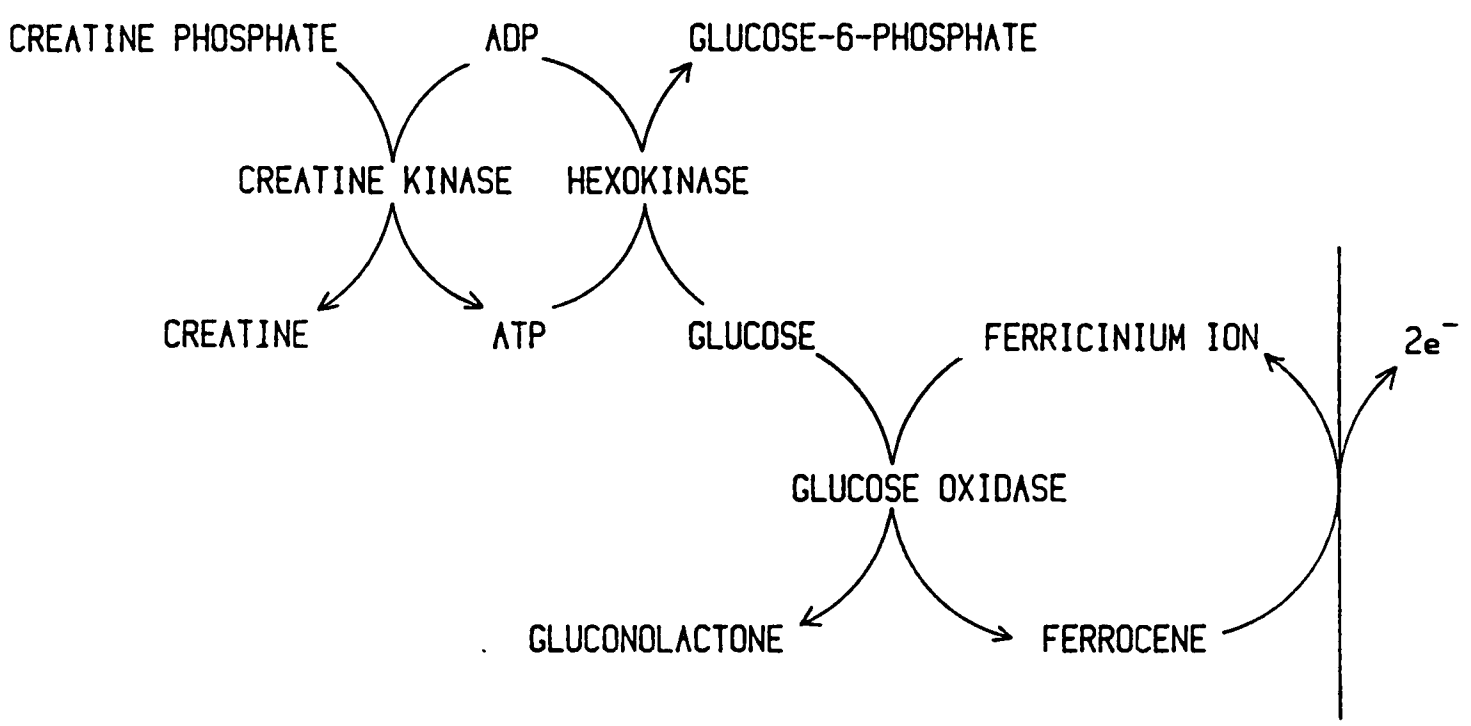

Figure 5.3 Coupled reaction sequence for a creatine kinase assay using the ferrocene-based glucose enzyme electrode.

Experimental

5.2.1 Reagents

Creatine phosphate, adenosine-5′-diphosphate, adenosine-5′-triphosphate, creatine kinase from rabbit muscle with an activity of 800 IU mg^{-1} at 37°C and hexokinase from yeast with an activity of 1600 IU ml^{-1} at 37°C were supplied by Boehringer. D-glucose and magnesium chloride were of AnalaR grade and supplied by BDH. In all experiments 25mM tris(hydroxymethyl)aminomethane, adjusted to pH 7.0 with HCl, was used.

5.2.2 Electrochemical experiments

D. C. cyclic voltammetry experiments were carried out with the cell described in section 3.1.2, using a 4mm diameter pyrolytic graphite working electrode.

Experiments in which the glucose enzyme electrode was used were performed with the first prototype design a 1ml three-compartment electrochemical cell, equipped with a stirrer bar. The rate of change in the steady-state glucose-dependent current was measured with the glucose enzyme electrode poised at 160mV vs SCE, using an Oxford electrodes potentiostat and a Bryan BS-271 chart recorder.

All assays were performed under thermostatic control at 37°C.

5.2.3 Plasma samples

Heparinised plasma samples were supplied frozen by the Clinical Biochemistry Laboratory of the John Radcliffe Hospital, Oxford.

Results and discussion

5.3.1 Uncoupling the glucose oxidase reaction

Figure 5.4(a), shows a D. C. cyclic voltammgram of ferrocene monocarboxylic acid in 25mM Tris-HCl buffer, pH 7.0, containing 20mM magnesium chloride and 10mM glucose. The voltammogram is similar to that shown in figure 4.5(a). Addition of glucose oxidase, figure 5.4(b), as expected, gave a typical catalytic current at oxidising potentials, resulting from the enzymatically coupled oxidation of glucose. When hexokinase 20 IU ml^{-1}, is added, no change in the voltammogram is observed. However, upon addition of ATP to a final concentration of 10mM, the catalytic behaviour is no longer observed and the voltammogram associated with reversible electrochemistry of the ferrocene is again obtained, as in figure 5.4(a). These observations are consistent with phosphorylation of glucose to form glucose-6-phosphate, thus removing from solution the substrate for the electrochemically coupled oxidation reaction. The voltammogram shown in figure 5.4(b) could be restored by further addition of glucose.

Since none of the components of the system interferred with the electrochemistry of ferrocene monocarboxylic acid, or showed any direct electrochemistry over the range of potential scanned, 0-450mV vs SCE, it was possible to investigate the response of the glucose enzyme electrode, firstly as an ATP monitor, and then for monitoring

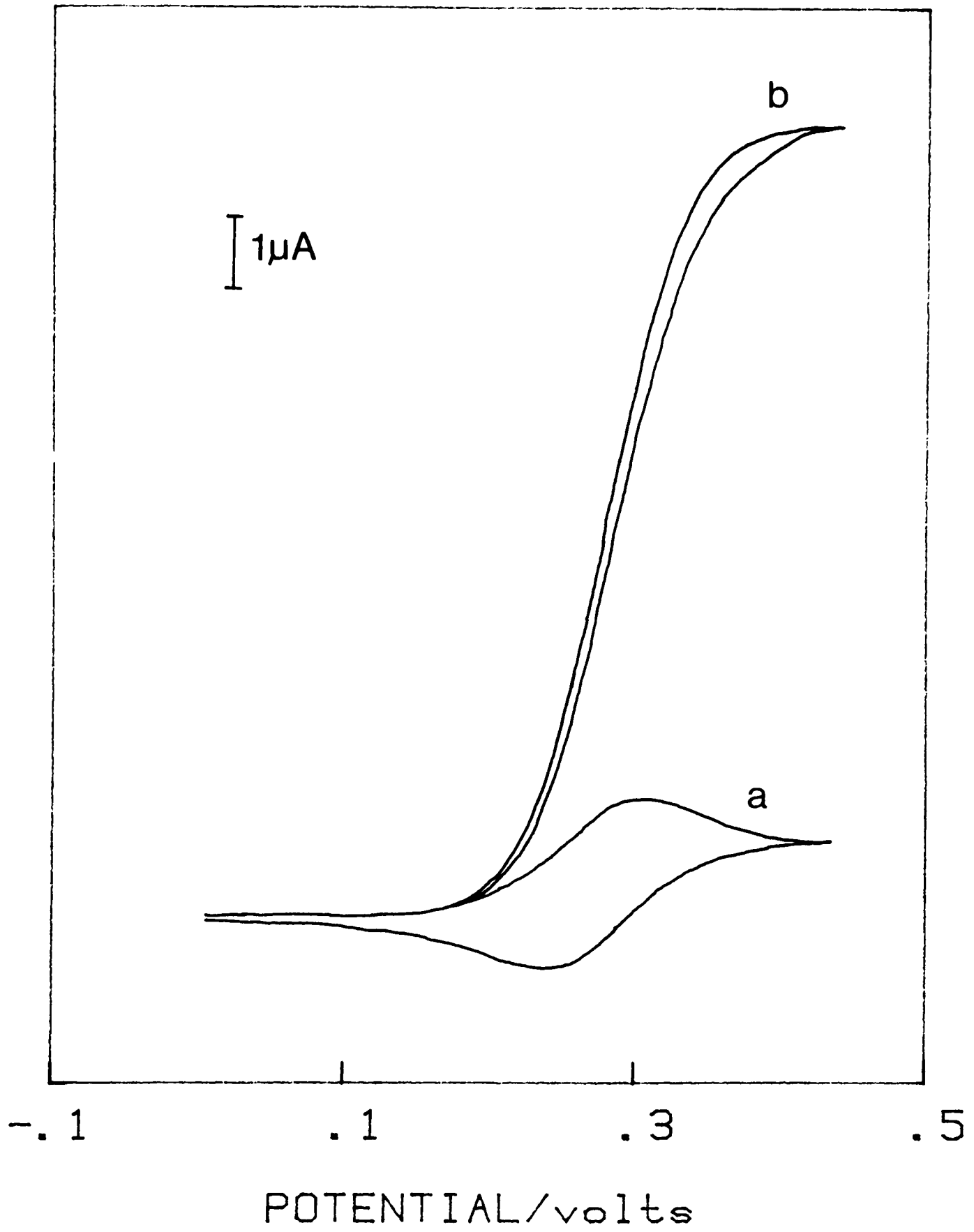

Figure 5.4 (a) D. C. cyclic voltammogram of ferrocene monocarboxylic acid (200μM) in 25mM Tris-HCl pH 7.0, containing 20mM $MgCl_2$ and 10mM glucose at a scan rate of $1mVs^{-1}$. (b) as for (a), but with the addition of 10.9μM glucose oxidase and 20 IU ml^{-1} of hexokinase. Subsequently, 10mM ATP was added and voltammogram (a) was obtained.

kinase activity.

5.3.2 Glucose enzyme electrode as an ATP sensor

Figure 5.5, shows a trace of the current-time response of a glucose enzyme electrode in 10mM glucose and hexokinase 20 IU ml^{-1}. A series of five aliquots of ATP (each to a final concentration of 2.0mM) were added and the decrease in the steady-state current was measured after each addition. Figure 5.6, plots the steady-state current as a function of ATP added. Figure 5.7, correlates the amount of glucose consumed with the amount of ATP added, from which a correlation coefficient of 0.99 was calculated. This experiment shows that the glucose enzyme electrode can be used to monitor stoichiometric consumption of glucose by ATP, in the presence of hexokinase. The electrode is re-usable: figure 5.5 shows that the electrode responds to further addition of glucose at the end of the experiment.

5.3.3 Glucose enzyme electrode based creatine kinase assay

Figure 5.8 shows that the current-time response of the glucose enzyme electrode in 20mM glucose is stable, after the further addition of hexokinase 20 IU ml^{-1}, ADP (5.0mM) and creatine phosphate (20mM). These reagent concentrations were found to be in sufficient excess to ensure that the rate of glucose consumption in the assay was limited by the activity of creatine kinase. When

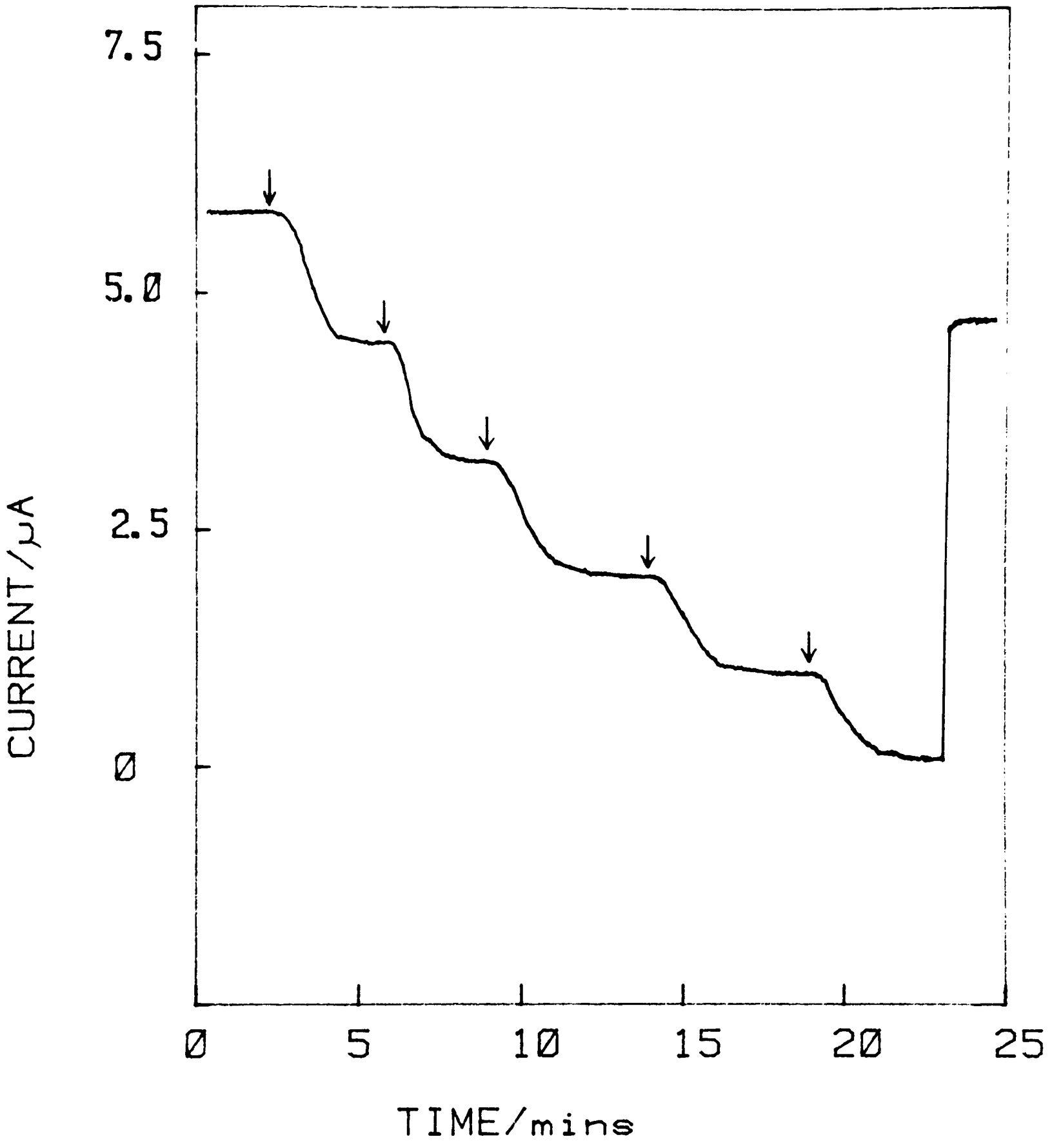

Figure 5.5 Current-time response of the glucose enzyme electrode poised at 160mV in 1ml of 25mM Tris-HCl pH 7.0, containing 20mM $MgCl_2$, 10mM glucose and 20IU ml^{-1} hexokinase. Five aliquots (↑) of 2.0μmoles ATP were added to the system and the change in the steady-state current measured. At the end of the experiment, glucose was added to give a final concentration of 8mM.

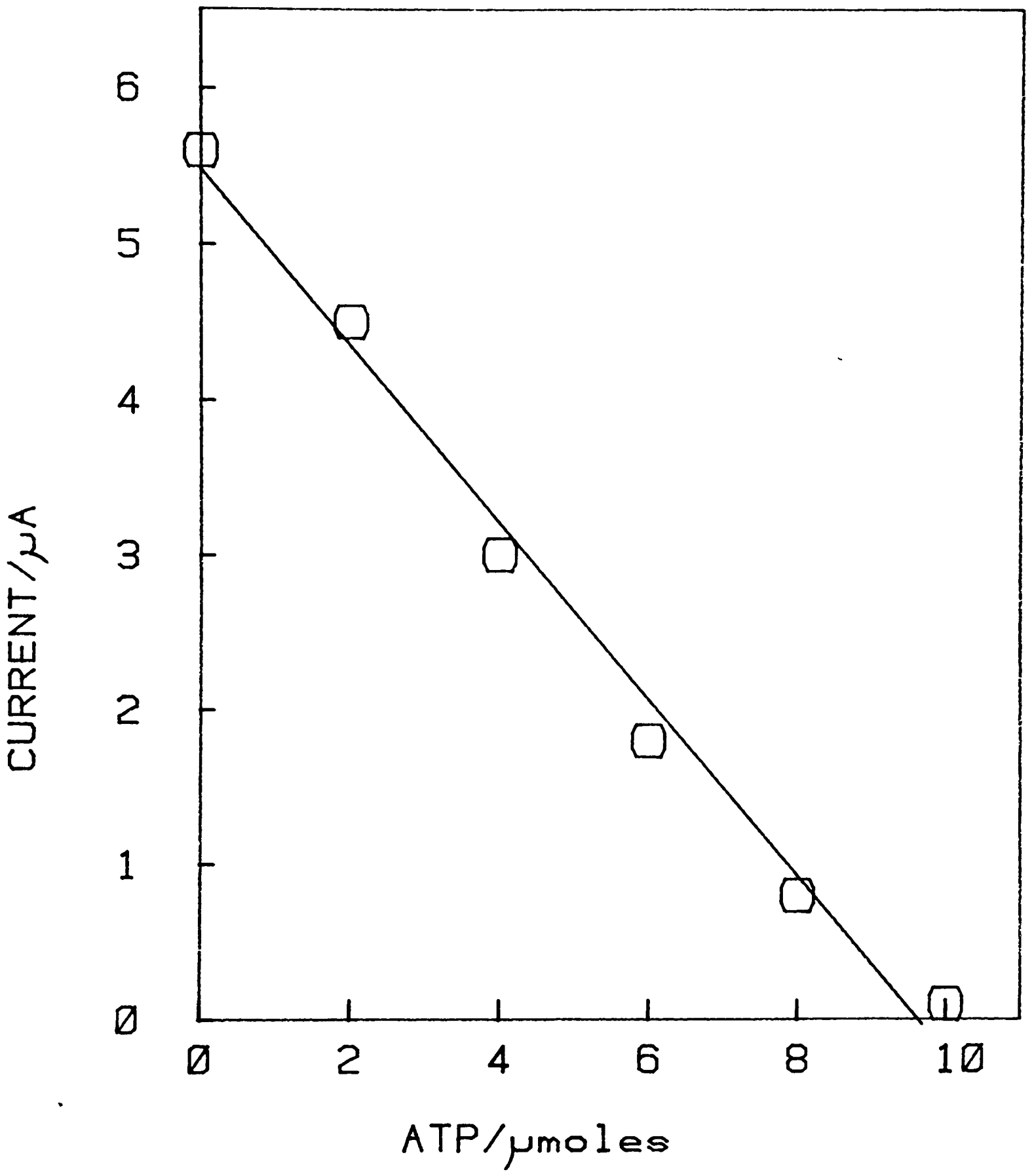

Figure 5.6 Plot of steady-state current as a function of the amount of ATP added, data obtained from figure 5.5.

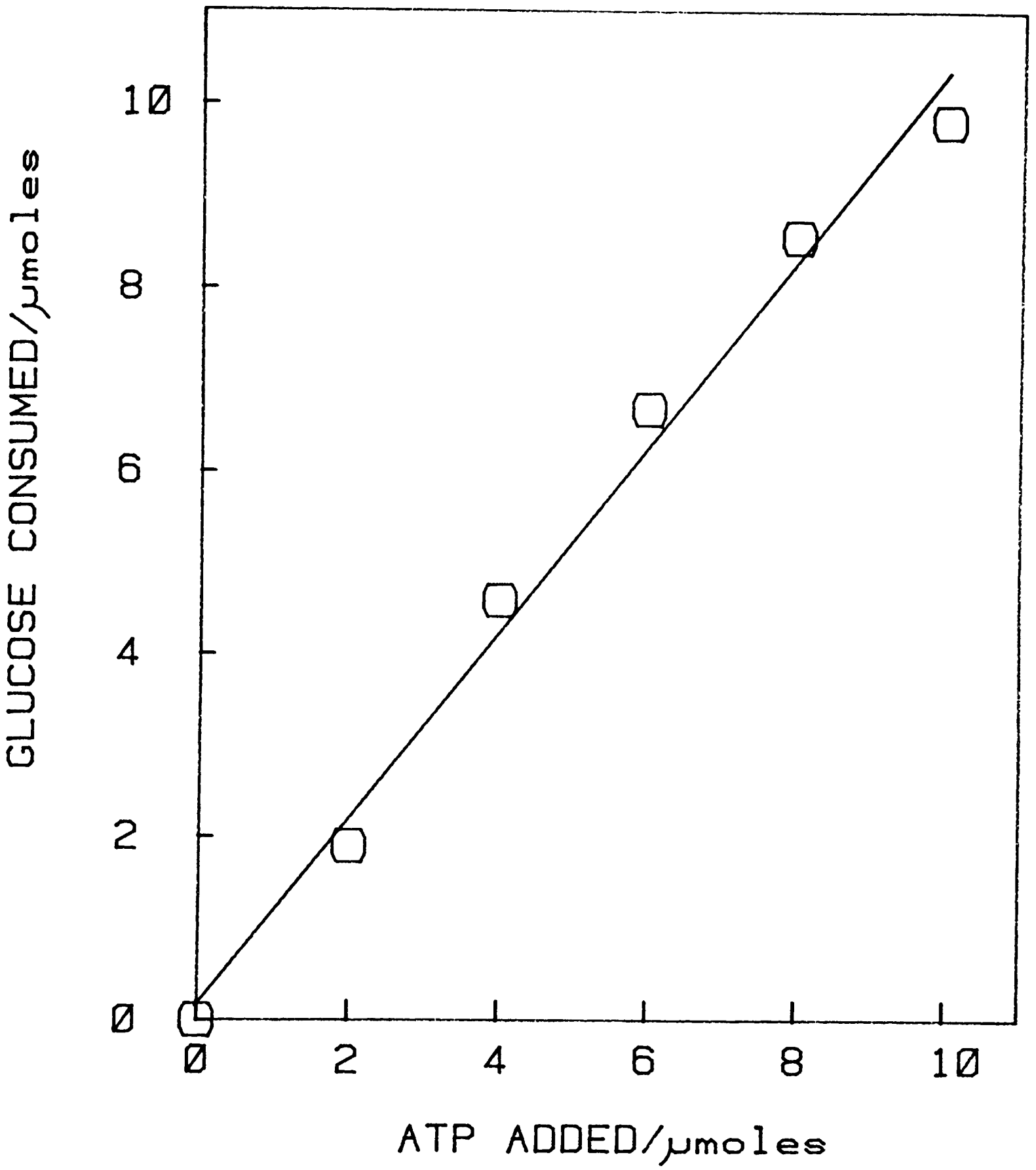

Figure 5.7 Correlation plot for the amount of glucose consumed versus the amount of ATP added to the system, data from figure 5.5.

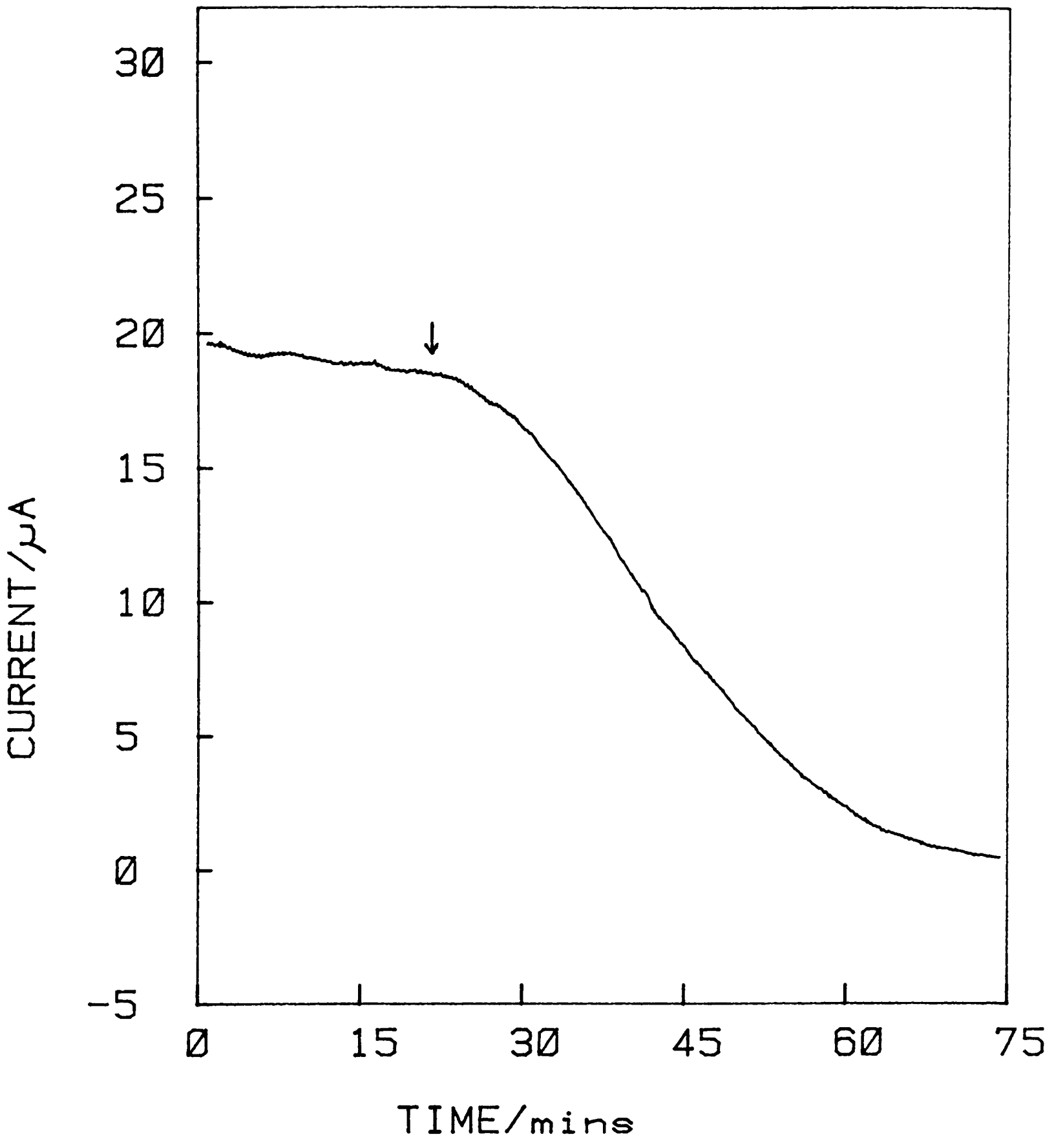

Figure 5.8 Current-time plot of the enzyme electrode in 25mM Tris-HCl pH 7.0, containing 20mM glucose, 20IU ml^{-1} hexokinase, 20mM creatine phosphate, 20mM $MgCl_2$ and 5mM ADP. The reaction was initiated (↑) by addition of 500IU l^{-1} creatine kinase.

creatine kinase, with a reported activity of 500 IU l^{-1} is added to the system, the current decreases with time. From the initial rate of decrease, the rate of glucose consumption was calculated. The rate of glucose consumption should be equivalent to the activity of creatine kinase in μmoles creatine phosphate consumed min^{-1} mg^{-1}. This is shown in the correlation plot, figure 5.9, for which a correlation coefficient of 0.99 was calculated.

5.3.4 Detection limits of Creatine kinase assay

In post-AMI patients, plasma CK activities in the range 30-2000 IU l^{-1} (0.03-2.0IU ml^{-1}), are common. From the data in figure 5.9, it is evident that the assay procedure, when investigated in buffered solutions, may be suitable for monitoring clinical levels of CK. The upper limit of the electrode response is ca. 10IU ml^{-1} (10 000 IU l^{-1}).

5.3.5 Assay of creatine kinase in plasma samples

It was not possible to obtain authentic plasma samples from post-AMI patients, so samples were simulated by adding clinically relevant concentrations of CK to human plasma. Aliquots of ADP, $MgCl_2$ and HK were also added to the plasma to give the same reagent concentrations as used in section 5.3.3. The initial glucose concentration present in the plasma was determined with the glucose enzyme electrode, as described in section 4.3.16, and was increased

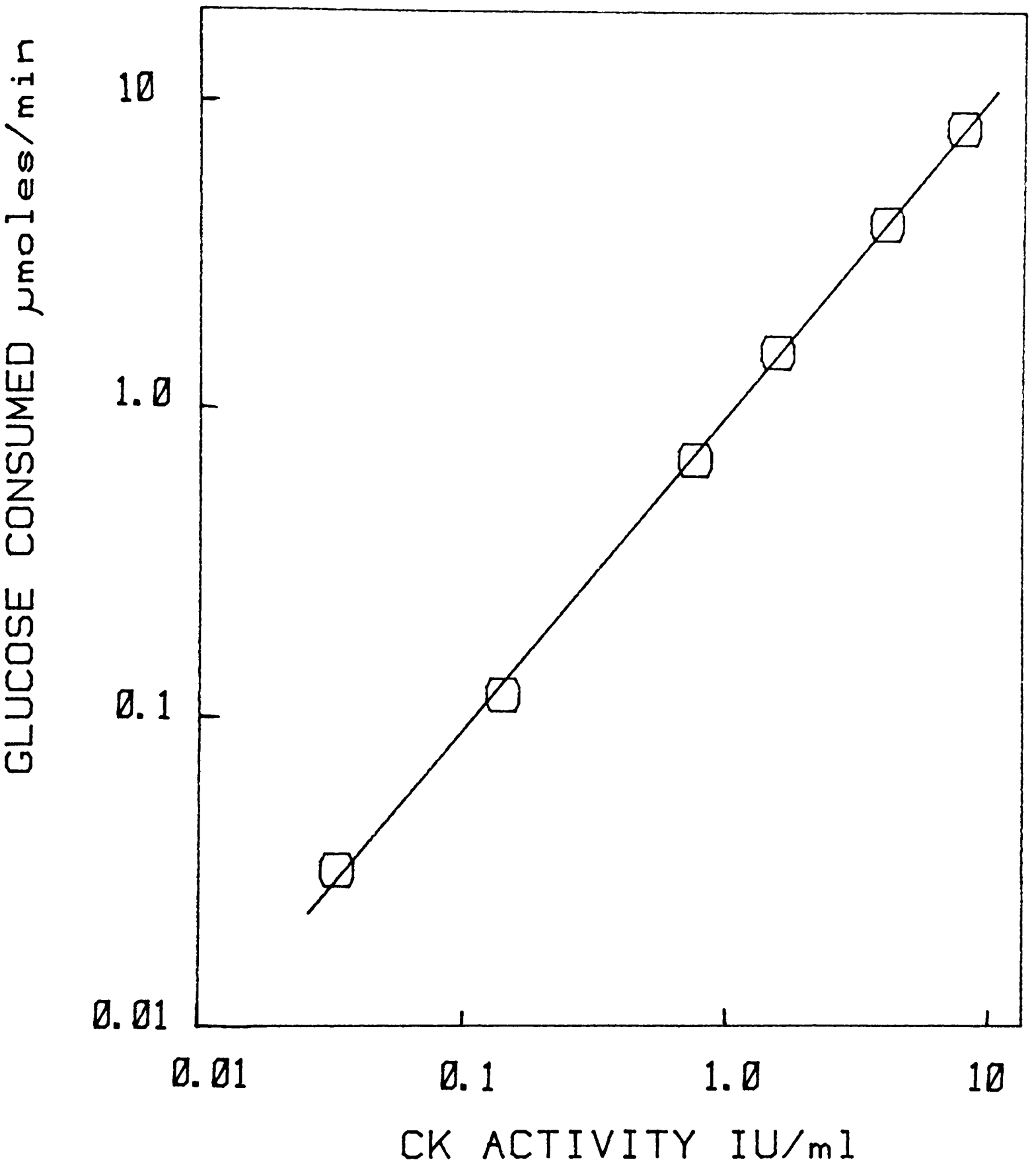

Figure 5.9 Correlation plot for the rate of glucose consumption versus the amount of CK activity present in buffered solution. Assays were performed as described in figure 5.8, with varying amounts of CK.

Table 5.2 Creatine kinase assays

CK Added IU/L	Buffer pH 7.0 IU/L	Plasma pH 7.7 IU/L	Plasma corrected to pH 7.0 IU/L
150	152	64.7	154
150	152	66.8	159
150	148	59.6	142
90	83	37.0	88
70	76	31.5	75
30	31	2.5	5.9
15	15	1.9	4.5
7.5	7.3	2.3	5.3
7.5	7.3	3.6	8.6

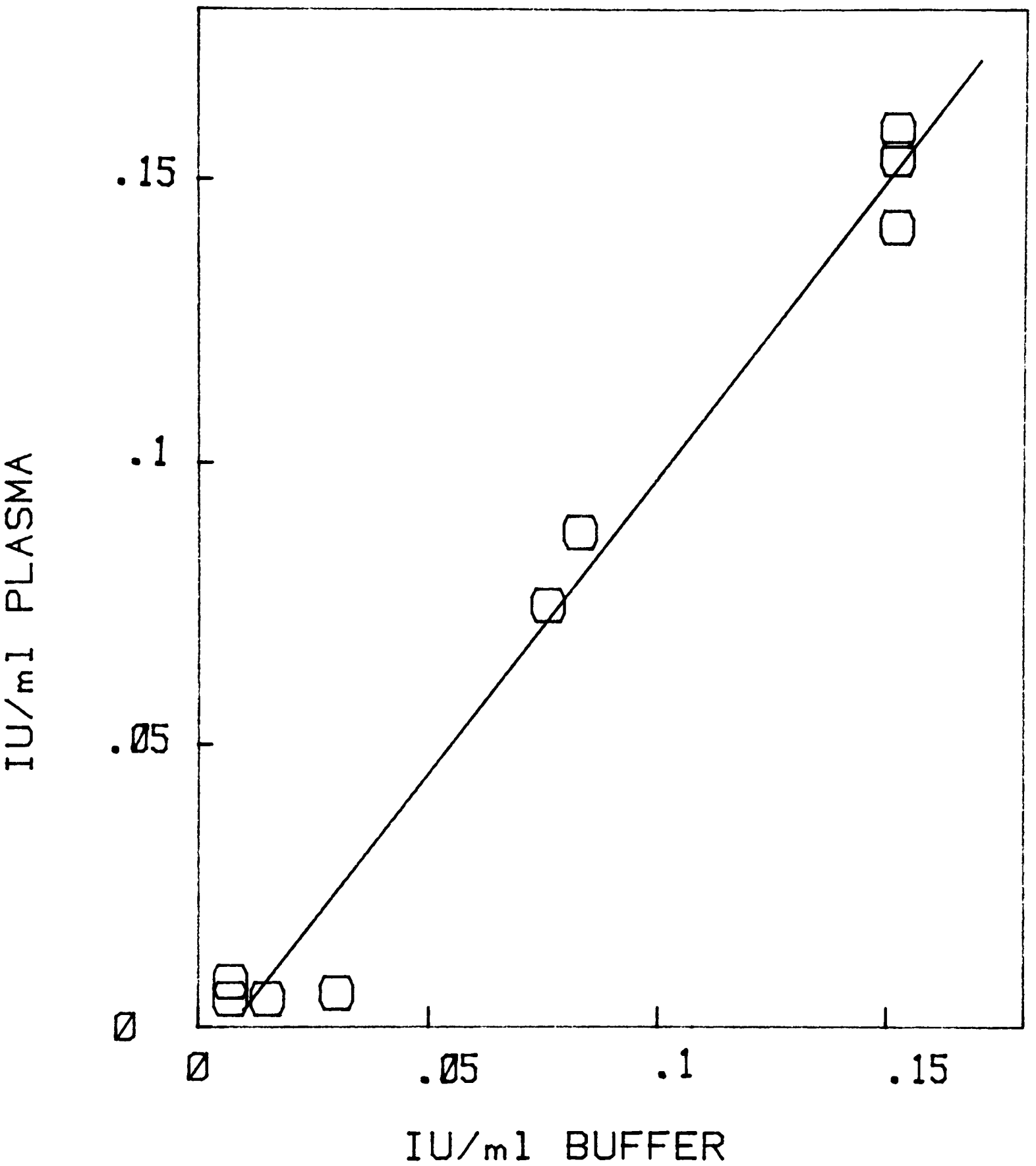

Figure 5.10 Correlation plot for CK assays performed in buffer and plasma samples. Data are normalised to pH 7.0.

to 20mM by adding glucose. The reaction was initiated by the addition of creatine phosphate. Table 5.2 shows data obtained for the activity of creatine kinase as supplied, in buffer at pH 7.0 and in plasma at pH 7.7. The data for plasma are normalised to pH 7.0, as the activity of CK (for the reverse reaction) is lower at pH 7.7 than at pH 7.0, as illustrated in figure 5.2. A correlation plot for the normalised data is presented in figure 5.10, from which a correlation coefficient of 0.97 was obtained, n=9, $y=-1.05\mp0.08$.

5.4.1 Conclusions

The performance of the glucose enzyme electrode-based assay for creatine kinase in plasma suggests that the method could undergo a more detailed comparison with present methods using authentic post-AMI samples. In addition, the enzyme electrode could be further refined by the co-immobilisation of glucose oxidase and hexokinase, thus eliminating the necessity to add the latter to the assay sample.

References

1. Blum, H. E., Weber, B., Deus, B. and Gerok, W. Z. Physiol. Chem. 359, 1058, (1978).

2. Lang, H. in: Creatine kinase isoenzymes. Lang, H. ed. New York: Springer-Verlag (1981).

3. Blum, H. E. in: Creatine kinase isoenzymes. Lang, H. ed. New York: Springer-Verlag (1981).

4. Wurzburg, U., Hennrich, N. and Lang, H. Klin. Woehenschr. 54, 357, (1976).

5. Hegler, R. in: Creatine kinase isoenzymes. Lang, H. ed. New York: Springer-Verlag (1981).

6. Oliver, I. T. Biochem. J. 61, 116, (1955).

7. Rosalki, S. B. J. Lab. Clin. Med. 69, 696, (1967).

8. Ottaviani, F. and Pagani, E. Ouad. Sclavo. Diagn. 12, 373, (1976).

9. Swanson, J. R. and Wilkinson, J. H. in: Standard methods in clinical chemistry. Cooper, G. R. ed. New York: Academic press (1972).

10. Gerhardt, W. and Kofoed, B. Scand. J. Clin. Lab. Invest. 35, 381, (1975).

11. Knob, M. and Rosenmund, H. Med. Lab. (Stuttg.) 31, 213, (1978).

12. Guilbault, G. G., Kuan, S. S. and Yuan, C-L. Anal. Chem. 53, 190, (1981).

CHAPTER 6

ELECTROCHEMICALLY COUPLED ENZYMATIC OXIDATION REACTIONS

Introduction

6.1.1 Ferricinium ion as a mediator for oxido-reductases

It has been shown that the ferricinium ion of a range of ferrocene derivatives will act as electron acceptors for glucose oxidase and that 1,1′-dimethylferrocene is a suitable mediator for incorporation into an amperometric enzyme electrode for the detection of glucose in biological samples. This chapter describes the assessment of ferrocene monocarboxylic acid as a mediator in other enzyme catalysed oxidations. The diagnostic value of D. C. cyclic voltammetry is applied to establish whether reactions catalysed by a range of oxido-reductases could be coupled electrochemically. Where possible, quantitative kinetic data for the reaction between the ferricinium ion and the enzyme were obtained.

Experimental

6.2.1 Materials

The flavo-proteins pyruvate oxidase (EC 1.2.3.3), xanthine oxidase (EC 1.2.3.2), cholesterol oxidase (EC 1.1.3.6), choline oxidase (EC 1.1.3.17), oxalate oxidase (EC 1.2.3.4), sarcosine oxidase (EC 1.5.3.1), lipoamide dehydrogenase (EC 1.6.3.4) and glutathione reductase (EC 1.6.4.2) were supplied by Boehringer and stored at $-20^{o}C$. The respective concentrations of the flavo-proteins are expressed in terms of the amount of catalytically-active flavin, as described in section 4.2.1.

Carbon monoxide oxido-reductase was isolated (23) from Pseudomonas thermocarboxydovorans by Dr. J. Colby, Biochemistry Department, Sunderland Polytechnic and supplied at a concentration of 8.6 mg ml^{-1}, in phosphate buffer containing 50% ethanediol as a stabilizer. Before use, the enzyme was dialysed against 20mM Tris-HCl (pH 7.5) at $4^{o}C$, and purified by FPLC using an analytical Mono-Q column. The enzyme was loaded on to the column at a concentration of 1.0 mg ml^{-1} in 20mM Tris-HCl pH 7.5 (buffer A) and eluted with a linear ionic strength gradient using buffer B (A + 1.0M KCl). Carbon monoxide oxido-reductase eluted as one major peak at an ionic strength equivalent to 35% buffer B, figure 6.1.

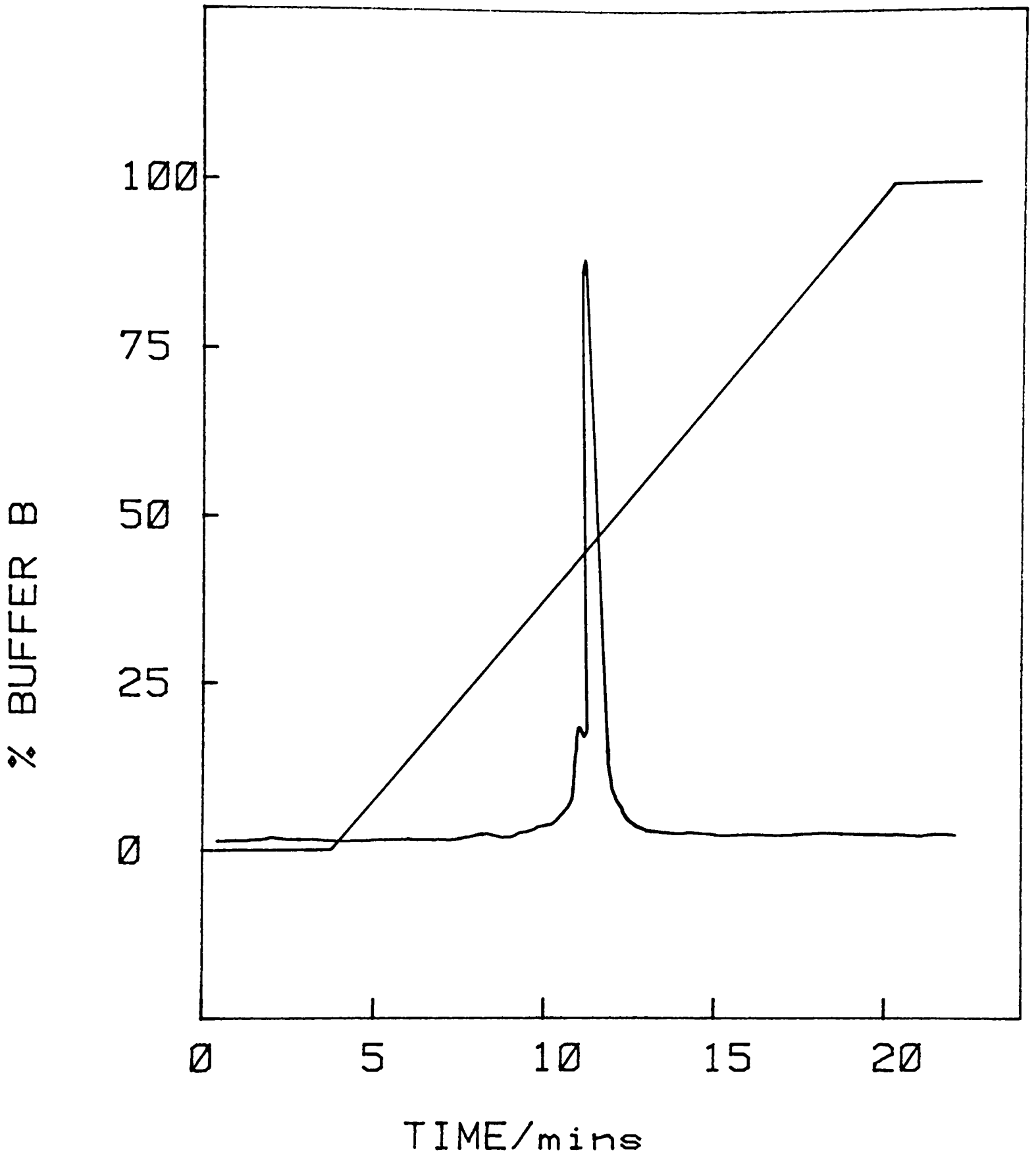

Figure 6.1 FPLC profile of carbon monoxide oxido-reductase from Pseudomonas thermocarboxydovorans.

Purification of the quino-protein alcohol dehydrogenase (EC 1.1.99.8) is described in section 6.2.1. Superoxide dismutase (EC 1.15.1.1) was the kind gift of Dr. J. Bannister. Lactate dehydrogenase (EC 1.1.1.27) and isocitrate dehydrogenase (EC 1.1.1.42) were supplied by Boehringer.

Sodium lactate, sodium isocitrate, sarcosine, sodium pyruvate, xanthine, cholesterol, potassium oxalate, choline, reduced nicotinamide adinine dinucleotide (NADH) and reduced nicotinamide adinine dinucleotide phosphate (NADPH) were supplied by Boehringer. Carbon monoxide was supplied by BOC. Ferrocene monocarboxylic acid was supplied by Flourochem. Horse heart cytochrome c type VI, was supplied by Sigma and purified before use to remove deamidated forms (1).

6.2.2 Electrolytes

All experiments used 100mM Tris-HCl buffer pH 7.0, except those involving oxalate oxidase which used 100mM succinate buffer pH 3.0, and those with alcohol dehydrogenase which used 100mM borax-NaOH, pH 10.5, containing 14mM NH_4Cl.

6.2.3 Electrochemical experiments

All experiments used the electrochemical cell described in section 3.2.2 incorporating a 4mm disc pyrolytic graphite working

electrode, except in experiments on lipoamide dehydrogenase and glutathione reductase where a 4mm disc gold electrode was used. In experiments where cytochromes c was investigated with carbon monoxide oxido-reductase, a bis(4,4′-pyridyl)-1,2-ethene modified gold electrode was used (2).

Results and discussion

6.3.1 Identification of electrochemically coupled reactions

D. C. cyclic voltammetry experiments were performed in argon-saturated solutions using the following protocol. Firstly, the reversible electrochemistry of ferrocene monocarboxylic acid (200μM) in a suitable electrolyte was established by recording voltammograms at different scan rates (ν=1-100mVs^{-1}) over the potential range 0-400mV. Substrate was then added to the cell, typically to a final concentration of 10mM and always in excess of the Michaelis-Menten constant for the enzyme. A set of voltammograms were recorded to assess the effect of the substrate upon the electrochemistry of the mediator. Enzyme was then added to final concentrations in the range 10-100μM. If an enhanced anodic current was obtained, and the dependence of the current function upon the scan rate was indicative of a catalytic reaction, the experiment was repeated adding the substrate as the final component to insure that the reaction was dependent upon the presence of substrate.

Under the conditions that were used, none of the substrates interferred with the electrochemistry of the ferrocene. Over the range 0-400mV vs SCE, none of the substrates or enzymes exhibited any direct electrochemistry.

6.3.2 Flavo-protein oxido-reductases

In 1978 Clark (3), listed twenty-seven flavo-protein oxidase that were known to generate hydrogen peroxide. Some were reported to use oxygen specifically as an electron acceptor e. g. cholesterol oxidase, whereas others like glucose oxidase used a variety of electron acceptors including phenazine methosulphate, N,N,N′,N′-tetramethyl-4-phenylene diamine and 2,6-dichlorophenol indophenol (4).

6.3.3 Oxygen-specific flavo-proteins

The flavo-proteins that had previously been reported to use oxygen specifically as an electron acceptor, choline oxidase, oxalate oxidase and cholesterol oxidase, table 6.1, did not use the ferricinium ion of ferrocene monocarboxylic acid as an oxidant, since no catalytic current was observed in the voltammograms in the presence of the respective enzymes and substrates. Consequently, amperometric enzyme electrodes based on ferrocene and incorporating these enzymes could not be developed.

6.3.4 Non-oxygen specific flavo-proteins

The flavo-proteins that were reported to be non-specific with respect to the electron acceptor, table 6.1, all gave an enhanced anodic current in the presence of their substrate, indicative of a

Table 6.1 Flavo-proteins

Flavo-protein	Substrate	RMM x 10^{-5}	Oxygen-specific
pyruvate oxidase	pyruvate	1.0	x
xanthine oxidase	xanthine, purines aldehydes	3.0	x
sarcosine oxidase	sarcosine	1.74	x
cholesterol oxidase	cholesterol	1.2	✓
oxalate oxidase	oxalate	1.2	✓
choline oxidase	choline	8.0	✓
lipoamide dehydrogenase	NADH	1.0	x
glutathione reductase	NADPH	1.0	x
CO oxido-reductase	CO	2.3	x

catalytically coupled oxidation reaction. For example, figure 6.2, shows the catalytically coupled oxidation of pyruvate via pyruvate oxidase.

Second order homogeneous rate constants were calculated from the data for the reactions of pyruvate oxidase (POX), xanthine oxidase (XOD), sarcosine oxidase (SOX), lipoamide dehydrogenase and glutathione reductase with ferricinium monocarboxylic acid, using the theory of Nicholson and Shain (5) described in section 2.1.5. These values are compared with that for glucose oxidase in table 6.2.

From this investigation it was concluded that, given suitable methods of enzyme immobilization, amperometric enzyme electrodes similar to that described in chapter 4 could be developed for pyruvate, xanthine(and purines and aldehydes) and sarcosine based on the following reactions, eqs 6.1-6.3,

$$\text{pyruvate} + H_2O + 2Fecp_2R^+ \xrightarrow{POX} \text{acetate} + CO_2 + 2Fecp_2R + 2H^+ \quad [6.1]$$

$$\text{xanthine} + H_2O + 2Fecp_2R^+ \xrightarrow{XOD} \text{urate} + 2Fecp_2R + H^+ \quad [6.2]$$

$$\text{sarcosine} + 2Fecp_2R^+ \xrightarrow{SOX} \text{glycine} + 2Fecp_2R + 2H^+ \quad [6.3]$$

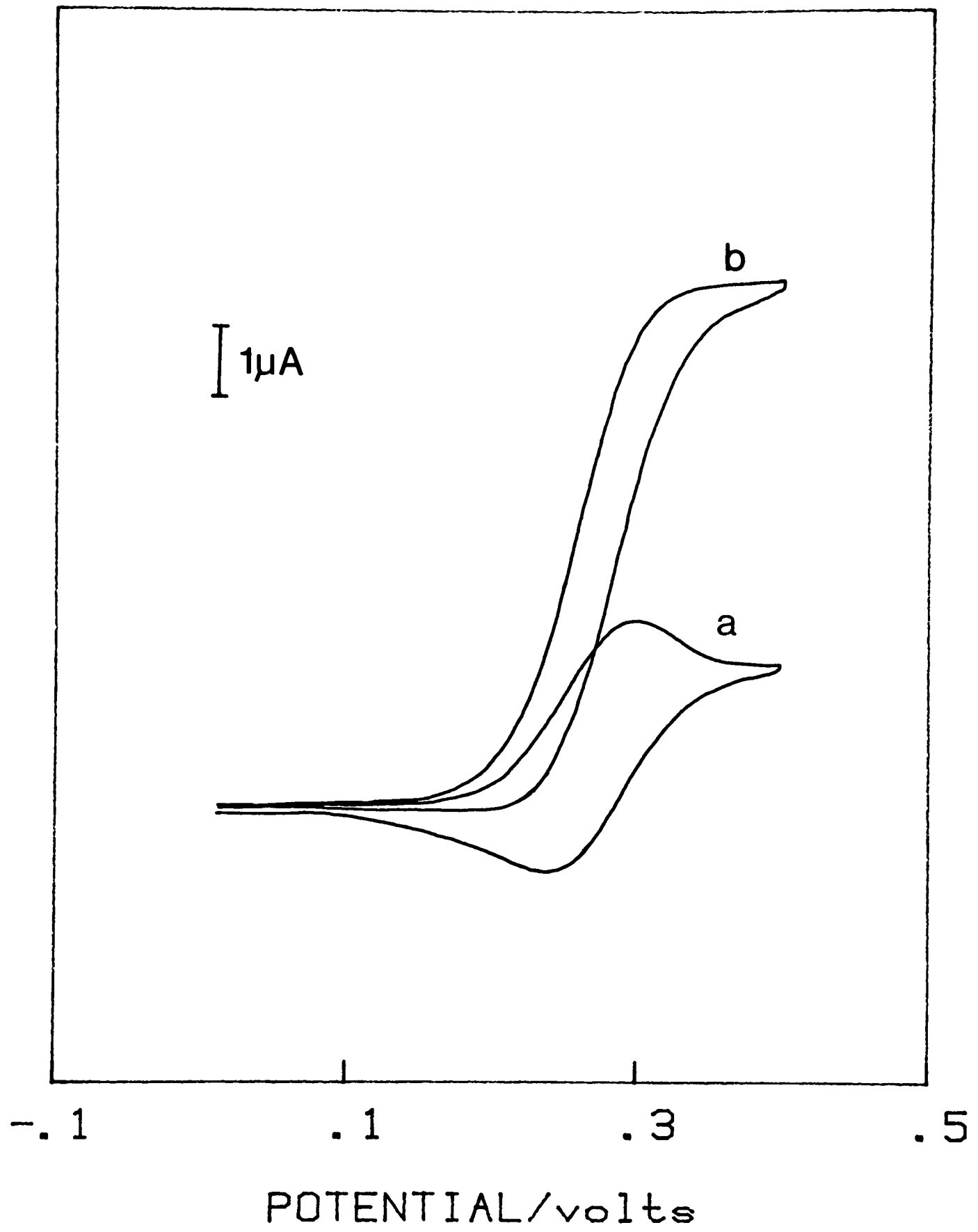

Figure 6.2 (a) D. C. cyclic voltammogram at a pyrolytic graphite electrode of ferrocene monocarboxylic acid (200μM) in 100mM Tris-HCl pH 7.0, in the presence of 20mM pyruvate at a scan rate of $1mVs^{-1}$. (b) as for (a), but with the addition of 10μM pyruvate oxidase.

Table 6.2 Ferricinium monocarboxylic acid rate constants

Enzyme	$k_s \times 10^{-5}$ l mol^{-1} s^{-1}
glucose oxidase	2.0
pyruvate oxidase	0.2
xanthine oxidase	4.0
sarcosine oxidase	0.1
cholesterol oxidase	-
choline oxidase	-
oxalate oxidase	-
lipoamide dehydrogenase	0.2
glutathione reductase	2.0
alcohol dehydrogenase	0.6
carbon monoxide oxido-reductase	4.0

All rates determined at pH 7.0 and 20°C.

6.3.5 NAD(P)H linked enzymes

Particularly interesting are the results for lipoamide dehydrogenase (LADH), eq 6.4, and glutathione reductase ($GSSG_{red}$), eq 6.5, which catalyse the oxidation of NADH and NADPH, respectively.

$$NADH + 2Fecp_2R^+ \xrightarrow{LADH} NAD^+ + H^+ + 2Fecp_2R \qquad [6.4]$$

$$NADPH + 2Fecp_2R^+ \xrightarrow{GSSG_{red}} NADP^+ + H^+ + 2Fecp_2R \qquad [6.5]$$

Whilst electro-oxidation of NAD(P)H can be effected non-enzymatically, these enzymatic methods may have some merit.

Direct oxidation of NAD(P)H at a pyrolytic graphite electrode has been reported (6,7). However, the process has a large over-potential ca. 600mV vs. SCE and is difficult to achieve reproducibly (6). In the process of direct electrochemical oxidation, formation of the partially oxidised $NAD(P)^{\bullet}$ occurs and this species is able to undergo further chemical reactions, predominantly dimerisation (6). Such reactions are undesirable in a catalytically coupled system, as this can lead to the depletion of enzymatically active NAD(P).

Alternatively, low-potential 2-electron acceptors can be used to effect the oxidation of NAD(P)H, these include benzoquinone (7),

phenazine methosulphate and 4-phenylenediamine (8). The problems associated with the incorporation of these molecules into an enzyme electrode have been discussed in section 3.1.5.

6.3.6 Systems with two enzymes acting sequentially

The effective coupling of NADPH and NADH oxidation, eqs 6.4 and 6.5, suggested further experiments in which a second enzyme was incorporated to catalyse the regeneration of NAD(P)H by the oxidation of a second substrate, SH_2, eq 6.6.

$$SH_2 + NAD(P)^+ \longrightarrow S + NAD(P)H + H^+ \qquad [6.6]$$

Figure 6.3(a), shows a voltammogram of ferrocene monocarboxylic acid in the presence of lipoamide dehydrogenase, NAD^+ and L-lactate. It is only upon addition of L-lactate dehydrogenase, to the system that a catalytic current is observed, figure 6.3(b). The ommision of any one of the components shown in the scheme, figure 6.4(a), results in an absence of catalytic behaviour.

In a similar set of experiments the NADP-linked enzyme isocitrate dehydrogenase, which catalyses the oxidation of isocitrate to α-ketoglutarate, was coupled electrochemically via glutathione reductase. A catalytic current was observed only when all the components shown in the scheme, figure 6.4(b), were present.

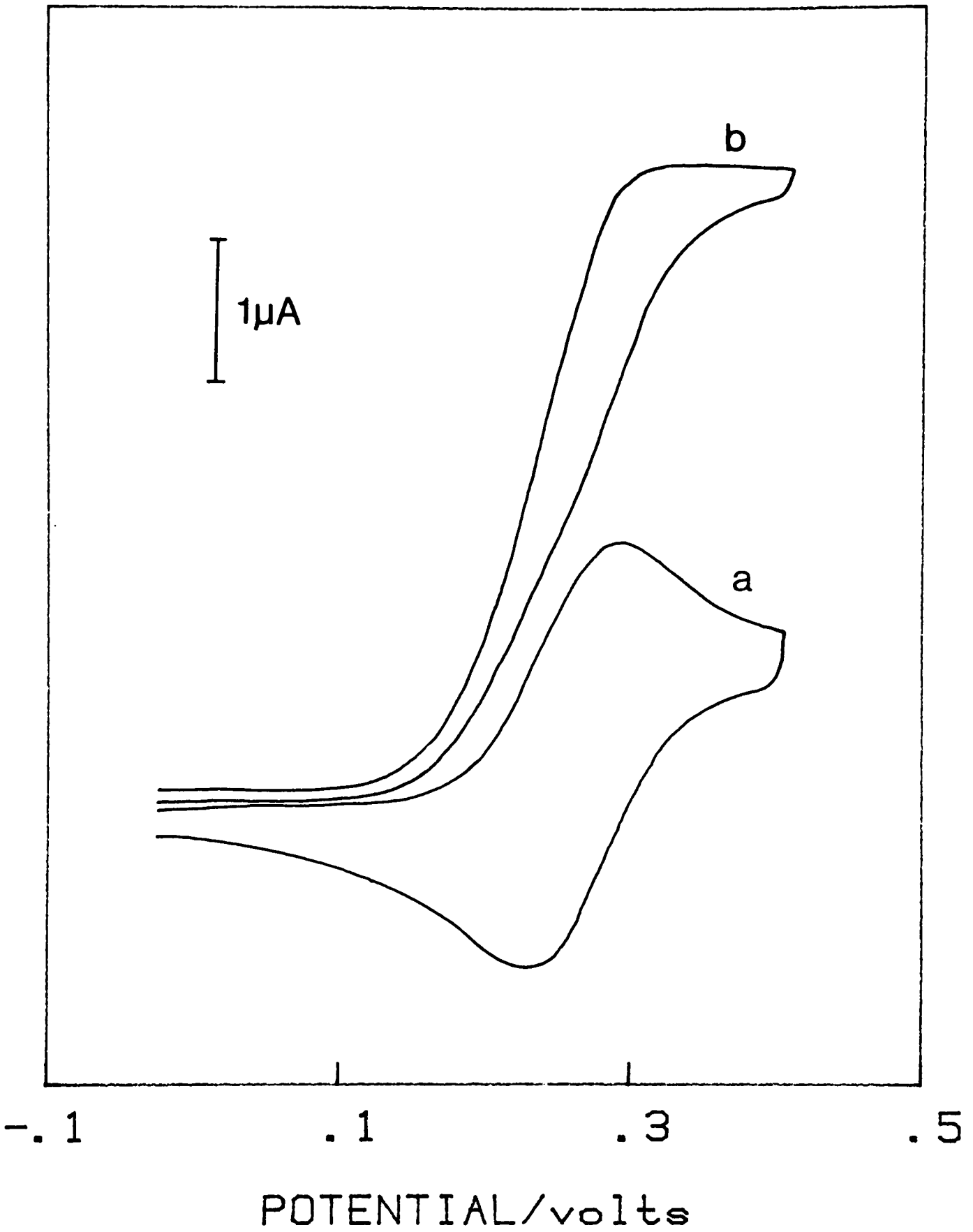

Figure 6.3 (a) D. C. cyclic voltammogram at a gold electrode of ferrocene monocarboxylic acid (200μM) in 100mM Tris-HCl pH 7.0, in the presence of 20μM lipoamide dehydrogenase, 1mM NAD and 10mM L-lactate at a scan rate of $1mVs^{-1}$. (b) as for (a), but with the addition of 5IU ml^{-1} lactate dehydrogenase.

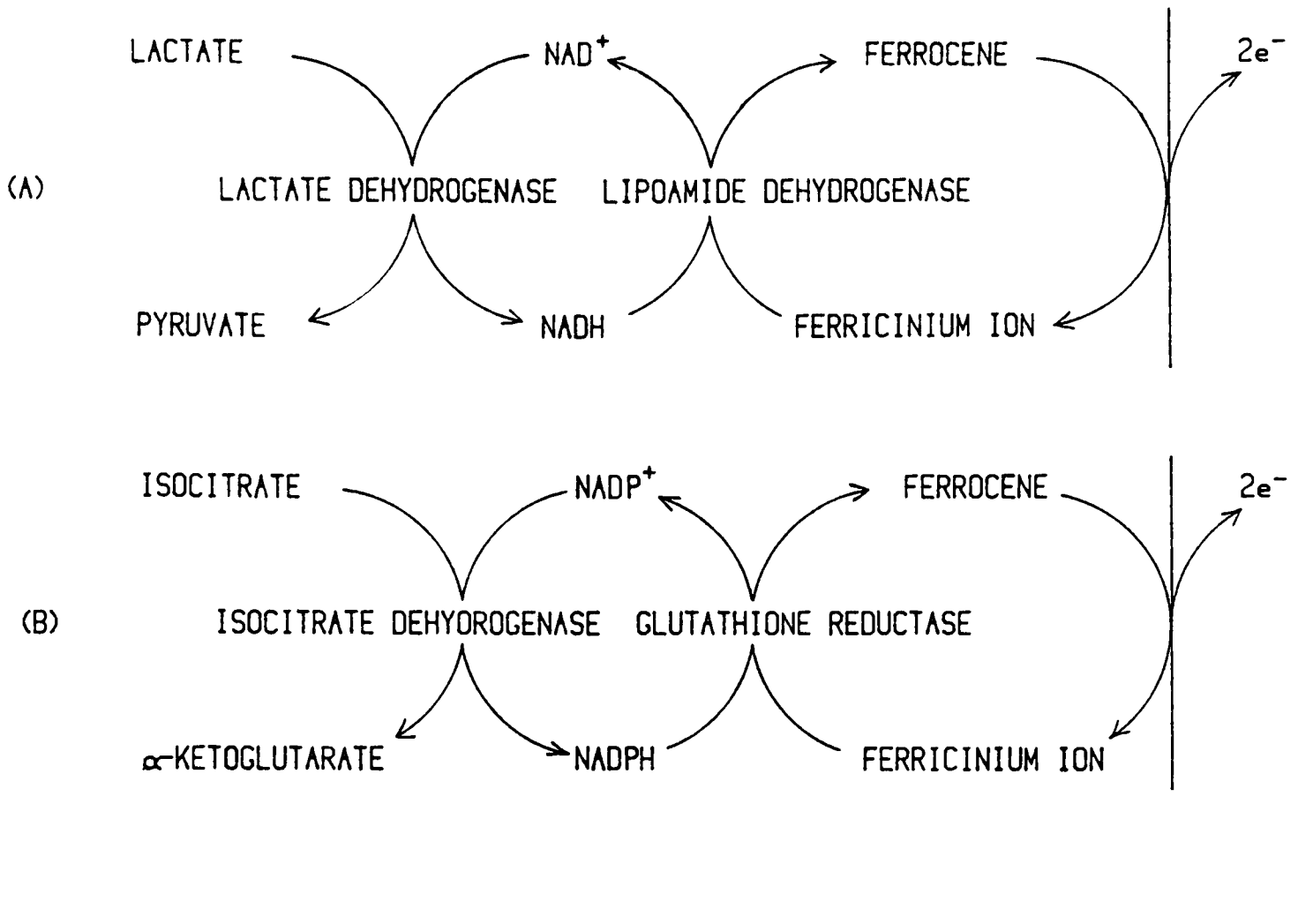

Figure 6.4 Schemes (A) and (B), show the respective reaction sequences for the electrochemically coupled enzymatic oxidation of L-lactate and isocitrate.

These coupled reactions illustrate the possibility of devising enzyme electrodes in which two enzymes are co-immobilised. The wide range of biological molecules that could be assayed by these systems is emphasised by the ubiquity of NAD(P)-linked enzymes.

6.3.7 Quino-proteins

In addition to oxido-reductases that use NAD(P) and flavins as co-factors, there are a limited number of dehydrogenases, termed quino-proteins, which contain a novel prosthetic group, figure 7.2. An important property of these enzymes is that they do not autoxidise, but, will use a range of organic dyes as electron acceptors (9). These enzymes, table 7.2, have recently been reviewed by Duine (10). A description of the biochemistry of the enzyme alcohol dehydrogenase, which catalyses the oxidation of methanol and other primary alcohols to aldehydes, is included in section 7.1.5.

Figure 6.5(a), shows a voltammogram of ferrocene monocarboxylic acid in the presence of methanol. When ADH is added, a catalytic current is observed, figure 6.5(b). The overall reaction catalysed by the enzyme is shown in equation 6.7.

$$CH_3OH + 2Fecp_2R^+ \xrightarrow{ADH} HCHO + 2Fecp_2R + 2H^+ \qquad [6.7]$$

The second order rate constant for the reaction between enzyme and mediator at the optimum pH for the oxidation of methanol (see

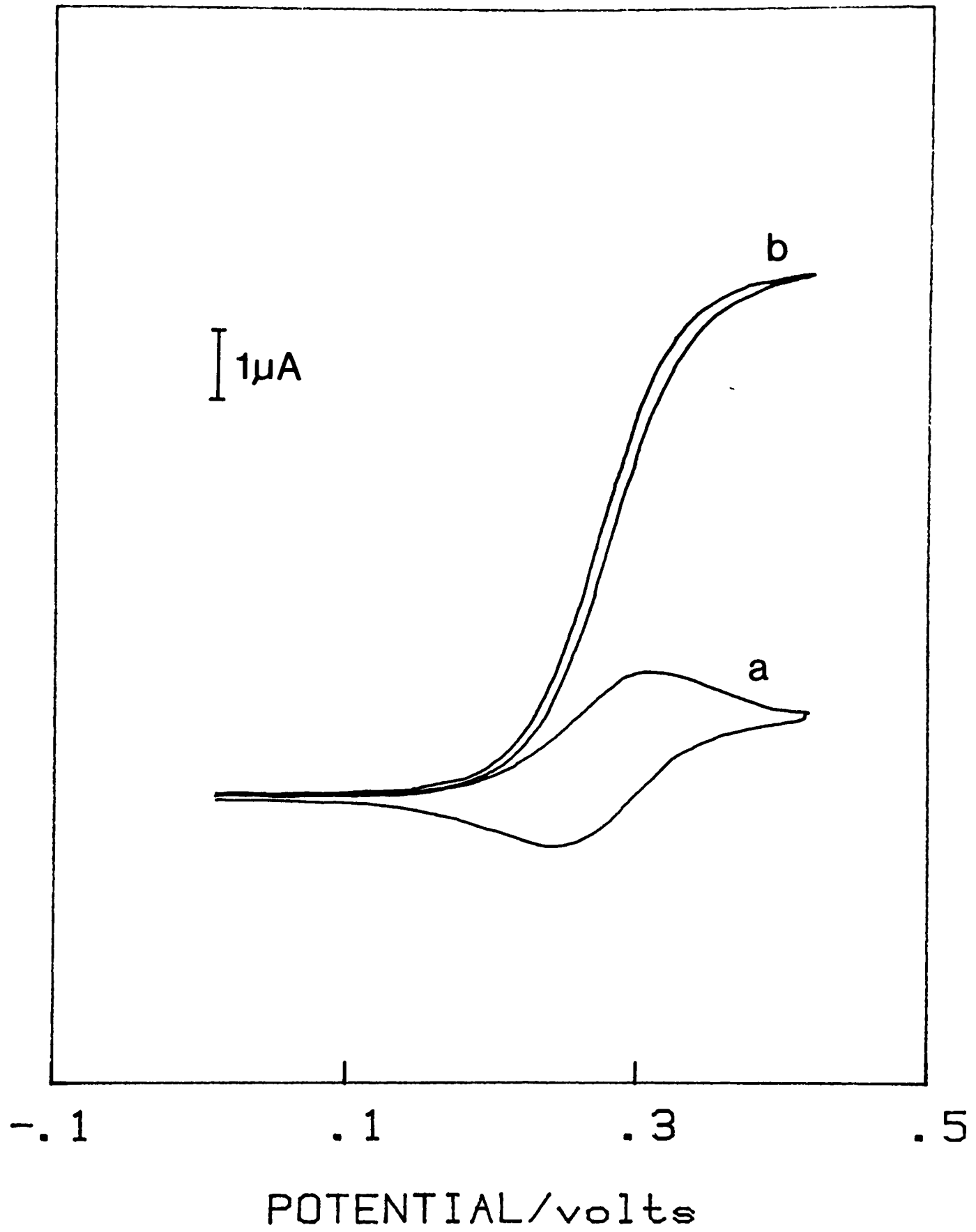

Figure 6.5 (a) D. C. cyclic voltammogram at a pyrolytic graphite electrode of ferrocene monocarboxylic acid (200μM) in 100mM Borax-NaOH pH 10.5, in the presence of 14mM NH_4Cl and 50mM methanol at a scan rate of $1mVs^{-1}$. (b) as for (a), but with the addition of 10μM alcohol dehydrogenase.

section 7.1.5), is included in table 6.2.

Since there is considerable interest in alcohol-monitoring for whole-blood analysis, water quality control, and fermentation control, an amperometric enzyme electrode based upon this coupled reaction is being developed in collaboration with the Cranfield Institute of Technology.

6.3.8 Carboxydo bacteria

Of all the atmospheric pollutants carbon monoxide is the most abundant. A limited range of sensors, based upon the electro-oxidation of CO at a gold electrode (1.4V vs. SCE), have been developed (11). However, when analysing authentic samples, the most important problem with these devices is a lack of selectivity, as many other gases are electro-active e. g. hydrogen sulphide, nitric oxide and nitrogen dioxide. To date, enzyme electrodes have largely been overlooked for gas sensing.

Carboxydo bacteria (12,13), which are able to grow aerobically on carbon monoxide as the sole carbon and energy source, contain an enzyme, carbon monoxide oxido-reductase (COOR), that specifically catalyses the oxidation of carbon monoxide to carbon dioxide, with water as the oxygen donor (14,15), eq 6.8.

$$CO + H_2O \xrightarrow{COOR} CO_2 + 2H^+ + 2e^- \qquad [6.8]$$

The properties of carbon monoxide oxido-reductase isolated from Pseudomonas thermocarboxydovorans are summarised in table 6.3. The enzyme is not NAD(P)-linked, but will use a range of non-physiological electron acceptors including methylene blue, phenazine methosulphate and N,N,N′,N′-tetramethyl-4-phenylenediamine (14).

6.3.9 Ferrocene as an oxidant for CO oxido-reductase

Ferrocene monocarboxylic acid was investigated as a novel electron acceptor for carbon monoxide oxido-reductase. The electrolyte was first degassed with argon and then saturated with CO, ca. 0.88mM (14), under these conditions the characteristic reversible electrochemistry of the mediator was unchanged, figure 6.6(a). Upon addition of COOR to the solution a voltammogram, figure 6.6(b) exhibiting a catalytic wave was obtained, indicative of a the following coupled reaction, eq 6.9.

$$CO + H_2O + 2Fecp_2R^+ \xrightarrow{COOR} CO_2 + 2H^+ + 2Fecp_2R \quad [6.9]$$

The second order homogeneous rate constant for the reaction between the ferricinium ion and the reduced enzyme is given in table 6.2. An enzyme electrode for the detection of carbon monoxide is being developed based on this system, in collaboration with Cranfield Institute of Technology.

Table 6.3 Properties of CO oxido-reductase

Source:	Pseudomonas thermocarboxydovorans
RMM:	230 000
Co-factors:	FAD, molybdenum, iron, labile sulphide in the ratio 1:1:4:4
K_M CO:	6.5μM
pH optimum:	7.0
Co-substrate:	Methylene blue
Inhibitors:	Methanol

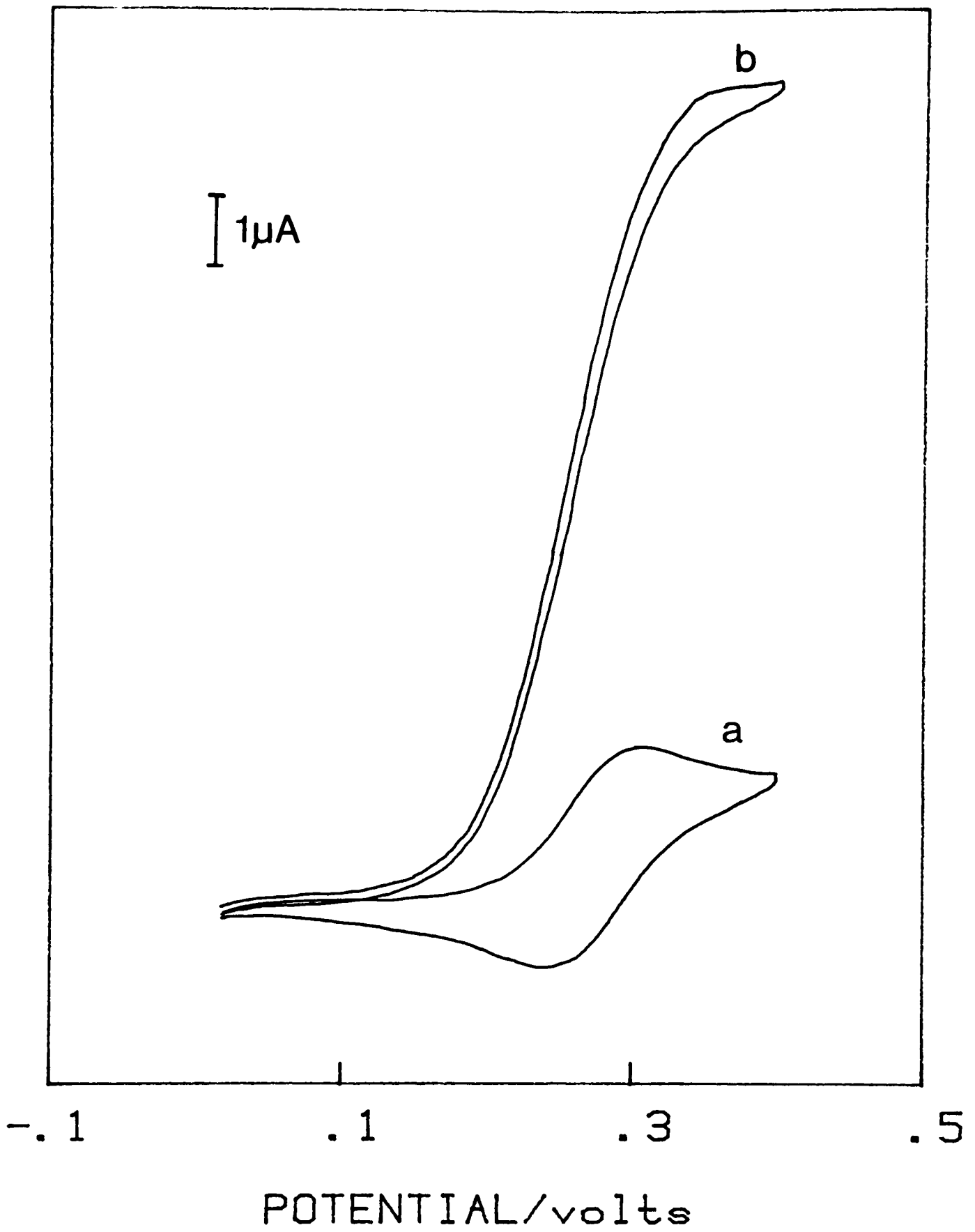

Figure 6.6 (a) D. C. cyclic voltammogram at a pyrolytic graphite electrode of ferrocene monocarboxylic acid (200μM) in 100mM Tris-HCl pH 7.0, saturated with carbon monoxide at a scan rate of $1mVs^{-1}$. (b) as for (a), but with the addition of 20μM carbon monoxide oxido-reductase.

6.3.10 Cytochrome c as an oxidant for CO oxido-reductase

A further investigation of the interaction of carbon monoxide oxido-reductase with horse heart cytochrome c (HHcyt c) was undertaken, based on the report by Meyer (14) that the enzyme will reduce this respiratory chain redox protein in aerobic solutions. Meyer, postulated that this reaction is mediated by the superoxide radical, since xanthine oxidase which resembles this enzyme in its co-factor complement (16), has been shown by Fridovich (17) to channel ca. 22% of its reducing equivalents into superoxide radical production, eq 6.10, the rest being converted to hydrogen peroxide, eq 6.11.

$$2O_2 + \text{xanthine} \xrightarrow{\text{XOD}} 2O_2^- + \text{urate} + 2H^+ \qquad [6.10]$$

$$O_2 + \text{xanthine} \xrightarrow{\text{XOD}} H_2O_2 + \text{urate} \qquad [6.11]$$

The superoxide radical can effect a number of secondary reactions, notably ferricytochrome c reduction (18), eq 6.12.

$$\text{HHcyt}^{3+}\underline{c} + O_2^- \longrightarrow \text{HHcyt}^{2+}\underline{c} + O_2 \qquad [6.12]$$

The reversible electrochemistry of horse heart cytochrome c at a bis(4,4′-pyridyl)-1,2-ethene modified gold electrode has been demonstrated by Eddowes and Hill (19). Hill and Walton (20,21) have shown that the terminal oxidase of the respiratory chain of

Pseudomonas aerogenosa can be supplied with reducing equivalents via cytochrome c for the reduction of oxygen to water.

Horse heart ferricytochrome c was investigated as an alternative oxidant to the ferricinium ion for carbon monoxide oxido-reductase. Figure 6.7(a), shows a D. C. cyclic voltammogram of the horse heart cytochrome c (500μM), in CO-saturated elctrolyte at pH 7.0. Upon addition of COOR to the solution, figure 6.7(b), an enhanced anodic current was obtained.

Since care had been taken to eliminate oxygen from the electrolyte before the experiment, the coupled reaction did not appear to be mediated by the superoxide radical. However, if the reduction of cytochrome depended upon, either traces of oxygen remaining in the electrolyte or being introduced as impurities in the gas supply, then addition of the enzyme superoxide dismutase (SOD) (34) which catalyses the following reaction, eq 6.13,

$$2O_2^- + 2H^+ \xrightarrow{SOD} H_2O_2 + O_2 \qquad [6.13]$$

would inhibitor cytochrome reduction. This should uncouple the catalytic process observed in figure 6.7(b). No change in figure 6.7(b), occurred upon addition of SOD (20 IU ml^{-1}) to the solution, suggesting that the coupled reaction involves direct reduction of ferricytochrome c by the reduced enzyme, eq 6.14.

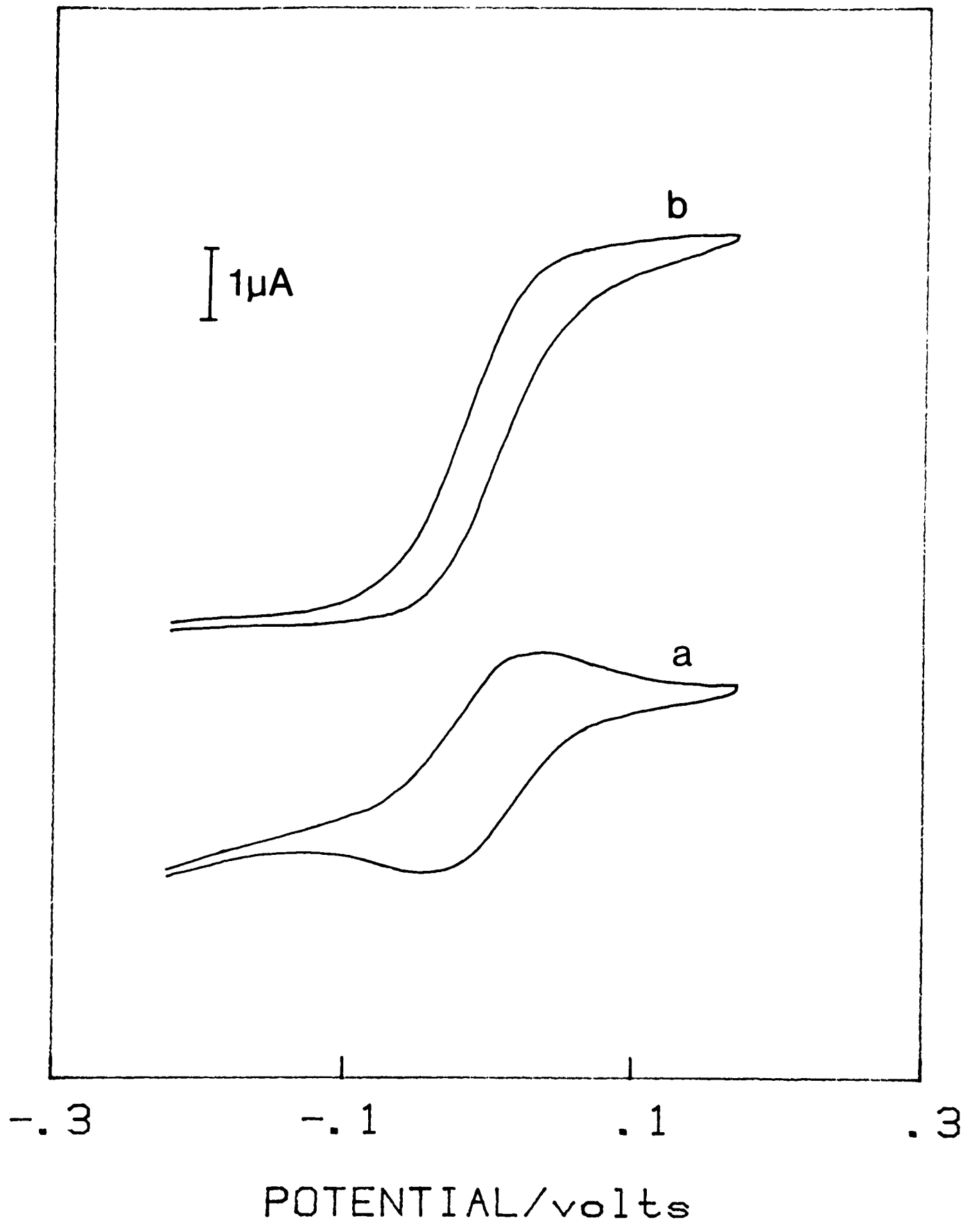

Figure 6.7 (a) D. C. cyclic voltammogram of Horse Heart cytochrome c at a gold electrode modified with bis(4,4′-pyridyl)ethene in 50mM Phosphate-perchlorate pH 7.0, saturated with carbon monoxide at a scan rate of $1mVs^{-1}$. (b) as for (a), but with the addition of 20μM carbon monoxide oxido-reductase.

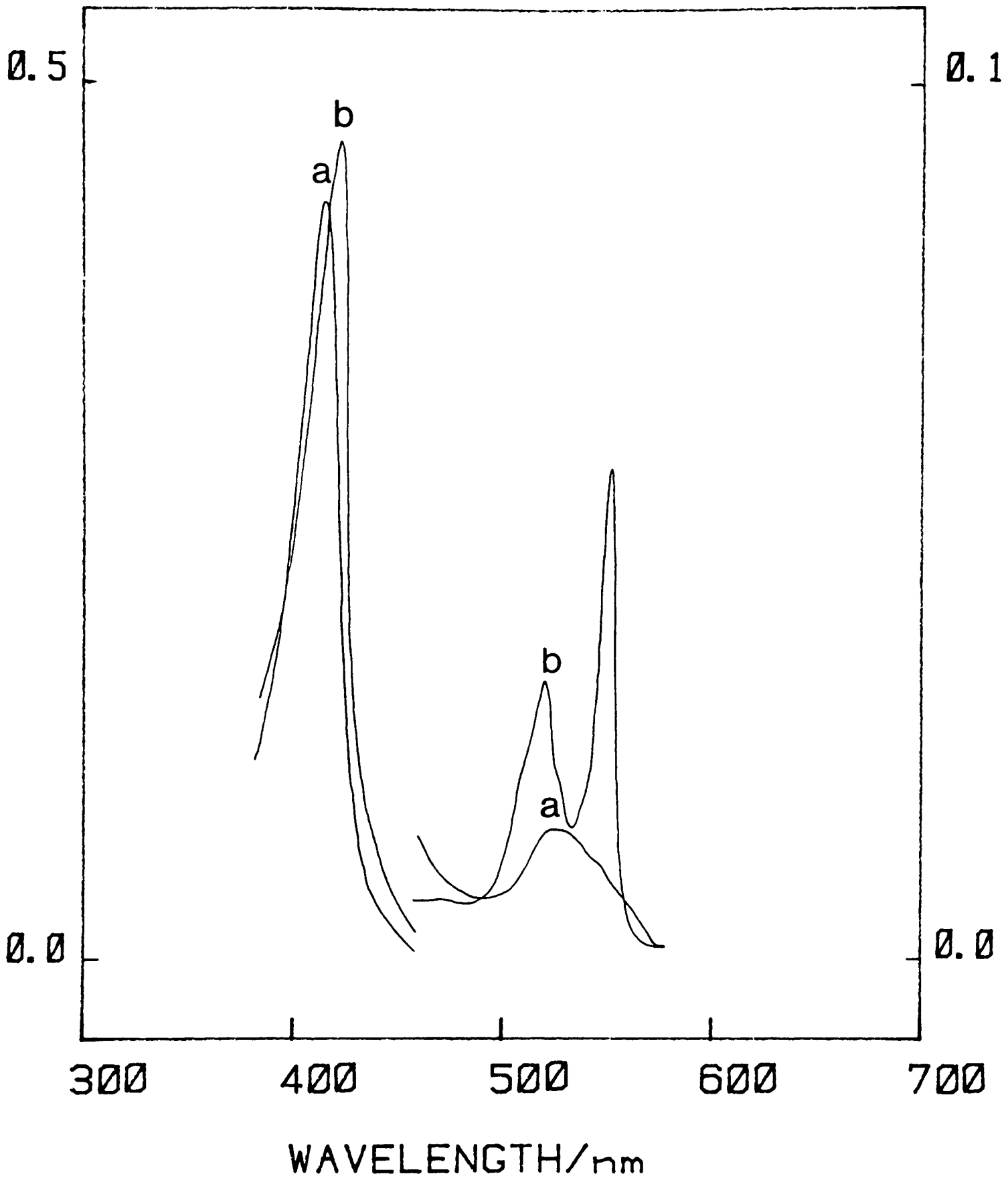

Figure 6.8 (a) UV spectrum of an aliquot of solution containing Horse Heart ferricytochrome c from figure 6.7(a), diluted 20 fold into buffer. (b) as for (a), but using an aliquot from figure 6.7(b).

$$2HHcyt^{3+}\underline{c} + CO + H_2O \xrightarrow{COOR} 2HHcyt^{2+}\underline{c} + CO_2 + 2H^+ \quad [6.14]$$

The homogeneous second order rate constant for the reaction between ferricytochrome c and the reduced enzyme was $3.0x10^4$ l mol^{-1} s^{-1} (pH 7.0, 20°C.).

Figure 6.8 shows the spectrum of an aliquot of the solution taken from the electrochemical cell before and after the addition of the enzyme. The changes in the absorption spectrum (18) are consistent with the reduction of ferricytochrome c, figure 6.8(a) to ferrocytochrome c figure 6.8(b), as shown in eq 6.14. The changes in the spectrum are dependent upon the presence of both the enzyme and substrate.

6.4.1 Conclusions

The range of oxido-reductases, table 6.2, that can utilise the ferricinium ion as an oxidant illustrates the value of this type of mediator to the development of enzyme electrodes. In addition to the possibility of devising an enzyme electrode, the use of the electron transfer protein, cytochrome c, with the enzyme carbon monoxide oxido-reductase emphasises new areas for research involving the use of physiological mediators (electron transfer proteins) for electron transfer between enzyme and electrode.

References

1. Brautigan, D. L., Ferguson-Miller, S. and Margoliash, E. Methods Enzymol. 53, 128, (1978).

2. Eddowes, M. J. and Hill, H. A. O. J. Amer. Chem. Soc. 101, 4463, (1979).

3. Clark, L. C. Biotechnol. Bioeng. Symp. 3, 377, (1972).

4. Aleksandrovskii, Y. A., Bezhikina, L. V. and Rodinov, Y. V. Biokhimica 46, 708, (1980).

5. Nicholson, R. S. and Shain, I. Anal. Chem. 36, 706, (1964).

6. Torstensson, A. and Gorton, L. J. Electroanal. Chem. 130, 199, (1981).

7. Huck, H. and Schmidt, H-L. Angew. Chem. Int. Ed. Eng. 20, 402, (1981).

8. Kitani, A. and Miller, L. L. J. Amer. Chem. Soc. 103, 3595, (1981).

9. Ghosh, R. and Quayle, J. R. Biochem. J. 199, 245, (1981).

10. Duine, J. A. and Frank, J. TIBS 6, 278, (1981).

11. Sedlak, J. M. and Blurton, K. F. J. Electrochem. Soc. 123, 1476, (1976).

12. Uffen, R. L. Enzyme microb. Tech. 3, 197, (1981).

13. Kim, Y. M. and Hegeman, G. D. J. Bacteriol. 148, 904, (1981).

14. Meyer, O. J. Biol. Chem. 257, 1333, (1982).

15. Drake, H. L., Ringsdale, S. W., Clark, J. E., Ljingdahl, L. G. and Lundie, L. L. J. Biol. Chem. 258, 2364, (1983).

16. Massey, V., Branby, P. E., Komai, H. and Palmer, G. J. Biol. Chem. 244, 1682, (1969).

17. Fridovich, I. J. Biol. Chem. 245, 4053, (1970).

18. McCord, J. and Fridovich, I. J. Biol. Chem. 243, 5753, (1968).

19. Albery, W. J., Eddowes, M. J., Hill, H. A. O. and Hillman, A. R. J. Amer. Chem. Soc. 103, 3904, (1981).

20. Hill, H. A. O., Higgins, I. J. and Walton, N. J. FEBS Lett. 126, 282, (1981).

21. Hill, H. A. O. and Walton, N. J. J. Amer. Chem. Soc. 104, 6515, (1982).

22. Lewis, N. S. and Wrighton, M. S. Science 211, 944, (1981).

23. Colby, J., Lyons, C. M. and Williams, E. Soc. Gen. Microbiol. Quart. 9, M7, (1983).

CHAPTER 7

METHANOL BASED BIOELECTROCHEMICAL FUEL CELL

Introduction

7.1.1 Theoretical background

A fuel cell is a device for the direct conversion of chemical energy to electrical energy (1). It requires an anode and a cathode, a supporting electrolyte and an external circuit to utilize the electricity. Reactants must be transported to the electrodes as a source of electrons at the anode and as a recipient of electrons at the cathode. Catalysts are incorporated to enhance the rate of reaction at each electrode. For a hydrogen-oxygen fuel cell, the anodic, eq 7.1, and cathodic, eq 7.2, half-cell and overall redox reaction, eq 7.3, are written as follows (at $a_{H^+} = 1$):

$$H_2 = 2H^+ + 2e^- \qquad E^o = 0V \qquad [7.1]$$

$$2H^+ + 2e^- + 1/2O_2 = H_2O \qquad E^o = 1.229V \qquad [7.2]$$

$$H_2 + 1/2O_2 = H_2O \qquad E^o = 1.229V \qquad [7.3]$$

The theoretical amount of work, W_u available depends on the net energy release, eq 7.4, for the overall reaction,

$$-\Delta G = nFE = W_u \qquad [7.4]$$

in this case 237.2 KJ mol^{-1}. The omission of a superscript on E implies that standard conditions are not required. The efficiency of a fuel cell is defined as, eq 7.5,

$$\Delta G/\Delta H = 1 - T\Delta S/\Delta H \qquad [7.5]$$

Given that the entropy term often amounts to ca. 10% of the enthalpy term, the efficiency can be as high as 90%. In practice, experimental values close to 60% are more common (2,3). When a current flows in a fuel cell, not all of the chemical potential is available for work. The unavailable part of the work, termed overpotential has three main sources: activation overpotentials arise from one of the chemical or electrochemical reactions being kinetically limited; concentration overpotentials result from diffusional limitations of the reactants; ohmic overpotentials are caused by slow transport of ionic species and to junction potentials (4,5).

7.1.2 Conventional fuel cells

Most inorganic fuel cells under development are based on hydrogen-oxygen and use various electrolytes including hydrogen bromide, phosphoric acid and potassium hydroxide (6). They require

high operating temperatures, 150-700°C, to realise sufficient current densities ca.100mA cm^2 from the catalysts that are incorporated. However, several problems remain to be solved before they find wide commercialisation. Improved catalysts of low cost are required, in addition to novel catalysts for electro-oxidation of fuels other than hydrogen. The types of materials available for fuel cell construction are severely restricted by the elevated temperature of operation and corrosiveness of the electrolytes that are used.

7.1.3 Biofuel cells

Fuel cells incorporating alternative biological catalysts merit investigation since they offer possible advantages over the present technology. The principal attractions are high substrate (fuel) affinity and fast rates of reaction at ambient temperatures and moderate pH. In addition, the ability of living organisms, particularly microorganisms, to metabolise numerous organic and inorganic molecules reflects the wide range of catalysts available for exploitation. In earlier work in this field, suspensions of respiring microbial cells were investigated as possible catalysts for glucose oxidation by incorporation into the anodic compartment of fuel cells. Microorganisms studied include, Saccharomyces cerevisiae (7), Pseudomonas ovalis (8) and Micrococcus cerificans (9). These reports use a variety of mediator molecules, to divert reducing equivalents from the respiratory chain of the organism to

the anode, with some success. However, the major problem with microbial systems is identifying mediators that can efficiently transport electrons from the organism without having a deleterious effect on other biochemical processes.

A more sucessful approach has been to incorporate a purified enzyme (plus cofactor) into a fuel cell to catalyse either the anodic or cathodic reactions. A summary of work on enzyme based fuel cells (10-16) is given in Table 7.1. Whilst, many of these systems give high thermodynamic efficiencies, 50-60% is typical, they are characterised by low current densities, ca. 1-10$\mu A\ cm^2$, when compared to conventional inorganic fuel cells. As a result, the technology, though promising, remains in its infancy.

7.1.4 Methanol based biofuel cell

At present, alcohols, especially methanol, are attracting considerable attention as fuels. Consequently, the development of an efficient (bio)fuel cell would expand the usefulness of these materials. Whilst direct electro-oxidation of methanol at a nickel electrode (17) and at a benzoquinone modified electrode (18) has been studied, conventional fuel cells based on these system have not been developed. In this context, however, methylotrophic bacteria are of special interest since energy derived during respiration is based upon the oxidation of methanol (or methane) to carbon dioxide (19), figure 7.1. The oxidation of methanol is catalysed by a

Table 7.1 Enzyme based fuel cells

Enzyme	Immobilisation	Mediator	Refs
glucose oxidase	glutaraldehyde	2,6-dichlorophenol indophenol	10
glucose oxidase	-	"	11
hyaluronidase	sepharose CNBr	"	12
alcohol dehydrogenase	-	phenazine methosulphate	13
hydrogenase	-	methylviologen	14
hydrogenase	polypropargyl pyridine gel	lithium tetracyano-quinonedimethane	15
methanol dehydrogenase	-	phenazine ethosulphate	16

Figure 7.1 Substrate utilization by methylotrophs

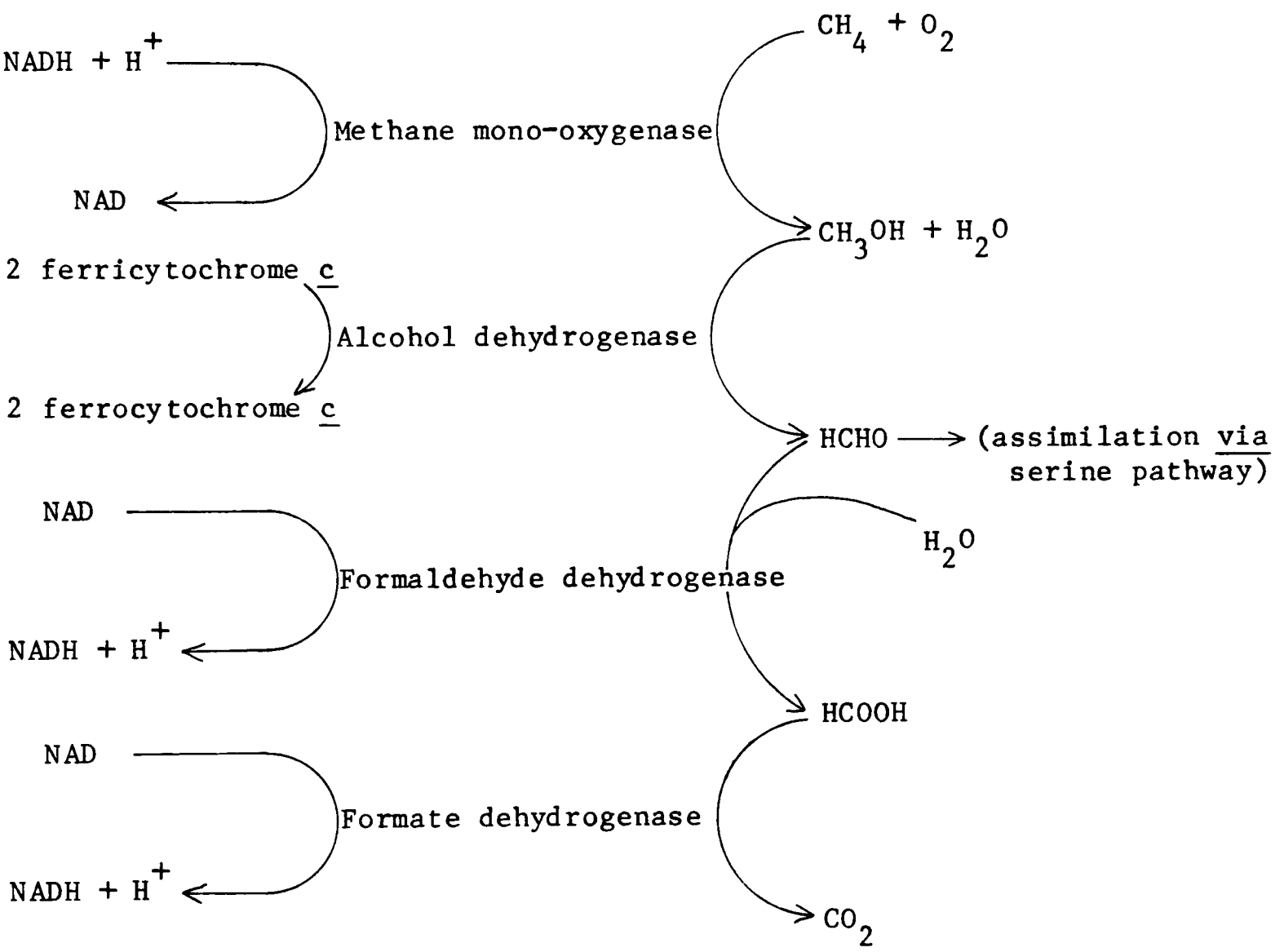

quinoprotein alcohol dehydrogenase (ADH) (alcohol:(acceptor) oxidoreductase, EC 1.1.99.8). This enzyme, which represents ca. 10% of the dry cell weight, was isolated from Pseudomonas extorquens and utilised as a catalyst for the anodic reaction of a methanol-based biofuel cell. Quinoproteins which oxidise a range of substrates have been isolated from various bacterial sources, table 7.2, and reviewed by Duine (20).

7.1.5 Biochemistry of Alcohol dehydrogenase

The novel biochemical properties of $NAD(P)^+$-independent alcohol dehydrogenases are particularly interesting. Enzymes have been isolated from several sources and appear to be closely related (20). In vivo, the enzyme is coupled to the respiratory chain at the level of cytochrome c, figure 7.1. However, this reaction which has a pH optimum at pH 7.0 only occurs with anaerobically prepared enzyme and is irreversibly destroyed on exposure to oxygen (21). Aerobically prepared ADH retains activity, if ammonia or primary amines are present as an activator and will use a range of organic dyes as electron acceptors (21). A dramatic increase in the optimum pH for the latter reaction is observed (20). The enzyme is dimeric with a molecular mass of 1.2×10^5 and contains two equivalents of the prosthetic group 2,7,9-tricarboxy-1H-pyrrolo(2,3-f)-quinoline 4,5-dione (PQQ). Forrest (22,23), found that the o-quinone structure was essential for activity and proposed a mechanism for methanol oxidation involving PQQ, figure 7.2. It was suggested that the

Table 7.2 Distribution of Quinoproteins

Quino-protein	Organisms
Alcohol dehydrogenase	Methylotrophic bacteria
Alcohol dehydrogenase	Acinetobacter calcoaceticus
Alcohol dehydrogenase	Acetic acid bacteria
Glucose dehydrogenase	Acinetobacter calcoaceticus
Glucose dehydrogenase	Pseudomonas aeruginosa
Glucose dehydrogenase	Gluconobacter oxydans
Methylamine dehydrogenase	Pseudomonas AM1
Methylamine dehydrogenase	Thiobacillus A2
Lactate dehydrogenase	Propionibacterium pentosaceum

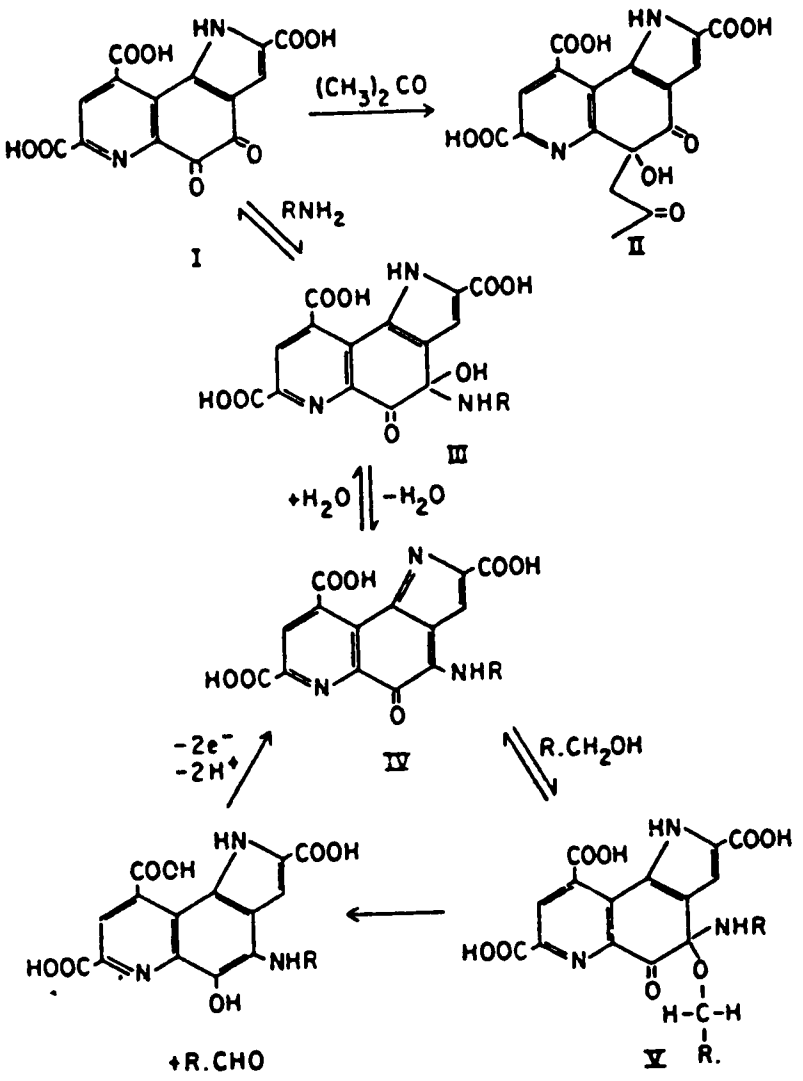

Figure 7.2 Proposed scheme for the PQQ-catalysed oxidation of primary alcohols. Addition of (I) to the apo-enzyme reconstituted activity towards the substrate. The active form of the co-factor (IV) is linked to the enzyme *via* an amine function. PQQ was first isolated as the acetone adduct (II)(23).

prosthetic group forms an addition compound with the ϵ-NH_2 of a lysine residue (or with ammonia or a primary amine) at the C-4 position. Addition of methanol is followed by a cyclic re-arrangement with release of the oxidised product. In addition to methanol, ADH will also use other primary alcohols and formaldehyde as substrates (21).

7.1.6 Experimental methanol biofuel cell

Oxidation of formaldehyde to yield formate is of particular significance to the fuel cell, as the overall oxidation of methanol becomes a four-electron process, eq 7.6.

$$CH_3OH + H_2O \xrightarrow{ADH} HCOOH + 4H^+ + 4e^- \qquad [7.6]$$

The experimental methanol based biofuel cell that has been developed is shown schematically in figure 7.3. In the anodic compartment, ADH oxidises methanol and reduces a redox mediator which is re-oxidised at the anode. From the anode electrons flow through the external circuit to the cathode where oxygen is reduced. The electrical circuit is completed by protons, derived from the enzymatic reaction, diffusing through a proton-permeable membrane to react at the cathode.

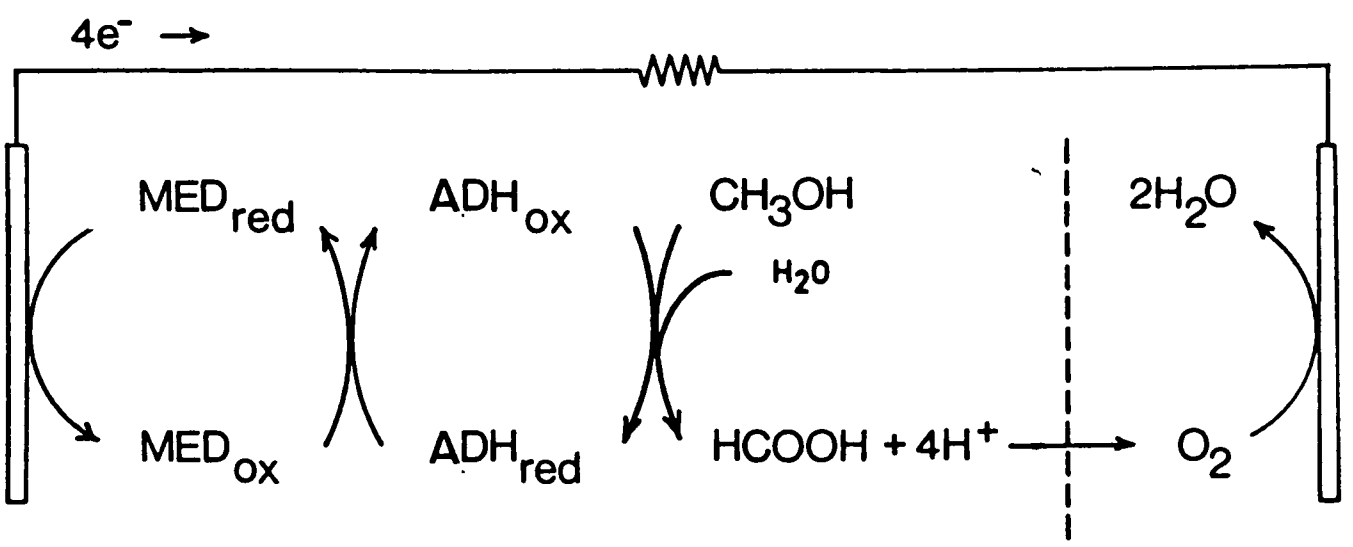

Figure 7.3 Schematic representation of the biofuel cell, where $MED_{(ox/red)}$ are the redox forms of the mediator and $ADH_{(ox/red)}$ are the redox forms of the prosthetic group of the quinoprotein. The anodic and cathodic compartments are separated by a proton permeable membrane.

The performance of a biofuel cell depends predominantly upon the rate of electron transfer from enzyme to mediator and the re-oxidation of the latter at the electrode surface. D. C. cyclic voltammetry is useful in the study of the kinetics of this process, enabling identification of the best mediator. In addition the technique is useful for studying the reaction as a function of additional variables e.g. pH, thus facilitating its optimisation.

In previous work (24), the MDH biofuel cell used phenazine (m)ethosulphate (PMS and PES) as mediators. However, slow decomposition of both mediators (25), a process accelerated by the high pH necessary for maximum enzyme activity, made them unsuitable for extended use in the biofuel cell. This prompted the evaluation of alternative stable soluble electron acceptors, including N,N,N′,N′-tetramethyl-4-phenylenediamine (TMPD), safranine-O, phenolsafranine, brilliant blue-B, malachite green, brilliant cresyl blue, 1-methoxyphenazine methosulphate and methyl violet-6B. Ferrocene monocarboxylic acid, which had been investigated with ADH, section 6.3.3, had a redox potential that was too positive for the anodic compartment of the fuel cell. Of all the mediators tested, the best results were obtained with TMPD.

Experimental

7.2.1 Protein preparation and purification

Alcohol dehydrogenase was purified from the methylotroph Pseudomonas extorquens held in the freeze-dried culture collection at the Biotechnology Centre, Cranfield Institute of Technology. The organism was grown under optimised conditions in a 20L fermenter (26). Cells were harvested using a Sharples Supercentrifuge (Penwalt, d'Ovres, France), and supplied frozen as pellets stored at -20^{o}C. Batches of cells were pooled, resuspended in 50mM Tris/HCl buffer at 4^{o}C and ruptured by a single passage at 25,000 psi through a Stansted cell disrupter (Stansted Fluid Power Ltd., Stansted, Essex). ADH was purified by the method of Anthony and Zatman (27). Final purification of the enzyme to homogeneity was achieved by fast protein liquid chromatography (FPLC) using a poly-anion SI exchange column. The enzyme was loaded on to the column in 20mM Tris-HCl pH 8.0 (buffer A) and eluted by applying a linear gradient of increasing ionic strength with buffer B (A + 1.0M NaCl), figure 7.4. ADH activity was limited to the major fraction eluting at an ionic strength equivalent to 25% buffer B. ADH had a purity ratio A_{280}/A_{342} = 10.7 which agreed with the reported literature value (4). The purified enzyme was concentrated to 5.2 mg ml^{-1}, measured by the method of Warburg (28), in buffer A and stored frozen at -20^{o}C. The specific activity of MDH was measured spectrophotometrically using

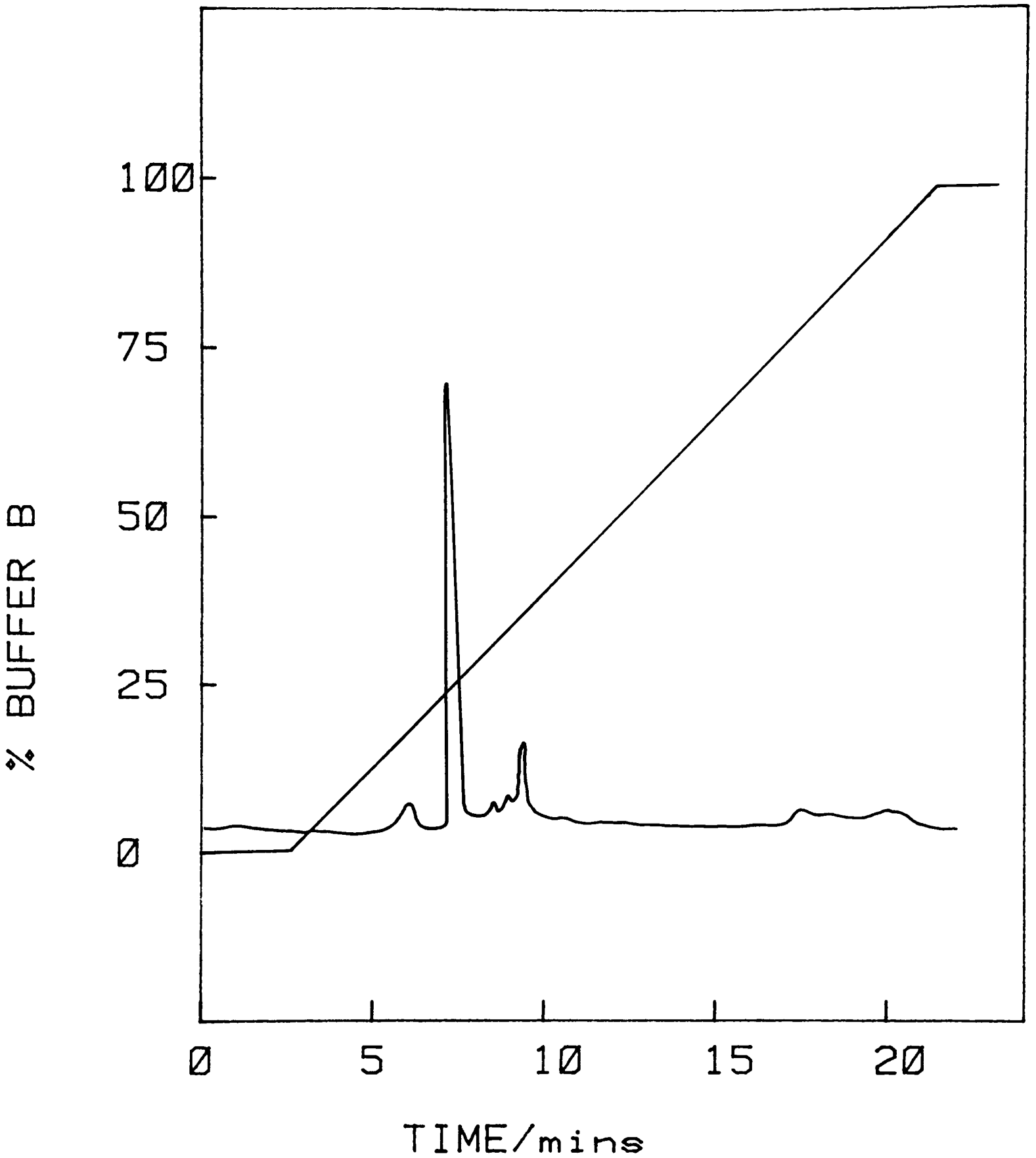

Figure 7.4 FPLC elution profile of alcohol dehydrogenase from Pseudomonas extorquens

N,N,N′,N′-tetramethyl-4-phenylenediamine (TMPD, oxidised form) as an electron acceptor which had a molar absorption coefficient of 11.6×10^3 l mol^{-1} cm^{-1} at 563nm. In argon-saturated 100mM borax-NaOH, pH 10.5, containing 14mM NH_4Cl and 50mM methanol, ADH had a specific activity of 1.07μmoles (TMPD reduced) min^{-1} mg^{-1}, at 20^oC.

Formate dehydrogenase with a specific activity of 24IU mg^{-1} was supplied by Sigma Chem. Co.

7.2.2 Electrolytes and substrates

All experiments were performed using 100mM Borax-NaOH as the electrolyte containing 14mM NH_4Cl, necessary for enzyme activity. Methanol and other alcohols were of AnalaR grade, supplied by BDH. At all times, thoroughly degassed solutions were used.

7.2.3 Electrochemical experiments

D. C. cyclic voltammetry experiments were performed, as described previously, with a 4mm platinum disc working electrode.

Experiments to determine the charge passed from the enzymatically coupled oxidation of measured quantities of substrates were performed using a cell of volume 10ml. The cell contained a $10cm^2$ gold gauze (80 mesh) working electrode, a platinum counter electrode behind a glass frit and an SCE as reference. To the cell

was added TMPD (1.0mM) and MDH (1.0μM) in 10ml of electrolyte pH 10.5. The potential of the working electrode was poised at +110mV (100mV positive of E^{o} for TMPD) and the system allowed to come to Nernstian equilibrium. The speed of this process was increased by stirring with a small magnetic stirrer bar. Aliquots of alcohols, made up as 60mM aqueous stock solutions, were added using a 100μl syringe (supplied by Scientific Glass Engineering Ltd). The current derived from the cell was recorded as a function of time with a Bryans 28000 Y-t chart recorder equipped with an integrator. Integration of the current-time curves obtained gave a measure of the total charge passed for each aliquot.

The experimental biofuel cell, figure 7.5, was made of perspex and comprised an anode compartment (1.6 x 1.6 x 3.5 cm) and a cathode compartment (1.6 x 1.1 x 3.5cm) which were separated by a cation exchange membrane supplied by BDH, Ltd. Both the anode and cathode were of platinum gauze rolled into cylinders, 50-mesh (1.6 x 4.8cm) and 80-mesh (1.6 x 2.5cm), respectively. Before use, the electrodes were cleaned by immersion in concentrated HNO_3 and electrochemically cycled in 0.5M H_2SO_4 (29).

Typically, the anodic compartment contained 3.6ml of electrolyte pH 10.5, 50mM methanol and various concentrations of MDH and mediator. The mixture was stirred rapidly using a small magnetic stirrer bar whilst nitrogen was blown over the surface of the solution. The cathodic compartment contained 3.0ml of the same

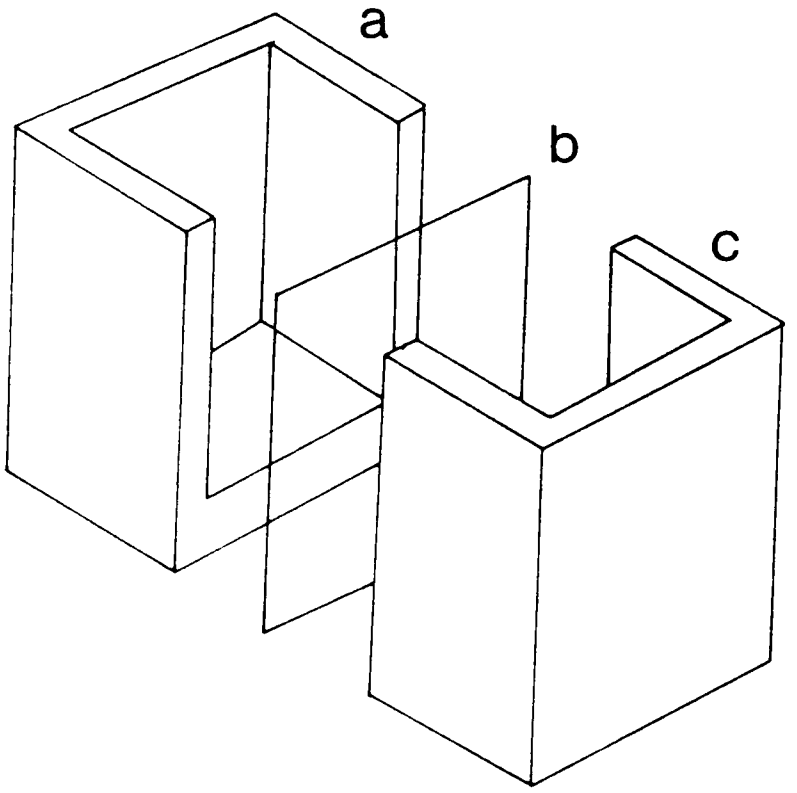

Figure 7.5 The perspex biofuel cell was assembled by clamping the the anodic (a) and cathodic (c) compartments together with a proton permeable membrane (b) separating the two compartments.

electrolyte saturated with air. The current generated by the cell, operated at 20^{o}C, was determined by measuring the voltage drop across a 10 ohm resistor and recorded on a Bryans 28000 Y-t chart recorder.

Results and discussion

7.3.1 Electrochemically coupled oxidation of methanol

A series of D. C. cyclic voltammograms of TMPD were recorded at scan rates of 1-100 mVs^{-1}, in the region pH 8-11. The data obtained confirmed previous reports (33) that the mediator is a reversible one-electron redox agent (E^{o} = 10mV vs SCE) over this pH range. Introduction of both methanol and ammonium chloride, the latter required for enzyme activity, had no discernable effect upon the electrochemistry of TMPD, figure 7.6(a). However, upon addition of ADH to the system, figure 7.6(b), a voltammogram indicative of the catalytic regeneration of reduced TMPD by the enzyme, was obtained. Given that figure 7.6(b) is only obtained in the presence of methanol (or other primary alcohols), the data are qualitatively consistent with the catalytically coupled sequence shown, eq 7.7-7.9.

$$CH_3OH + ADH/PQQ \longrightarrow HCHO + ADH/PQQH_2 \qquad [7.7]$$

$$ADH/PQQH_2 + 2TMPD_{(ox)} \longrightarrow ADH/PQQ + 2TMPD_{(red)} + 2H^{+} \qquad [7.8]$$

$$2TMPD_{(red)} \rightleftharpoons 2TMPD_{(ox)} + 2e^{-} \qquad [7.9]$$

Quantitative kinetic data for the homogeneous reaction between ADH and TMPD, were obtained under conditions of substrate excess, 50mM

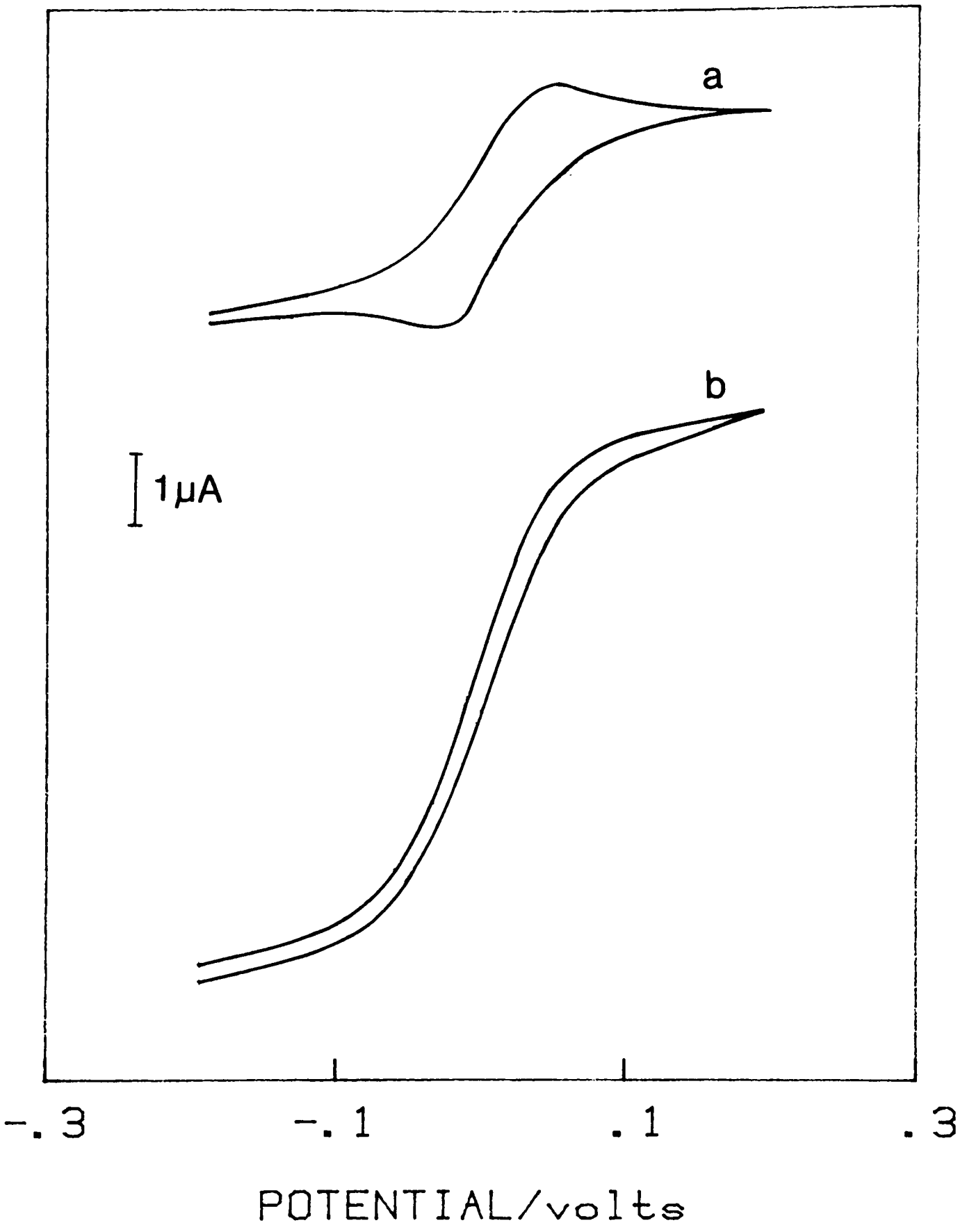

Figure 7.6 (a) D. C. cyclic voltammogram of 500μM TMPD in 50mM Borax-NaOH buffer pH 10.5, containing 14mM NH_4Cl and 50mM methanol at 20°C and at a scan rate of $1mVs^{-1}$. (b) as for (a), but with the addition of 7.0μM ADH.

methanol. By this method a second order homogeneous rate constant for the reaction between enzyme and mediator, eq 7.8, was obtained, $k_f/[ADH] = k = 6.4 \times 10^4$ l mol^{-1} s^{-1} at pH 10.5 and 20°C.

7.3.2 Optimum pH for methanol oxidation

To evaluate the optimum operational pH for the reaction occuring in the anodic compartment of the fuel cell, the second order rate constant was determined as a function of pH. Figure 7.7 shows that there is a substantial increase in the rate constant with increasing pH, to an optimum value at pH 10.5. Such high optimum pH values are also typical of NAD-dependent alcohol dehydrogenases from both yeast and horse liver (30), though these enzymes do not require ammonia as an activator.

The TMPD/ADH/methanol system remained catalytically coupled without substantial deterioration at pH 10.5 and at 20°C for more than 20 days. Such remarkable combined enzyme and mediator stability suggested the system constituted a suitable bio-anode for a methanol based biofuel cell.

7.3.3 Optimum substrate for the fuel cell

The broad substrate specificity of ADH indicated that a range of primary alcohols could be used to power the biofuel cell. A number of potential fuels were investigated to determine the charge

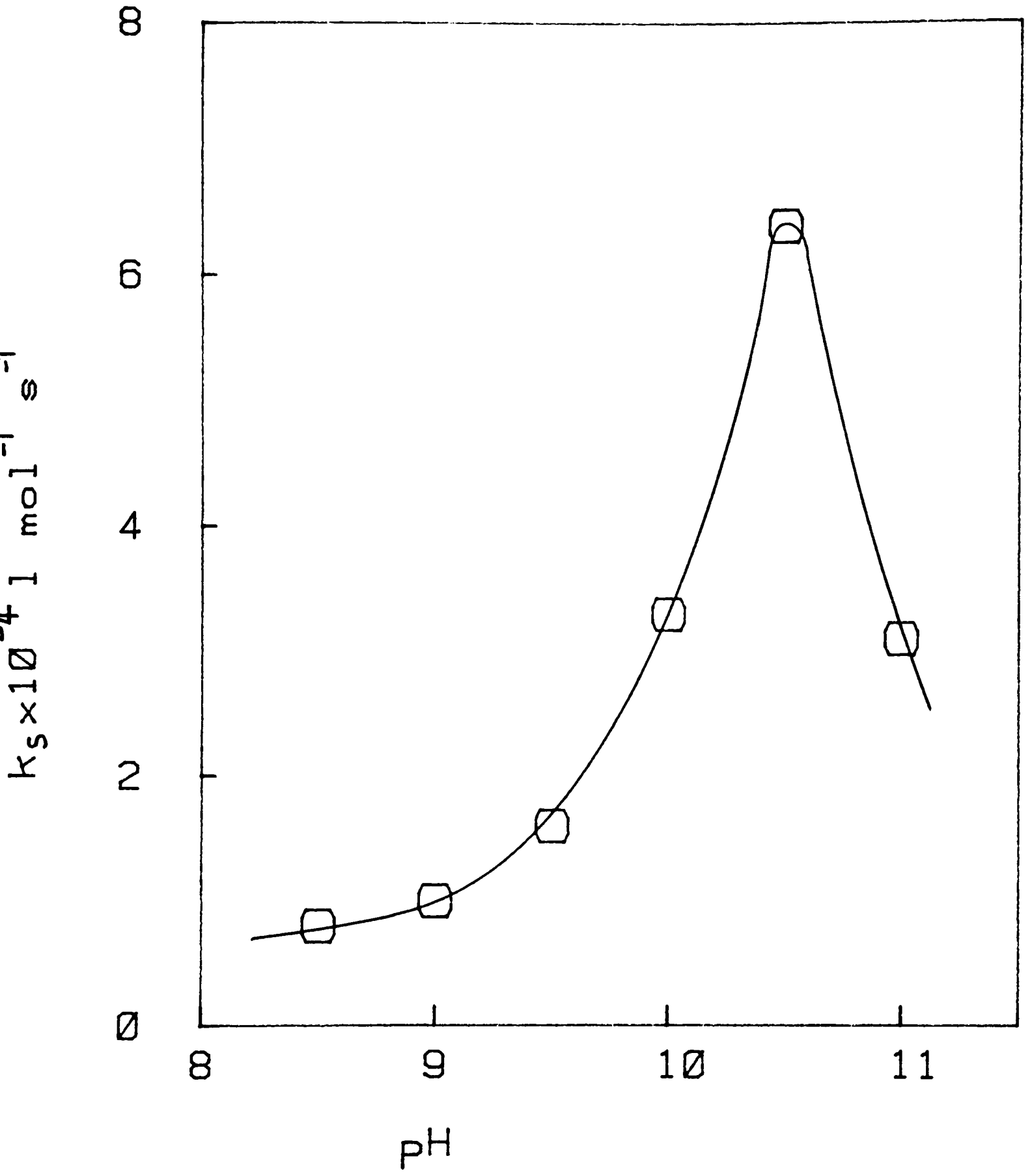

Figure 7.7 Plot of the second order rate constant for the reaction between TMPD and ADH at 20°C as a function of pH. Other conditions as for figure 7.6.

passed per mole of fuel. Aliquots of different alcohols of known concentration, were added to a cell containing TMPD and MDH. Upon addition, a current flowed until all of the substrate had been oxidised. By integration of the current-time curves obtained, a value for the total charge passed during the experiment was estimated. Figure 7.8, presents a sample calibration curve in which charge passed is plotted versus the amount of methanol added, in the range $2\text{-}10\times10^{-9}$ moles substrate. Data for butan-1-ol are also included in Figure 7.8. Whilst the charge passed is directly proportional to the amount of substrate added, the total charge is different for each substrate. This method was used as to determine values for other straight chain primary alcohols up to hexan-1-ol, also for 1,4-butanediol, 1,3-propanediol and formaldehyde, table 7.3. Confirmation of the enzymes specificity for primary alcohols was obtained by adding secondary and tertiary alcohols, propan-2-ol and iso-butanol respectively. Neither of these substrates yielded a current. From the gradient of plots such as those shown in figure 7.8, the oxidation of methanol, 1,4-butanediol and 1,3-propanediol is associated with the passage of ca. 4 Faradays per mole, whereas butan-1-ol, formaldehyde and all other primary alcohols give values close to 2 Faradays per mole. The results are generally consistent with a 2-electron oxidation of a primary alcohol to an aldehyde. However,the results for methanol and formaldehyde indicate that the former is the best substrate for the biofuel cell since it is oxidised to formate. Oxidation of formaldehyde probably results from this aldehyde existing in aqueous solution predominantly as a

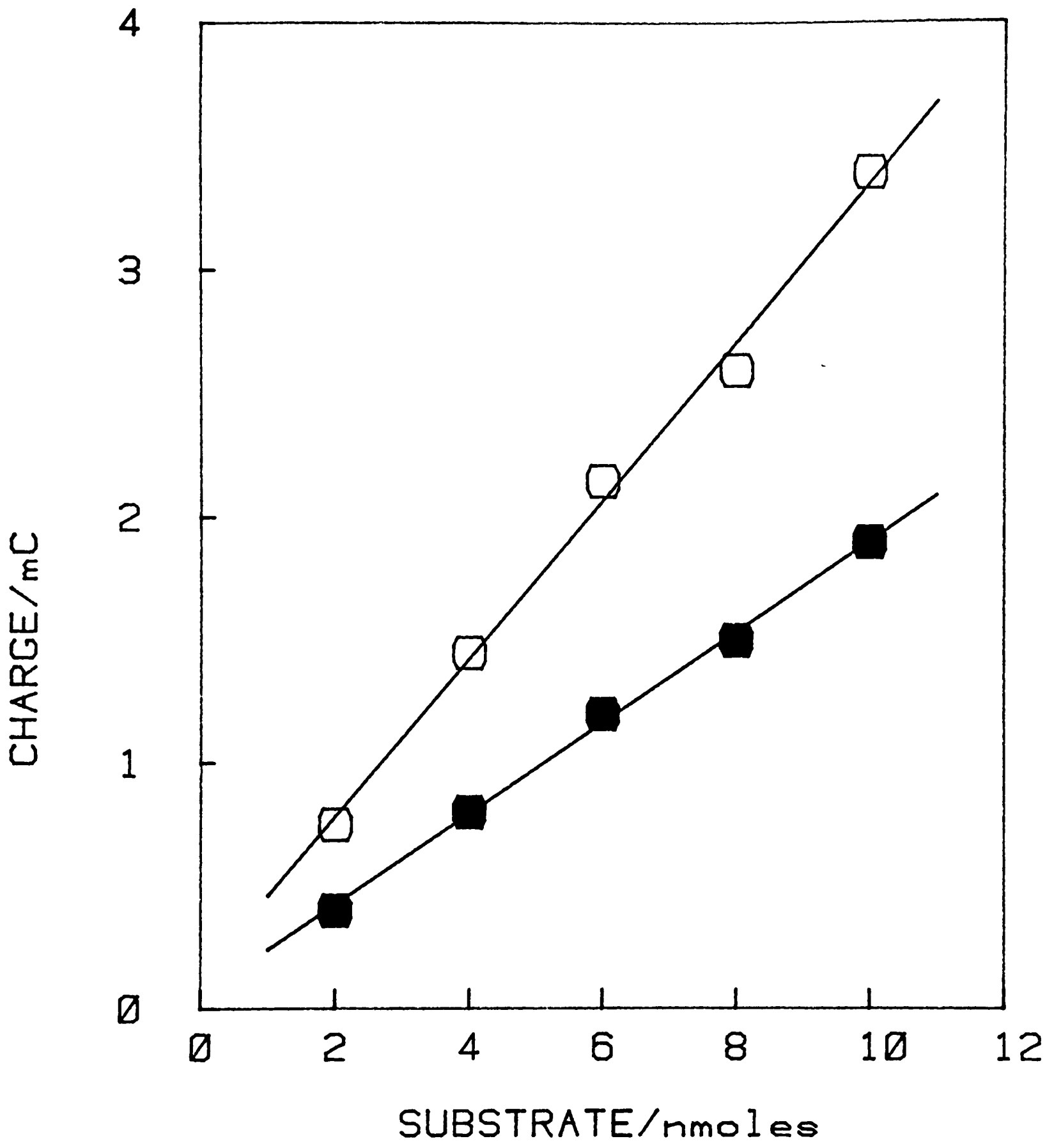

Figure 7.8 Plot of the total charge passed in millicoulombs upon addition of aliquots of methanol (O) and butan-1-ol (●).

Table 7.3 Fuels for biofuel cell

Substrate	Charge passed Faradays per mole
methanol	3.5
formaldehyde	2.0
ethanol	2.1
acetaldehyde	0.0
propanol	1.7
isopropanol	0.0
n-butanol	2.2
iso-butanol	0.0
n-hexanol	1.8
1,3-propanediol	2.9
1,4-butanediol	3.5
pentaerythritol	0.0
trichloroacetal	1.7

hydrated gem-diol $CH_2(OH)_2$ (26). Indirect evidence that this is the enzymatically active form of the substrate was obtained using this coulometric assay. It was shown that the gem-diol, trichloroacetal underwent a 2-electron oxidation, whereas addition of acetaldehyde gave no current.

7.3.4 Alcohol dehydrogenase-based biofuel cell

Fast and efficient conversion of substrate to electrical power is obviously dependent on the optimisation of the enzymatic reaction and the transfer of electrons to the anode. The production of a practical fuel cell, however, requires the effective containment of these reactions within the anodic compartment, under conditions compatible with maximum power output and stability. As a result, the choice of membrane for the fuel cell is extremely important since the material used must be freely permeable to protons, giving the cell a low internal resistance, whilst remaining impermeable to the mediator and oxygen if a short circuiting of the cell is to be prevented. Previously, a number of membrane materials were studied to assess proton, mediator and oxygen permeability (31). Whilst none of them proved ideal, a cation exchange membrane was the best compromise.

7.3.5 Fuel cell stability

The performance of the experimental fuel cell, incorporating

this membrane, was tested with MDH and TMPD under conditions suitable for maximum enzyme activity figure 7.9(a). Whilst the maximum current output was slightly lower than that obtained with PES, figure 7.9(b), the cell showed substantially improved current stability with time. In typical experiments, continuous operation of the TMPD-based fuel cell yielded a steady current output decreasing by less than 10% over a 24h period. Precautions were taken to ensure that the overall current output was limited by the rate of transduction within the anodic compartment and not by the cathodic reaction. This was achieved by using a platinum cathode of sufficiently high surface area so that no observable increase in the current occurred when the air-saturated electrolyte in cathodic compartment, figure 7.9(a), was saturated with oxygen.

7.3.6 Current as a function of reagent concentrations

The fuel cell was always operated with excess methanol (50mM), which is aproximately two orders of magnitude greater than the K_M of the enzyme for this substrate. The relationship between enzyme and mediator concentrations and the current output of the experimental cell were investigated. The effect of enzyme concentration on the current is shown in figure 7.10. Aliquots of MDH were added to the anodic compartment of the biofuel cell and the maximum current after each addition was measured. Initially, the current was directly proportional to the amount of enzyme added. Further addition of MDH (above 0.1mg), however, did not increase the current above 0.13mA.

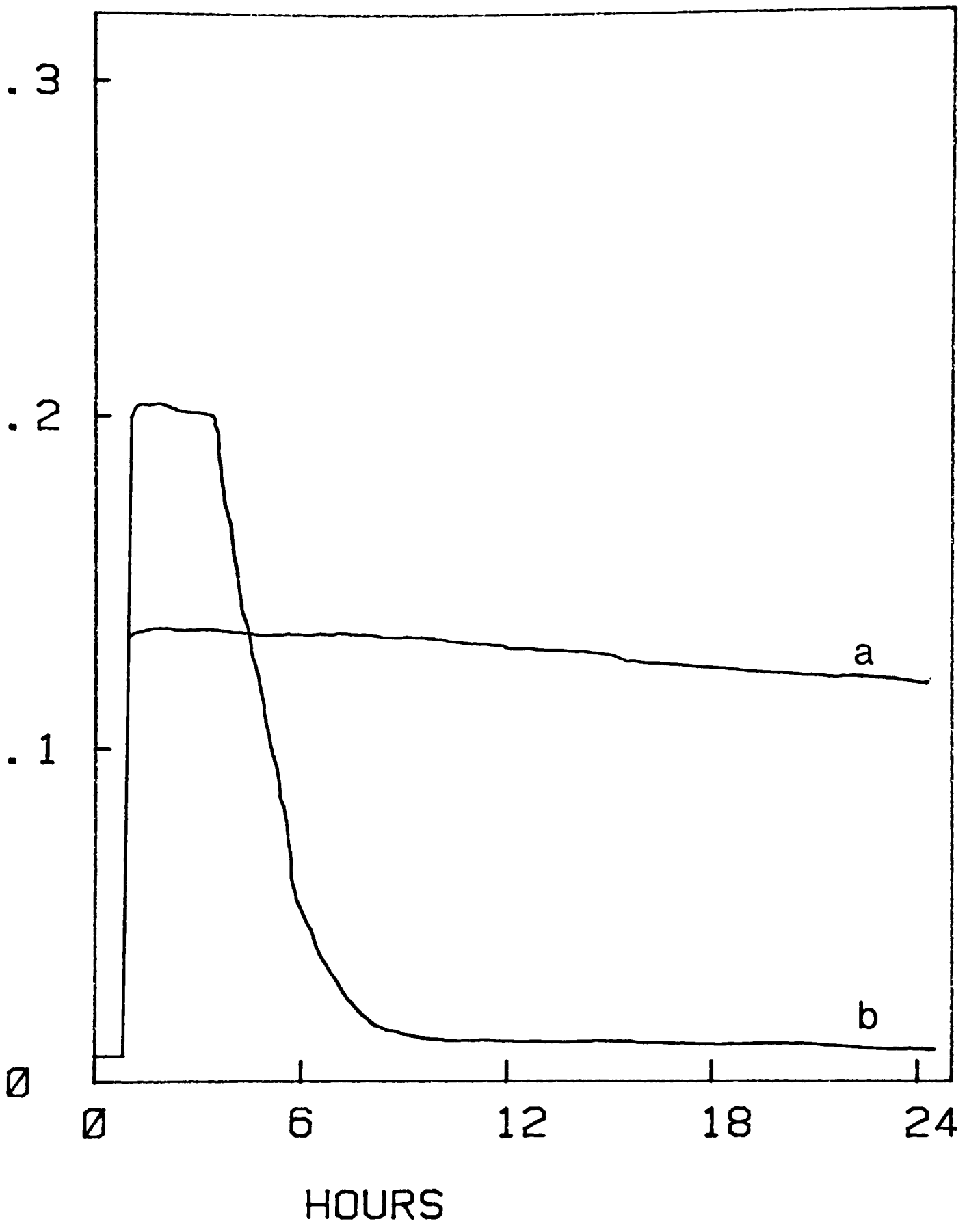

Figure 7.9 Current output of fuel cell using 4.0mM TMPD (a) and 4.0mM PES (b) over a 24h period. The anodic compartment contained 3.6ml of argon-saturated 100mM Borax-NaOH pH 10.5, plus 4.6mg ADH, 14mM NH_4Cl and 50mM methanol. The cathodic compartment contained 3.0ml of the electrolyte saturated with air. The respective surface areas of the anode and cathode were $7.0cm^2$ and $4.4cm^2$.

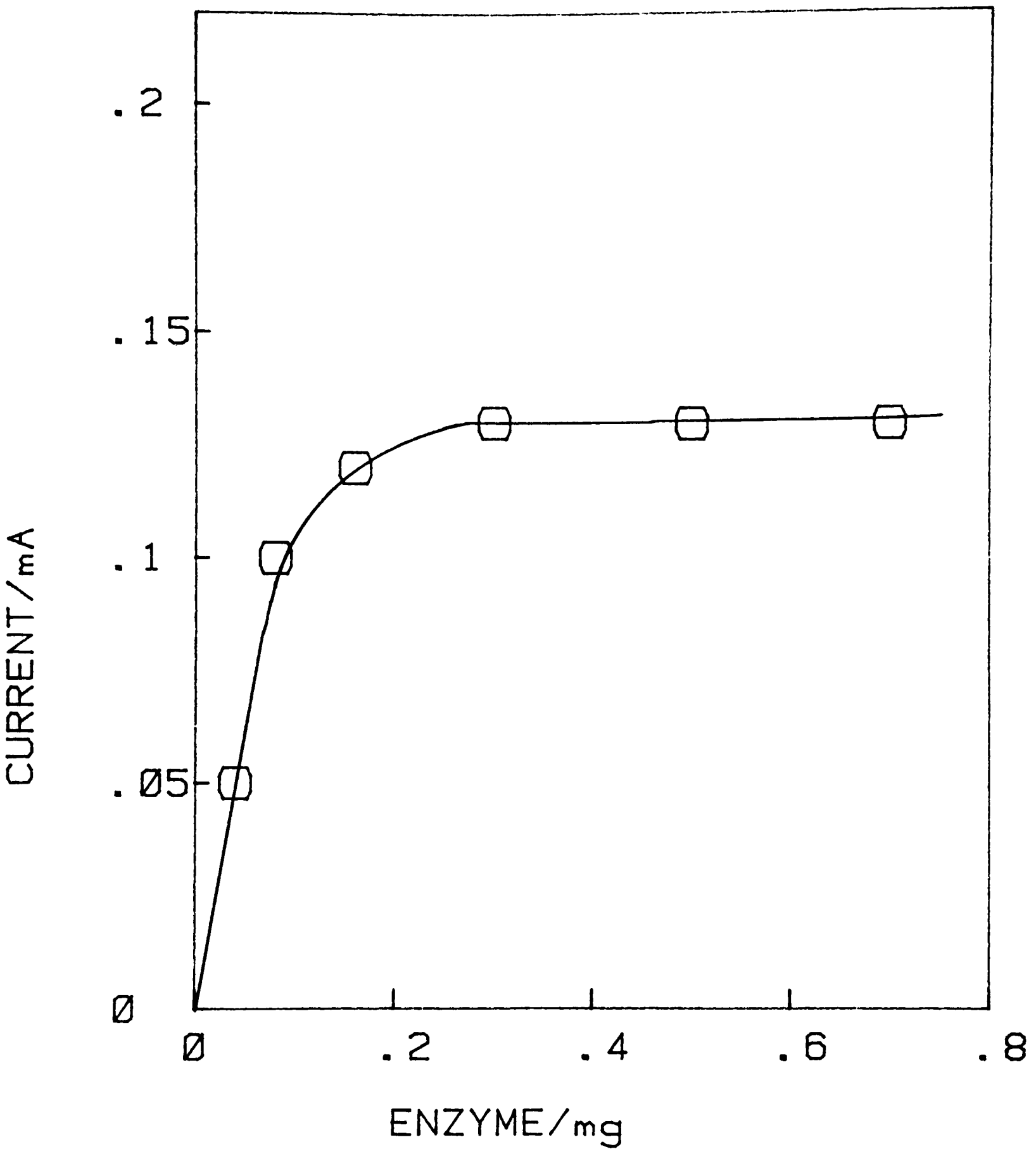

Figure 7.10 Effect of the ADH concentration on current output. Conditions as for figure 7.9.

The effect of TMPD concentration on the current is shown in figure 7.11. The current was initially proportional to the mediator concentration (up to 2.0mM) though again further addition of TMPD did not increase the current above 0.13mA. Clearly, at MDH concentrations exceeding 1.0μM, factors other than enzyme activity are limiting the current. Since the current was found to increase markedly with increased rates of stirring, this was attributed to the rate of mass transport of reduced TMPD to the electrode, i. e. the result of a concentration overpotential. The maximum current density for the platinum gauze anode was 20 μA cm^{-2} geometric area using a 10 ohm external resistance.

7.3.7 Biofuel cell efficiency

The efficiency with which MDH transduces the chemical energy of methanol into current, under conditions where enzyme activity limits the current, was calculated from the data presented in figure 7.10. From the specific activity of the enzyme, 1.07μmoles mg^{-1} min^{-1} the theoretical efficiency (26) eq. 7.10,

$$\text{efficiency} = nF \times \text{specific activity}/60 \qquad [7.10]$$

was calculated to be 1.7mA mg $protein^{-1}$. The observed current output of 1.25mA mg $protein^{-1}$ represents 73% of the enzyme activity realised as current.

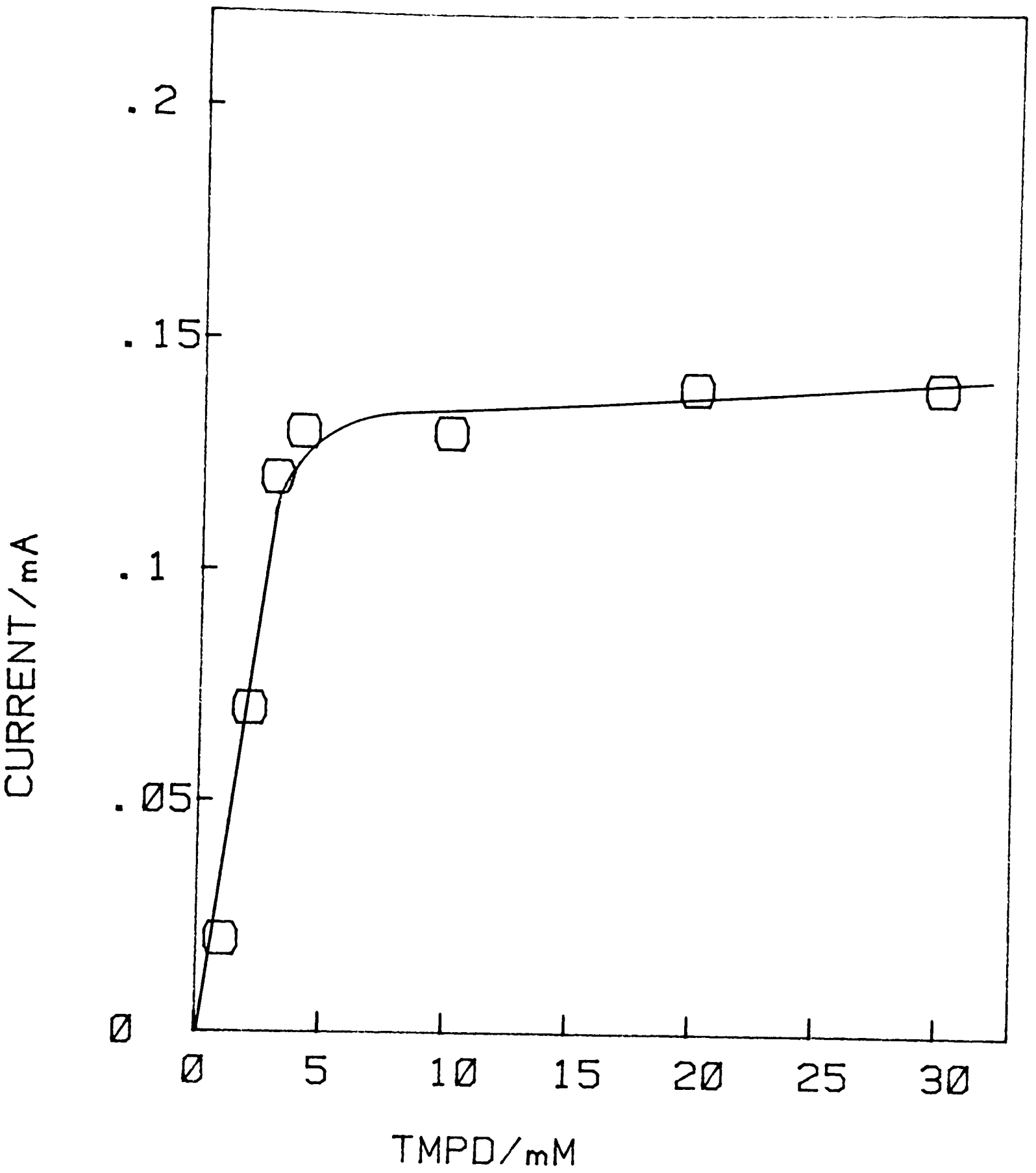

Figure 7.11 Effect of the TMPD concentration on current output. Conditions as for figure 7.9.

7.3.8 Power output

The most important criteria for evaluating fuel cells are based on the voltage-current, figure 7.12, and power-current, figure 7.13, relationships. The decrease in voltage as more current is drawn from the cell is characteristic of many fuel cells (6). Figure 7.13 show that the maximum power derived from the cell was 12μW, (equivalent to 14KW mol^{-1} catalyst), with a power density of 2μW cm^{-2}.

7.3.9 Deficiencies of the fuel cell

One of the deficiencies of the cell is the incomplete oxidation of the substrate methanol and resultant accumulation of the product formate, which is an inhibitor of the enzyme (20). One method of solving this problem was investigated. The NAD-linked enzyme formate dehydrogenase (FDH; EC 1.2.1.2 from Pseudomonas oxalaticus, Sigma) was incorporated into the fuel cell to catalyse the oxidation of formate to CO_2. Whilst NADH will use 4-phenylenediamine derivatives as electron acceptors (32), the activity of FDH decreases above pH 7 (19). As a consequence, it was not possible to find a pH value at which a cell containing both MDH and FDH oxidised methanol to CO_2 with an enhanced current, compared to the cell as originally comprised.

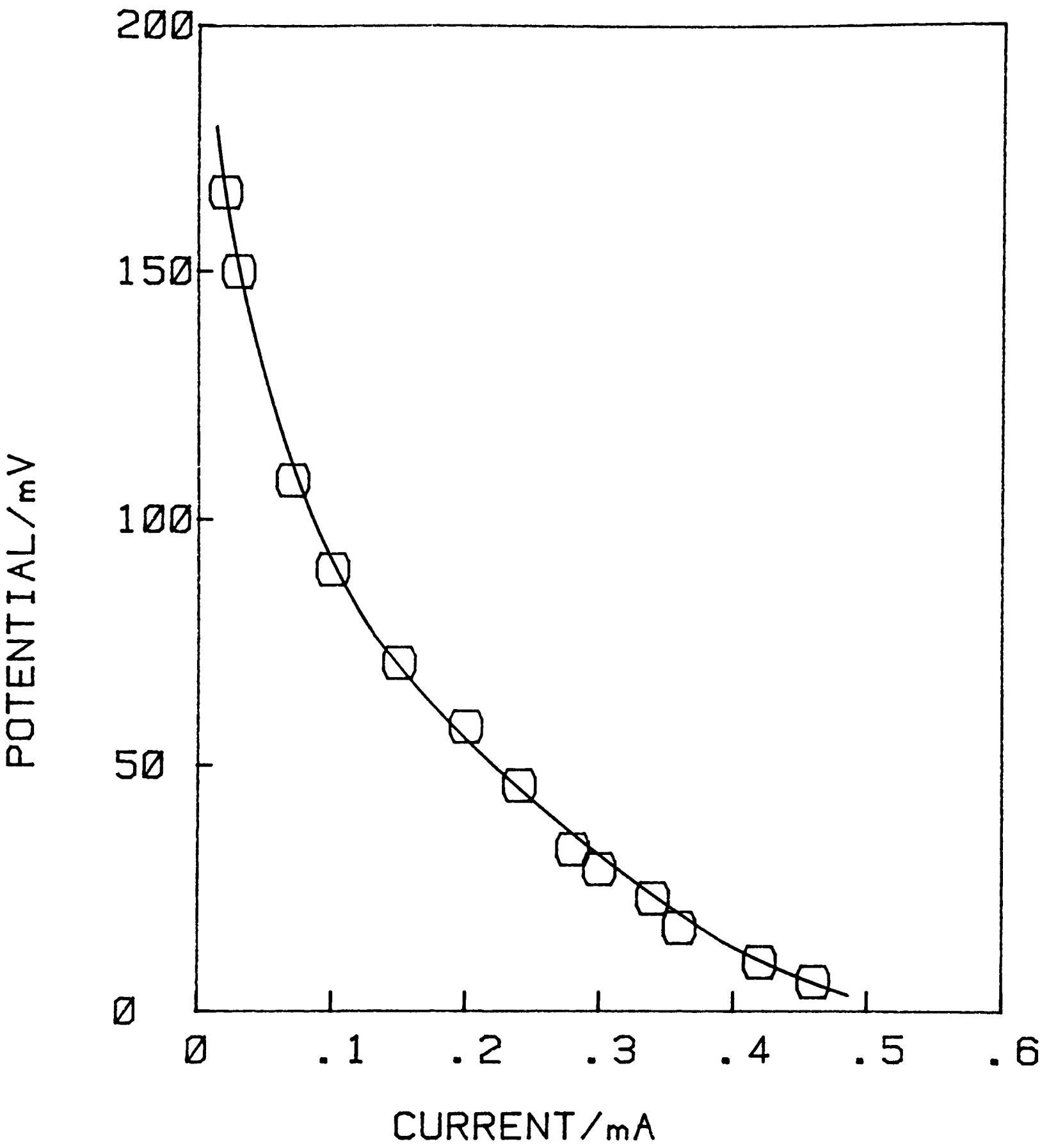

Figure 7.12 Voltage-current relationship for fuel cell.

Conditions as for figure 7.9. The external resistance was varied between 1 and 133×10^3 ohm.

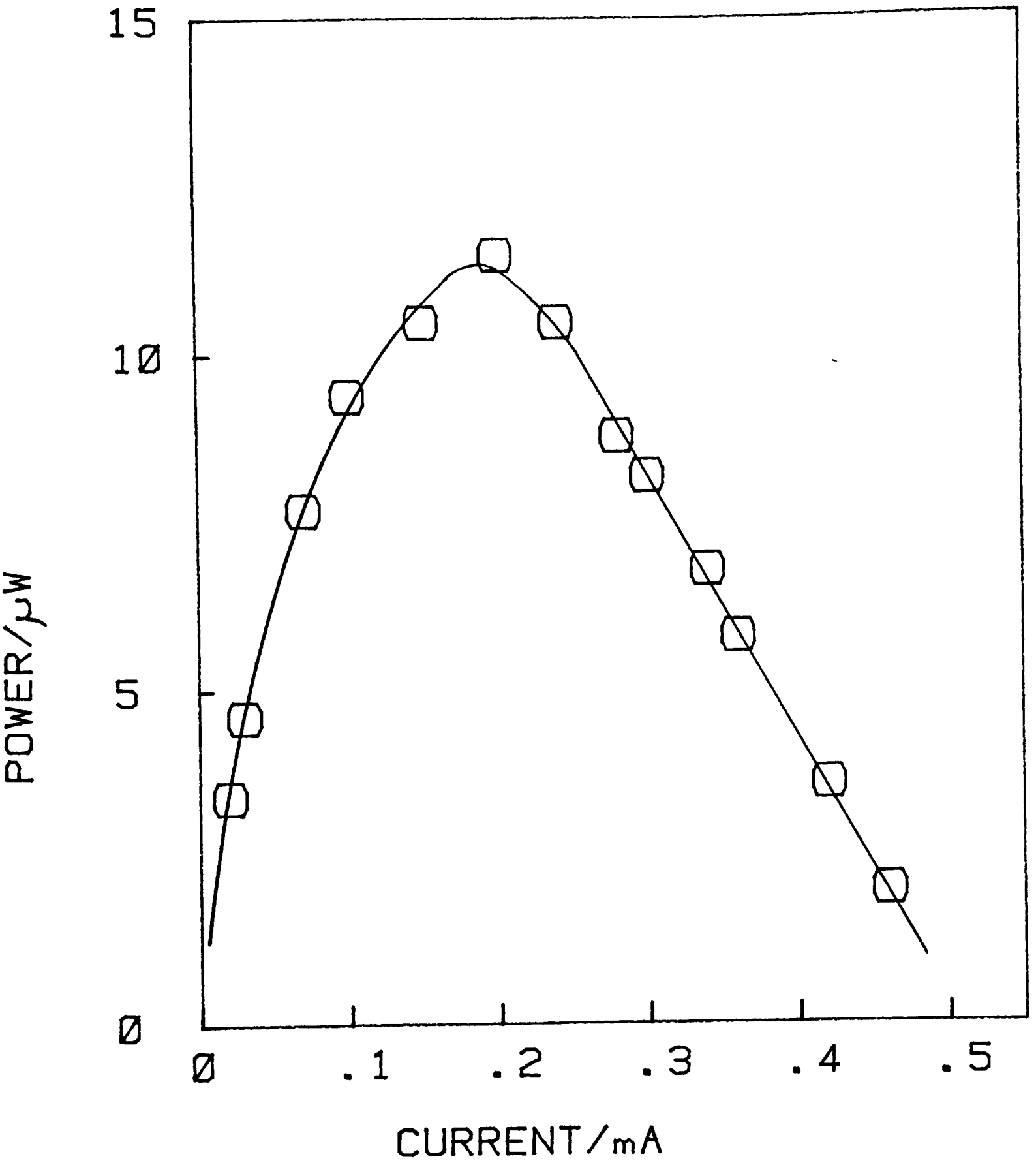

Figure 7.13 Power-current relationship for fuel cell calculated from data presented in figure 7.12.

7.4.1 Conclusions

When compared with conventional fuel cells, the respective current and power densities obtained with this configuration do not represent a realistic method of power production. However, the successful operation of the system demonstrates the potential for using a biological catalyst in fuel cells.

References

1. Been, F. J. Proc. 14th Intersoc. Energy Conv. Eng. Conf. 1, 544, (1979).

2. Bockris, J. O'M. and Reddy, A. K. N. Modern elecrochemistry. New York: Plenum (1970).

3. Benjamin, T. G., Camara, E. H. and Selman, J. R. Proc. Intersoc. Energy Conv. Eng. Conf. 1, 579, (1979).

4. Bockris, J. O'M. and Srinivasan, S. Fuel cells their electrochemistry. New York: McGraw-Hill (1969).

5. Vetter, K. J. Electrochemical kinetics. New York: Academic press (1967).

6. Gallagher-Dagitt, G. E. ed: Fuel cells. Proc. SERC appraisal meeting. London (1982).

7. Videla, H. A. and Arvia, A. J. Experimentia suppl. 18, 667, (1971).

8. Videla, H. A. and Arvia, A. J. Biotechnol. Bioeng. 17, 1529, (1975).

9. Disalvo, E. A and Arvia, A. J. Bioelectrochem. Bioenerg. 6, 185, (1979).

10. Lahoda, E. J., Lui, C. C. and Wingard, L. B. Biotechnol. Bioeng. 17, 413, (1975).

11. Weibel, M. K. and Dodge, C. Arch. Biochem. Biophys. 169, 146, (1975).

12. Kulis, Y. Y. Proc. 3rd Joint US/USSR Enz. Eng. US Govt. PB283 328T (1978).

13. Varfolomeev, S. D. and Yaropolov, A. I. Bioelectrochem. Bioenerg. 4, 314, (1977).

14. Gogotov, I. N. and Varfolomeev, S. D. Mol. Biol. (Moscow), 12, 63, (1978).

15. Berezin, I. V. and Bogdanovskaya, V. A. Dokl. Acad. Nauk. USSR 240, 615, (1978).

16. Suzuki, S., Karube, I., Matsunga, T., Kuriyama, S. and Takamura, Y. Biochemie 62, 353, (1980).

17. Maximovitch, S. and Bronoel, G. Electrochimica Acta 26, 1331, (1981).

18. Kuwana, T., Fujihira, M., Tasaki, S. and Osa, T. J. Electroanal. Chem. 137, 163, (1982).

19. Higgins, I. J., Best, D. J., Hammond, R. C. and Scott, D. Microb. Rev. 45, 556, (1981).

20. Duine, J. A. and Frank, J. TIBS 6, 278, (1981).

21. Duine, J. A., Frank, J. and Ruites, L. G. J. Gen. Microbiol. 115, 523, (1979).

22. Forrest, H. S., Salisbury, S. A., Cruse, N. B. and Kennard, O. Nature 280, 843, (1979).

23. Forrest, H. S., Salisbury, S. A., Kilty, C. G. Biochem. Biophys. Res. Comm. 97, 248, (1980).

24. Plotkin, E. V., Higgins, I. J. and Hill, H. A. O. Biotechnol. Lett. 3, 187, (1981).

25. Ghosh, R. and Quayle, J. R. Anal. Biochem. 99, 112, (1978).

26. Davis, G., Hill, H. A. O., Higgins, I. J., Turner, A. P. F. and Aston, W. J. Enzyme Microb. Technol. 5, 383, (1983).

27. Antony, C. and Zatman, L. J. Biochem. J. 96, 808, (1965).

28. Warburg, O. and Christian, W. Methods Enzymol. 3, 451, (1957).

29. Sawyer, D. T. and Roberts, J. L. Experimental electrochemistry for chemists. New York: Wiley (1974).

30. Wiseman, A. and Williams, N. J. Biochim. Biophys. Acta. 250, 1, (1971).

31. Davis, G., Hill, H. A. O., Higgins, I. J., Turner, A. P. F. and Aston, W. J. Biotechnol. Bioeng. Suppl. 12, 402, (1982).

32. Kitani, A. and Miller, L. L. J. Amer. Chem. Soc. 103, 3595, (1981).

33. Prince, R. C., Linkletter, S. J. and Dutton, L. P. Biochim. Biophys. Acta. 635, 3595, (1971).